ENVIRONMENTAL CRACKING OF WELDED MARAGING STEEL IN HYDROGEN SULPHIDE

by

J.B. MURPHY M.I.M. M.Inst.W.

Thesis submitted to the Council for National Academic Awards for the Degree of MASTER OF PHILOSOPHY

APRIL 1976

CONTENTS

PREFACE

During the period of study, the author has participated in the following courses and conferences:-

1. Statistics and Design of Experiments
2. Electron Microscopy
3. High Strength Steels

at Sheffield Polytechnic, together with a Short Course on Fracture at the University of Newcastle upon Tyne (1970). The work described in this thesis was carried out in the Department of Metallurgy, Sheffield Polytechnic except where specifically stated otherwise, and no part of it has been presented for a higher degree at any other University or College.

The author wishes to express his sincere thanks to his external supervisor Mr J E Trueman in particular, for guidance, friendship and constant encouragement throughout the course of this work. His thanks are also due to Dr P L James for valuable discussions during supervision, and to Dr A W D Hills for his continued support.

The generous supply of maraging steel plate by Messrs. Firth Brown Ltd is gratefully acknowledged as is the provision of fatigue testing and welding facilities at Firth Brown Ltd and Bristol Aerojet Ltd respectively. It is a pleasure to thank Mr P S Cassy and Mr N J Rhodes of Sheffield Polytechnic for their assistance with macro-photography and chemical techniques respectively.

Finally, the author's thanks are due to his wife for her patience, to Miss J Bradley for typing the script and to his colleagues at Sheffield Polytechnic for their sustained tolerance to levels of hydrogen sulphide which might have proved toxic to lesser mortals.

J B Murphy
April 1976

1. SYNOPSIS

A comprehensive survey of the literature concerning environmental cracking in maraging steels has been carried out, with particular reference to the behaviour of welded joints.

The major part of the present experimental work was centred on the performance of submerged-arc welded plate in aqueous hydrogen sulphide. By using pre-cracked specimens, stress-intensity/endurance relationships were determined for weld and parent metals together with mixed structure material from two positions within the heat-affected-zone.

From these data, estimated threshold stress-intensities of 20-30 $MN/m^{3/2}$ showed little difference between materials from any of the four positions. Endurances themselves, however, were generally lower for weld metal than for parent material.

Stage II crack propagation occurred at rates of the order of 10^{-4} - 10^{-3} mm/sec, predominantly along prior-austenite grain boundaries.

An unusual feature of many tests was an apparent drop in propogation rate after growth was initiated. There followed growth at more or less constant rates before final acceleration just prior to fracture.

Fractography showed preferential cracking along specimen edges ahead of the main crack front. This suggested either

faster growth under plane stress conditions or a diffusion barrier affecting hydrogen ingress. Scanning electron microscopy confirmed the purely intergranular nature of cracking, and the presence of stretch zones.

2. INTRODUCTION

Risk of structural failure, often with catastrophic consequences, becomes increasingly serious as material strengths and operating stresses rise. A major cause of many such failures is environmental interaction with stressed material resulting in cracks, the insidious growth of which is the forerunner of unstable fracture. High yield-strength martensitic steels have a reduced tolerance for such cracks due to their poor fracture toughness, which factor may restrict attainment of their potential.

A partial solution to the Gordian knot of concomitant strength and ductility is offered by maraging steels, whose high yield stresses are matched by excellent toughness, albeit at increased cost. These steels owe their remarkable properties to the formation of alloy martensites which are less highly stressed than martensites in more conventional steels, but whose strength is increased by precipitation. Nevertheless, such structures are susceptible to embrittlement by hydrogen and their tolerance of defects may thereby be affected. Any factors such as welding, which still further reduce this tolerance, are therefore regarded with concern.

The danger of including crack-like defects in multi-pass welds increases with material thickness, so that processes with high deposition rates such as the submerged-arc technique are used. Unfortunately, the heat inputs associated with

this process can lead to excessive grain growth and segregation, which may in turn reduce fracture toughness and resistance to environmental cracking.

Little information is available on the performance of maraging steel welds in any environment other than air, and none relating to submerged-arc welds. Consequently, the aim of the present investigation was to examine and compare the behaviour of such welds in an environment known to cause rapid failure under stress, namely hydrogen sulphide. The results have allowed estimates of threshold stresses and propagation rates to be made, which show little deterioration compared with other published data on welds tested in salt solutions.

3. LITERATURE REVIEW

3.1 GENERAL METALLURGY OF MARAGING STEELS

The term maraging evolved from the concept of age-hardening martensitic structures to effect significant improvements in mechanical strength. Concommitant achievement of high strength and adequate toughness in simple iron-carbon martensites proved impossible, however, by reason of their crack-sensitive and highly stressed body-centred tetragonal crystal structure. Fortunately, alloy modification affords a satisfactory solution to this problem.

As the carbon content is lowered, conventional martensite formation in plain-carbon steels becomes progressively more difficult. With carbon levels below 0.05%, the structure of martensite changes from internally twinned acicular material to a more ductile body-centred cubic 'lath' or 'massive' martensite, with a much reduced internal stress.

Three distinct types of product can result from austenite transformation, depending upon cooling rate and composition.[1] They are:

(1) Massive ferrite,
(2) Massive martensite, and
(3) Acicular martensite.

Massive ferrite denotes ragged b.c.c. grains formed by a rapid short-range diffusion process, with a fairly high tangled dislocation density structure and high-angle boundaries. Massive martensite is characterised by b.c.c. laths with typically jagged boundaries formed by a shear process. The

low-angle boundary structure has a higher dislocation density than massive ferrite. Acicular martensite is characterised by individual or grouped lenticular b.c.c. plates formed by shear, and is often embedded in untransformed austenite. Its substructure is internally twinned, and it has the greatest tangled dislocation density of each product.

Of the three structures, the first although ductile, is the least strong, while the last is too crack-sensitive for structural use. The constitutional problem with maraging steels is therefore, that of obtaining complete transformation of austenite to massive martensite under the wide range of cooling conditions which obtain during heat-treatment of constructional thicknesses.

Solution of the problem lay in the addition of nickel to low-carbon iron as discovered by Bieber[2] during the period 1956-60, work which resulted in the first commercial maraging steels.

3.1.1 Constitution

The physical metallurgy of maraging steels has been the subject of comprehensive reviews by Contractor,[3] Floreen[4] and by Magnee et al.[5] Only the principal aspects relevant to behaviour during welding are therefore included in this section.

At room temperature, ferrite is the equilibrium phase in low-carbon iron alloys containing less than 10% nickel, but as the cooling rate from $900^{o}C$ is increased, lath

martensite can form more easily,[6,7] the transformation temperature and product being determined by the nickel content.

For alloys containing 10-25% nickel, the equilibrium room temperature phases are ferrite and austenite, as indicated by Owen and Liu.[8] In practice, however, the high temperature austenite in alloys containing more than 10% nickel will not transform to the equilibrium phases. Instead, b.c.c. lath martensite is eventually formed on cooling. Not only is time required for this reaction, but there is also a considerable hysteresis if the transformed martensite is subsequently reheated. The extent to which hysteresis is affected by nickel content is shown in the metastable equilibrium diagram of Jones and Pumphrey[9] reproduced in Figure 1. Although simplified, in that martensite can be made to form in alloys containing less than 10% nickel, the diagram indicates that above this value, martensite will form even at very slow cooling rates, and will therefore allow through-thickness hardening in plate thickness materials. Furthermore, the transformation hysteresis allows artificial ageing to take place at 400-500°C without reversion to austenite.

With nickel contents greater than 25%, the austenite - martensite transformation temperature is less than 0°C, so that the alloys remain austenitic at room temperature. This presents a problem during welding, since solute rejection

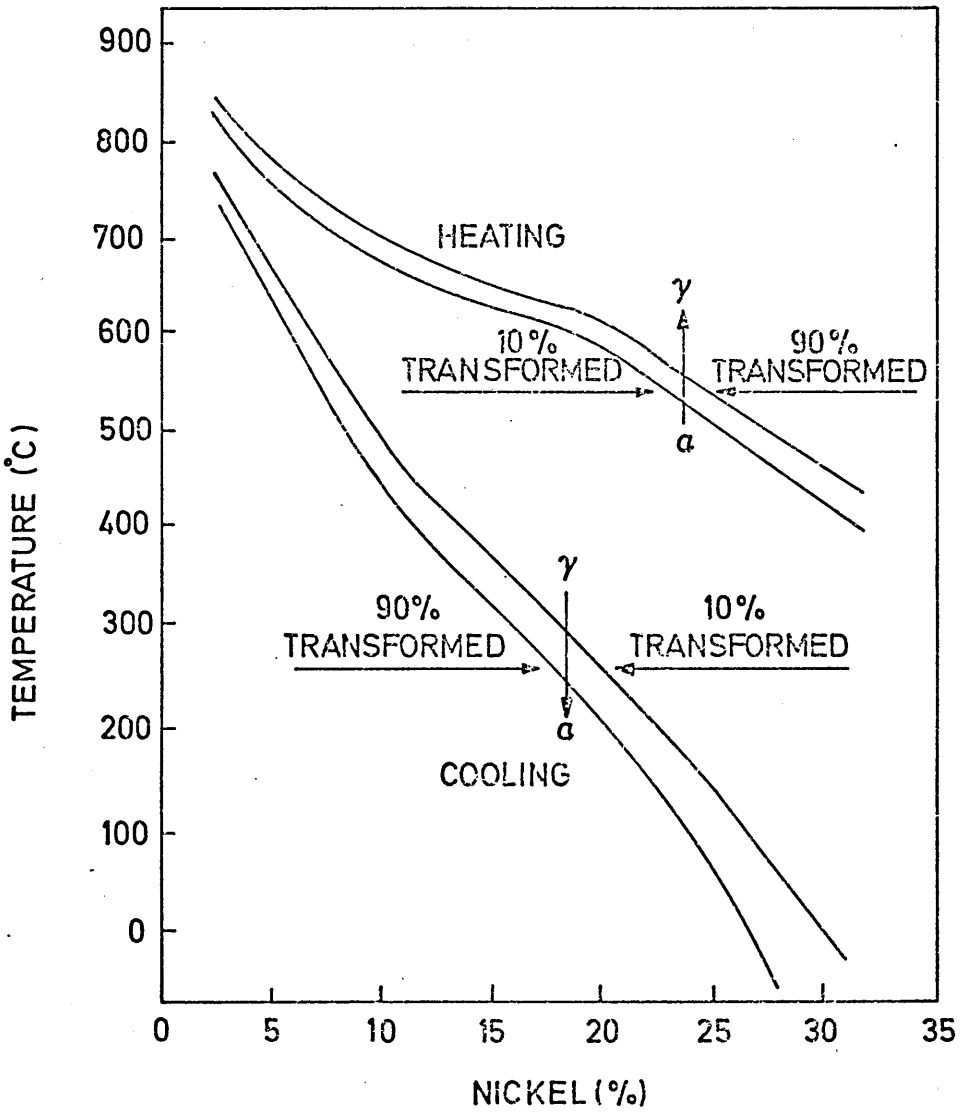

FIG. 1 Iron-nickel transformation diagram (after Jones and Pumphrey (9).

ahead of the freezing front results in nickel enriched pools of austenite which remain unchanged during subsequent heat-treatment, and have a detrimental effect on weld properties. Nevertheless, hysteresis in the 25% nickel alloys permits aus-ageing at 700°C, during which time coarse precipitation of Ni_3Ti effectively reduces the nickel content of the matrix, so that subsequent refrigeration at -80°C will produce martensite. The attendant dislocation tangles can then act as sites for a second ageing treatment at the conventional temperature of 480°C. It is the uniformly fine distribution of such tangles and lath boundaries acting as sites for subsequent precipitation that is a principal feature of maraging steels.

In addition to nickel, two principal alloying elements present in commercial maraging steels are cobalt and molybdenum. Decker et al[10] found that these elements act synergystically in producing a greater hardening response when present together than when present as individual additions. Whilst additions of molybdenum alone do allow maraging to occur, there is no response if only cobalt is present. The effects when both elements are present together may be judged from the hardness results reproduced in Figures 2 and 3, which show increased ageing of alloys containing 7% cobalt. With molybdenum alone, maximum hardness is achieved at 10% Mo, but a steeper linear increase is shown for the combined alloy with up to 5% Mo.

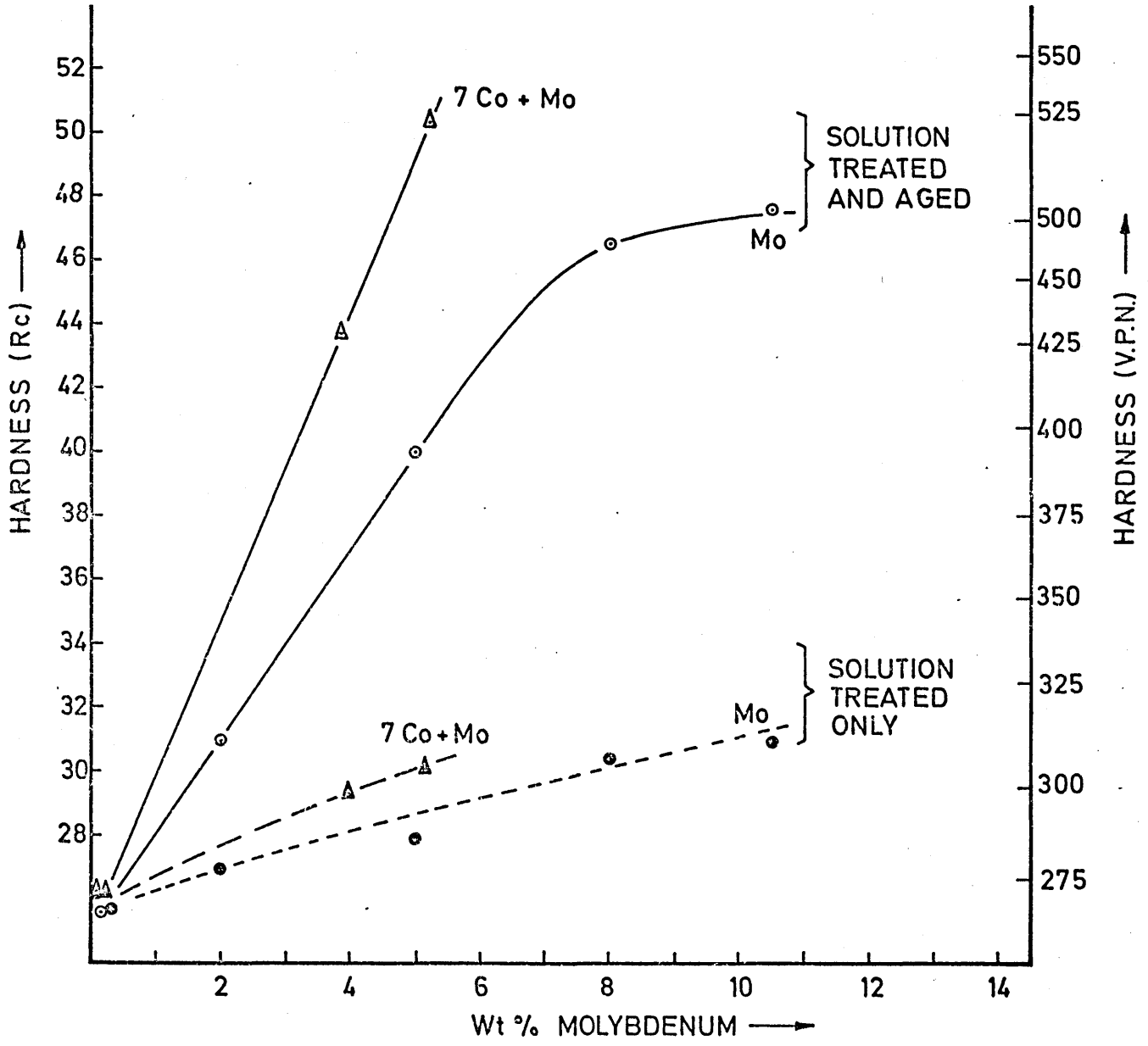

FIG. 2 EFFECT OF MOLYBDENUM AND COBALT ON MAXIMUM HARDNESS OF MARAGING STEELS (AFTER DECKER)[10]

Decker concluded that the hardness of both aged and annealed conditions was directly proportional to the product (%Mo x %Co) up to limits of 5.4%Mo and 7%Co, (Figure 3). Surprisingly, the individual solid-solution strengthening effects of each element are small compared with their influence on aged properties. No formal explanation of their intriguing interaction has yet been advanced although this feature provides the modus operandi for the remarkable properties of maraging steels.

Minor, but nevertheless significant, further alloying additions are those of titanium and aluminium, with vanadium a further possibility. These elements assist in a precipitation sequence, the precise nature of which is still debatable, in spite of the extensive studies summarised by Floreen.[4] Not only basis composition, but also ageing temperature and time influence the precipitates formed, with some initial precipitates redissolving to allow others to appear. The effect of temperature is, of course, paramount in influencing the properties of welds and their heat-affected zones.

In 18%Ni 8%Co 5%Mo steels aged at 480^{o}C for three hours rod or ribbon-form Ni_3Mo is generally agreed to be the main precipitate.[11,12,13] After longer times or at higher temperatures, this precipitate is replaced by either Fe_2Mo or by σ-Fe(Ti,V).

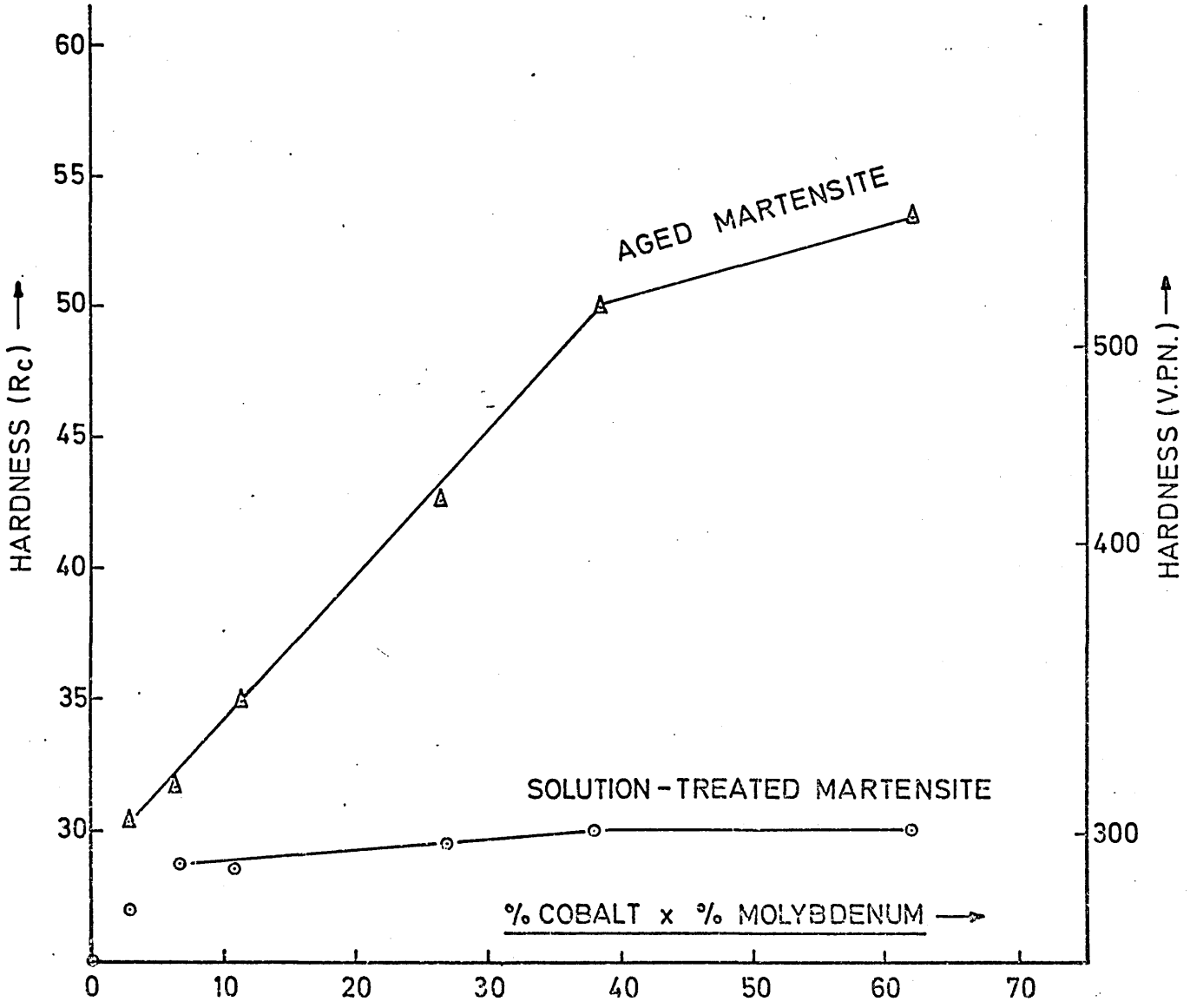

FIG. 3 EFFECT OF COBALT-MOLYBDENUM INTERACTION ON HARDNESS OF Fe-Ni ALLOYS (10)

It is difficult to be specific about the roles of these supplementary precipitation elements. Titanium itself can form as η-Ni_3Ti which, with its structural similarity to Ni_3Mo, makes simultaneous detection problematical. (A substitutional form $Ni_3(Mo,Ti)$ is also possible.) In addition, titanium acts as a refining agent in tieing up residual carbon and nitrogen as Ti(C,N), which then segregates to austenite grain boundaries and causes losses in ductility.[14] Vanadium additions also appear in the form of σ-FeV, whereas in aluminium containing steels, the precipitate appears to be cubic Fe_3Al. Aluminium, however, acts mainly as a grain refiner rather than a precipitate former.

3.1.2 Austenite Reversion and Retension

As already stated, the equilibrium phases in iron 18% nickel alloys are ferrite and austenite, so that all martensitic structures produced by air-cooling such alloys are metastable. Reheating would normally enable equilibrium to be re-established via diffusion, but the reaction is so slow even at ageing temperatures (450-500°C), that austenite is found only after very prolonged times. However, if this reaction is allowed to occur at ageing temperature, then the reverted austenite so formed contains approximately 30% nickel and thus becomes highly stable on cooling. Temperatures higher than A_3 occur in the H.A.Z. during welding, and cause austenite to form more rapidly by a shear process so that

its nickel content remains at the prior matrix level of 18%.

A third mechanism for austenite formation, of particular relevance to welding, is that of solute rejection during freezing, which leads to pools of stable austenite at triple points in weld metal. This form, termed retained austenite, can also occur in fabricated material as a legacy from the original cast structure.

Thus three mechanisms exist by which austenite can form in welded maraging steels, two of the modes leading to pools of practically untransformable material at grain boundaries, and which prove to have significant effects on weld properties.

It will be appreciated that the term reverted austenite is in reality a misnomer since austenite is the product of martensite reversion, not vice versa. There is still much interplay between the terms reverted and retained austenites in published literature in spite of the importance of their distinction.

3.2 MECHANICAL PROPERTIES

3.2.1 General Compositional Effects

Of the alloys originally examined by Bieber,[2] those based on Fe18%Ni emerged as the optimum solution to the twin engineering requirements of strength and toughness.[15] At the same time, these alloys have the least sensitivity to differences in processing such as melting procedure.

Within the 18% nickel range, four alloys are now available, denoted by their yield strength values which, in p.s.i. x 10^3, are the 200, 250, 300 and 350 grades of materials. The latter two alloys are also often referred to as 'ultra high-strength' steels.

Table 1 gives the nominal composition ranges of these four alloys, from which it is evident that differences in strength are achieved by slight changes in cobalt and molybdenum levels together with proportionally greater increases in titanium content. Substantially greater cobalt and titanium contents are required to raise the yield strength from 300 into the 350 classification, and this appears to be the maximum strength as far as development of the 18%Ni alloys is concerned. The quest for ever higher strengths continues unabated, however, and two further grades denoted 400 and 500 have recently been developed[16] based on lower nickel content, but with increased cobalt and molybdenum contents. A reduction of titanium to 0.2% in these later alloys is noteworthy, especially in view of the tendency of this element to segregate and produce retained austenite in weld metal.

There is no doubt that the excellent mechanical properties possessed by all the alloys stem from the strength of solution hardened lath martensite combined with the fine dispersion of precipitates formed on ageing. Magnee et al[5] have summarised typical room temperature properties

Grade	%Ni	%Co	%Mo	%Ti	%Al
200	17-19	8-9	3-3.5	0.15-0.25	0.05-0.15
250	17-19	7-8.5	4.6-5.2	0.3-0.5	0.05-0.15
300	18-19	8.5-9.5	4.6-5.2	0.5-0.8	0.05-0.15
350	17.5-18.5	12-12.5	3.8-4.6	1.4-1.7	0.10-0.15

(Residual elements limited to: C 0.03% max., Si,Mn 0.10% max. S,P 0.01% max. Figures in wt%)

Table 1: Nominal Composition ranges of 18% Ni maraging steels

Grade	0.2% Y.S. (MN/m^2)	U.T.S. (MN/m^2)	% ε (on 50mm)	Reduction of Area (%)	Hardness (Rc)	C.V.N. impact (J)	Fracture Toughness ($MN/m^{3/2}$)
200	1310-1550	1345-1585	6-12	35-67	44-68	35-68	110-176
250	1655-1825	1690-1860	6-10	35-60	48-50	24-45	99-165
300	1790-2070	1825-2105	5-10	30-50	51-55	16-26	88-143
350	2179-2427	2268-2468	6-8	24-43	-	9-16 (at $-40^{o}C$)	-

Table 2: Typical Room Temperature Mechanical Properties of 18% Ni Maraging Steels

of the four grades of 18%Ni maraging steels in Table 2. All the data quoted refer to materials conventionally solution treated for 1 hour at 815°C followed by 3 hours artificial ageing at 480°C.

The reduction in fracture toughness which accompanies increases in strength, especially yield strength, is immediately apparent, and is also reflected in lower impact and ductility values. Whilst this behaviour is only to be expected, the toughness of all the maraging steels compares very favourably with other carbon-low alloy steels of similar strength levels.[17]

With toughness a major consideration, it has been emphasised that control of residual elements, especially carbon, sulphur and nitrogen, is particularly important if losses due to grain boundary embrittlement are to be avoided.[18] Thus, an upper limit of 0.005% has been set for carbon in the 300 grade material, while the simultaneous presence of silicon and manganese at the 0.15% level in reported to be highly detrimental.[19] On the other hand, traces of phosphorus, antimony, arsenic, tin, lead and bismuth are without effect on toughness, although their upper limits are not known, while chromium, copper and tungsten are each harmless up to 0.5%.[20] Indeed the beneficial effect chromium has on normal corrosion resistance resistance is the basis of its use in stainless grades of maraging steel, which has excellent toughness[21] but inferior stress-corrosion resistance at equivalent strength levels.

3.2.2 Processing Effects

Substantial improvements in those properties which demand the minimum levels of segregation and impurities, e.g. short transverse-direction ductility and fatigue strength, have been achieved by the almost universal adoption of vacuum and consumable electrode remelting. The effect of melting practice depends, however, on base composition, as observed by Maynor and Bush,[22] who found an air-melted maraging steel with 1.2%Ti to be tougher than a similar vacuum remelted composition. With 0.6%Ti, the effect was not repeated. Decker[10] noted that the most significant improvements were obtained in alloys with the highest yield strengths.

It is likely that sensitivity to property changes only becomes evident at very low levels of residual elements. Spaeder [23] found a significant drop in C.V.N. impact energy with test temperature in a high purity maraging steel, whereas a steel with a normal residual level showed very little change with temperature. This effect was ascribed to the influence residuals have in causing grain boundary failure at low plastic strains.

Interdenditic segregation of major alloying elements such as nickel, molybdenum and titanium to form parallel bands which persisted from the cast state through reduction and heat-treatment, was a feature of early heats, and detrimental to toughness.[24] This was traced to solute

rejection during freezing (c.f. weld pool solidification) which resulted in bands containing reverted austenite. Homogenisation treatments and changes in rolling schedule have reduced the problem considerably.

Repeated thermal cycling between 20 and 800°C was found by Goldberg[25] to reduce maximum hardness due to austenite retention, although grain size has only a small effect on either yield strength or U.T.S.[26] Any differences in crack propogation within the H.A.Z. of maraging steel welds are therefore likely to be a consequence of strength rather than structural changes.

3.3 WELDING

From the outset, the ability of maraging steels to be welded in either the solution treated or fully aged conditions was heralded as one of their outstanding characteristics.[27,28] The recurrent problem of hard-zone or cold cracking, which bedevils medium carbon and many low-alloy steels, is obviated in maraging steels by the ductility of low-carbon martensite, formed over the full range of cooling rates encountered during welding. Moreover, their insensitivity to quenching rate ensures a full response to post-weld ageing. This suggests that the tensile efficiencies of weldments should approach the theoretical maximum.

It is scarcely suprising that a series of papers between 1962 and 1967, comprehensively reviewed by Lang and Kenyon,[29] extolled the weldability of maraging steels by almost every

process available.[27,28] Only one case of cold cracking was encountered, although low hydrogen content materials were recommended, while instances of hot-cracking were rare. As expected, the recovery of tensile properties after post-weld ageing gave efficiencies of between 80 and 100%.

3.3.1 Process Applicability

Witherall and Fragetta [30] had earlier described welding of 25mm plate using the covered electrode, TIG and submerged-arc welding methods. By 1965, excellent properties including toughness were being obtained, especially on TIG welded sheet materials.[31,32,33] Generally, argon has proved to be a satisfactory shielding gas for the TIG and MIG processes and their variants, although some arc instability was reported. The addition of 1-5% oxygen or carbon dioxide to the shielding atmosphere improved arc consistency but adversely affected weld metal toughness. For covered electrode work, special low-hydrogen flux coatings were recommended, although these are not generally available.

Electron beam welding appears to offer the greatest chance of obtaining 100% tensile efficiency, since its low heat input minimises the overall metallurgical damage and provides fast cooling rates by comparison with the MIG or TIG processes. Adams and Travis[34] and also Kohn and Schaper[35] found that electron-beam welds developed up to 94% tensile efficiency simply on post-weld ageing, whereas complete resolution treatment was required to obtain similar

strengths in weld made by other processes. Boniszewski and Kenyon[36] confirmed the higher strengths of electron beam welds, but found marked microsegregation of titanium and molybdenum in as-deposited weld metal. Subsequent ageing redistriduted the molybdenum, but left titanium unaffected - a phenomenon ascribed to stable Ti_2S and Ti(C,N) compound formation. One disturbing feature of this work however, was the tendency for micro-defects to occur especially in weld roots, with attendant reductions in ductility and toughness.

Reduced fracture toughness of MIG compared with TIG welds was also noted by Knoth and Lang,[32] although it is not clear whether the losses were a microstructural feature or due to defects.

Paley[33] after examining the response of welds to ageing, found that the toughness of TIG weld metal increased and became independent of the initial heat input if ageing was carried out at 426°C. In contrast, weld metal aged at 480°C had 50% lower impact strength and 16% lower fracture toughness for heat inputs between 0.35 and 2.0 KJ/mm. Fracture paths were found to follow the boundaries of reverted austenite in areas of high segregation, and the improvements at lower ageing temperatures accrued from a reduction in this austenite. Advantage of the effect cannot normally be taken in commercial practise however, since post-weld ageing is used to ensure optimum properties

in the component as a whole, and these occur at 480°C.

Towards the opposite extreme of heat input, submerged arc welding probably represents the practical maximum as far as maraging steels are concerned, since the more powerful electroslag welding[37] is a method feasible only for material thickness exceeding 25 mm. Duffey and Sutar[38] discussed submerged arc welding of 250 grade maraging steels with particular reference to the effect of its heat input on the development of austenite pools during ageing. Such pools form most readily at around 650°C, although general formation also occurs during ageing at 480°C, and they have a detrimental effect on weld toughness.

Wilson and Wildman[39] examined a number of specially formulated fluxes for submerged arc welding in attempts to control titanium recovery and hence improve weld properties. The optimum results were obtained from ferro-titanium additions to an agglomerated basic alumino-chalk mixture. With this flux, tensile efficiencies of 82-85% were obtained, which could only be marginally improved by complete re-heat-treatment after welding.

The low ductility and fracture toughness of submerged arc welds compared with those deposited by inert gas shielded processes, are perhaps the most serious of the problems encountered during welding of maraging steels. There is some doubt whether critical defect sizes for submerged arc weld metals are within the range of currently available non-destructive testing techniques.[29]

3.3.2 Filler Alloy Compositions

Normally, filler alloys are designed to match parent metal compositions, with minor adjustments to titanium and aluminium contents for effective deoxidisation and to counter volatalisation and porosity. It is generally accepted that filler alloy wires should be fabricated from vacuum melted stock and vacuum annealed finally, so that their gas contents are minimal..[39]

Knoth and Lang[32] found significant variations in weld properties resulting from differences in filler compositions. Weld strengths could be increased by as much as 10% by small additions of cobalt, molybdenum, titanium and aluminium, but at the expense of ductility. Adverse effects on toughness were also discussed, although no data were presented.

At the same time, Contractor[41] emphasised the importance of filler composition control if maximum toughness was to be achieved. In examining fracture modes in 250 grade maraging TIG and MIG weld metals, Kenyon[42] also obtained marked differences in retained austenite content by changes in filler composition. On substituting aluminium and cobalt for the segregating elements titanium and molybdenum, austenite formation in weld metals could be reduced to zero with consequent improvements in toughness.

3.3.3 Strength and Toughness Data

A summary of tensile properties and toughness as measured by either Charpy shelf energies or by fracture mechanisms is given for welded maraging steels in Table 3. Most of the data have been abstracted from the review by Lang and Kenyon,[29] to which results published after 1971 have been added. Parent metal filler alloys were used in each case, and only materials aged at 480°C have been included.

Although tensile properties are little affected by process overall, the drop in toughness in the case of submerged-arc welds is evident. Both weld metals and heat-affected zones suffer in this respect,[43] and toughness varies depending on the extent of retained or reverted austenite formed.

In a recent attempt to combat low toughness, Kenyon and Floreen[44] examined composite multi-run deposits made with fillers markedly different in composition from the parent plate. Surface layers only were deposited with parent metal fillers. Improved toughness, albeit with lower strength was reported, but more significantly, the stress corrosion resistance was substantially improved. Advancing cracks were arrested by the less susceptible inner layers of weld metal.

GRADE	WELDING PROCESS	THICKNESS	YIELD STRESS 0.2% (MN/m^2)	ULTIMATE TENSILE STRESS (MN/m^2)	ELONGATION (% on 25mm)	CHARPY VEENOTCH ENERGY	FRACTURE TOUGHNESS K_{1C} ($MN/m^{3/2}$)
200	Automatic TIG	Plate	1370-1460	1420-1500	10-13	47-50	99-143
	Automatic MIG	Plate	1357-1495	1412-1516	6-11	23-32	-
	Submerged-arc	Plate	1426	1488	6	-	45-62
250	Automatic TIG	Plate	1515-1674	1564-1681	10-13	15-31	68-88
	Automatic MIG	Plate	1515-1702	1585-1736	1.5-4	9-16	71-88
	Submerged-arc	Plate	1592-1729	1639-1839	1-6	5-12	39-47
300	Automatic TIG	Plate	1392	1674	8	-	65
	Automatic TIG	Sheet	1647-1929	1826-1964	-	-	-
	Automatic MIG	Plate	1598	1688	3	-	59
350	Automatic TIG	Sheet	1964	2026	1.5	-	36

Table 3: Mechanical Properties of Welded Maraging Steels by Grade (after Lang and Kenyon[29])
(All materials tested with reinforement removed, and aged after welding)

3.3.4 Microstructural Features

Microstructural changes in welds and heat-affected zones are of major importance as they control both the properties and mode of any subsequent fracture.

Since maraging structures depend mainly on the maximum temperatures reached during the weld cycle, and very little upon cooling rate, it is convenient to relate microstructures purely to peak temperatures. In multipass welds, intermediate runs will themselves be reheated to varying extents depending on their distance from the fusion isotherm, and therefore also exhibit heat-affected zone features.

Generally, four different microstructures are encountered in welded maraging steels, these being:-

(a) Weld metal,
(b) Fusion interface zones
(c) Dark etching zones, and
(d) Unaffected parent metal

The development of regions (a) - (c) is a function of the heat-input per pass and hence upon the processes used.

Weld metals per se are comprised of dendritic low-carbon martensite cells aligned in the direction of principal heat extraction during freezing. Their structure is characteristic of competitive growth during rapid solidification, having relatively short side branching with stubby secondary branching. The prior-austenite grain boundaries are defined by discontinuities in the dendrite patterns.

At cell boundaries and triple points, constitutional micro-segregation results in pools of reverted austenite forming during ageing and which remain white on etching. Under light microscopy, occasional islands of austenite may also appear trapped within the martensite cells.

On etching the aged structure, cell boundaries appear dark and diffuse with a structure unresolvable by light microscopy. Under electron microscopy however, fine reverted austenite particles are found distributed throughout these dark regions and also within the matrix.

D'Annessa[45] confirmed by electron-probe micro analysis that reverted austenite forms as a result of microsegregation, principally of titanium and molybdenum. During ageing, only molybdenum appears able to rediffuse from such regions, leaving titanium in situ. Microsegregation of these two elements also occurs as bands transverse to the welding direction and similar to those which can occur during zone melting. They are formed as a result of changes in the growth rate[46] during solidification, with the fastest freezing producing the highest solute content. D'Annessa also found that overall microsegregation decreased towards the top centre of the weld bead.[47]

The role of austenite however formed, is by no means clear, despite the association of low toughness with high austenite content and vice versa.[42] Its distribution may be a more significant factor than its quantity, since

submerged-arc welds were found to contain only 9% of austenite compared with up to 38% in the dark etching bands of multi-run TIG welds.[48]

Both sulphur and nitrogen are generally present in maraging steels, albeit in small quantities. Together with carbon, these elements form the compounds Ti(C,N) and Ti_2S during fusion. Such particles can be detected both by light microscopy of welds and by scanning electron microscopy of the fracture surface. The particles are often associated with reverted austenite. It has been suggested therefore that differences in toughness between submerged arc and TIG weld metals may also be due to sulphide and carbonitride particles which could initiate cracks.[48]

Coleman and Jordan[43] have related heat-affected zone structures to peak temperature, using resistance heating to simulate the thermal cycles involved at various distances from the fusion interface. The structures developed are summarised as in Table 4.

Although Coleman and Jordan found no evidence of hot cracking, at least two other investigations[49,50] found that liquation of Ti_2S lead to sub-surface micro-cracking, particularly in multipass submerged-arc welds.

Pepe and Savage[49] found that liquated Ti_2S also affected grain boundary migration at the fusion boundary, which anomalously reduced the grain size in this region. Ghost grain boundaries were also formed.

Peak Temperature (^{o}C)	Microstructure
600	Unchanged, aged massive martensite
650	Aged massive martensite + fine reverted austenite particles, giving overall mottled effect on macroscopic scale. ("Dark etching band")
800	Aged martensite, similar to parent metal
1000	Acicularity develops in cellular martensite
1200	Acicular martensite formed with domains of various orientation within prior austenite boundaries. Reverted austenite develops in ribbon-like form
1325	As at 1200^{o}, but larger grain size. Further ribbon austenite associated with liquated Ti_2S
1400	Strongly acicular martensite. Grain size 36-66μ . Slightly less ribbon austenite, but some liquation of Ti(C,N)

Table 4: Heat Affected Zone Structures Developed Near Maraging Steel Welds[43]

As far as mechanical properties are concerned, fracture toughness was found to be significantly higher in the regions corresponding to 650^{o} and 1200-1400^{o}C peak temperatures,[43] compared with the original parent values. Toughness and mechanical properties were, as expected, inversely related.

One further effect which could reduce both weld and heat-affected zone hardness is the degradation observed by Goldberg.[51] On repeated thermal cycling, as in multipass or repair welding, hardness could drop significantly, although no mechanism was proposed. The observation, however, could account for the increases in toughness found by Coleman and Jordan.

3.4 ENVIRONMENTAL CRACKING

Catastrophic failure of alloys under stresses lower than the yield value and due to environmental interaction, is a phenomenon which has been extensively examined in recent years. The driving force for such investigations has been the increasing use of expensive, ultra high-strength materials operating at stresses close to their maxima and the subsequent need for component integrity. In consequence, the reduced defect tolerance has led to an increasing incidence of, and concern about, environmental failures.

Characteristically, environmental failures result from the slow development of small, crack-like defects, which

may or may not have originated during service. When such defects reach a critical size, dependent only upon material toughness and prevailing stress-intensity, then rapid unstable fracture inevitably follows.

Under given conditions of stress and environment, the useful life of engineering components is therefore governed by the growth rate of sub-critical defects, and by the time involved in their development. Crack growth-rate emerges as a function which is highly dependent upon the environment, the specificity of which is a principal characteristic.

Unfortunately, many laboratory test data have been obtained on nominally crack-free material, and yet crack initiation perhaps by ordinary corrosion processes can occupy up to 90% of the component endurance before appreciable growth even commences. As a design criterion therefore, endurance based on crack-free samples has little to offer. Even if growth-rate data were more generally available, estimates of probable component life could only then be realistic given the quality control methods able to detect sub-critical size cracks.

The overriding problem with high strength steels is that in taking advantage of their mechanical properties, one has to accept a smaller critical defect size than in more ductile steels, and this leads to detection difficulties. Fortunately, maraging steels will tolerate larger defects than most other steels at similar stress-levels, a factor

which may offset to some extent, their greater cost.

In view of the importance of crack growth in limiting the life of components, it is suprising that test data are so sparse. This is especially true as far as welded joints are concerned, with their in-built additional cracking propensity due to the structural and geometrical factors.

3.4.1 Terminology

Stress-corrosion cracking is now recognised as displaying a wide range of interactions between stress and corrosion, in which each has varying predominance.[52] At one extreme, stress is the principal controlling factor and results in almost completely brittle failure. In these cases, the role of corrosion may be to provide cathodic (or anodic) hydrogen which embrittles the material ahead of the crack front, as with martensitic stainless steel,[53] or with precracked titanium in methanol.[54] At the other end of the spectrum, stress is only marginally effective in increasing corrosion, which proceeds along anodic paths, usually intergranular, as in aluminium-copper alloys exposed to sea water. Difficulties arise with materials in which cracking may occur under both modes, possibly at the same time. Since hydrogen embrittlement could imply failure in the complete absence of corrosion, the term 'environmental cracking' is often preferred to describe the behaviour of systems in which the mechanism of cracking is not clear.

3.4.2 Test Methods and Data Comparison

Multiplicity of methods and test conditions leads to increasing difficulty in examining the influence process variables have on endurance, and especially in relating results from different sources.

Severe criticisms can be levelled at most of the test methods used in the past, chiefly on the grounds of poorly defined stress conditions, which are markedly influenced by test-piece geometry. In self-stressing methods such as the U-bend, stress relaxes as cracking proceeds, so that initiation time is the only reliable parameter this test provides. Crack initiation may occur under plane-strain or plane-stress conditions depending upon the specimen thickness, and the times quoted depend heavily upon human reliability. Comparisons based solely upon 'not failed' observations are almost meaningless.

Constant load tests give increasing rather than constant stress conditions, which may be more realistic, although the results are still subject to the influence of thickness. Nevertheless, in high-strength steels at least, cracks once started usually progress at increasing rates, so that failure times offer a more reproducible criterion of material performance.

Further difficulties arise in assessing material performances when tests have been carried out both on smooth and on notched or precracked specimens. Considerable

discrepancies have been shown to exist between results of such tests, especially in strongly passive materials such as titanium, previously thought to be immune from environmental cracking.[55]

The major problem in comparing experimental data generally stems from the fact that no clear parameter other than endurance at nominal stress levels has emerged, and which adequately describes specimen performance. Endurance itself is a highly variable statistic, the distribution of which was shown to be log-normal, at least for aluminium-magnesium alloys.[56] The logarithmic values of endurances may therefore be used with advantage when comparing different material conditions under the same test.

With smooth specimens, endurance is also notably stress-dependent, yet materials are often compared purely on the basis of tests at a fixed proportion of their yield stresses, e.g. 0.75 σ_y, rather than on a series of tests over a range of stresses. When the latter method is adopted, evidence of threshold limits below which cracks do not propagate are often observed. Threshold-stress values are of most use when the stress conditions within a component are known, but this is rare in practice. In spite of these criticisms, however, smooth specimen tests do have economic advantages, and they generally rank materials in the accepted order of their resistance to environmental cracking.[57]

During the past decade, increasing use has been made of tests involving specimens precracked in fatigue and in which the stress conditions at the crack-tip can be predicted by fracture mechanics, at least at the commencement of exposure. Such specimens are used in the Brown test[58] to determine both the limiting intensity below which slow growth does not commence, (K_{1SCC}), and also the variation in cracking rate with stress-intensity. Figure 4 shows the schematic relationship between endurance and initial stress-intensity.

Regardless of their complexity compared with simple tension or bend tests, much present day stress-corrosion research employs fracture mechanics tests to determine behavioural differences ,especially between strong materials. Of their principal advantages, one is that the results are characteristic of the material and the environment only, since the stress conditions are known and determined by test-piece geometry. A second is that uncertainties regarding the growth of corrosion pits prior to cracking are eliminated. In addition, the resulting test data, perhaps in the form of defect tolerance limits, could potentially form part of inspection and maintenance standards for components having fracture toughness as a design criterion.

The use of precracked specimens can be criticised on the grounds of the excessive specimen sizes required for

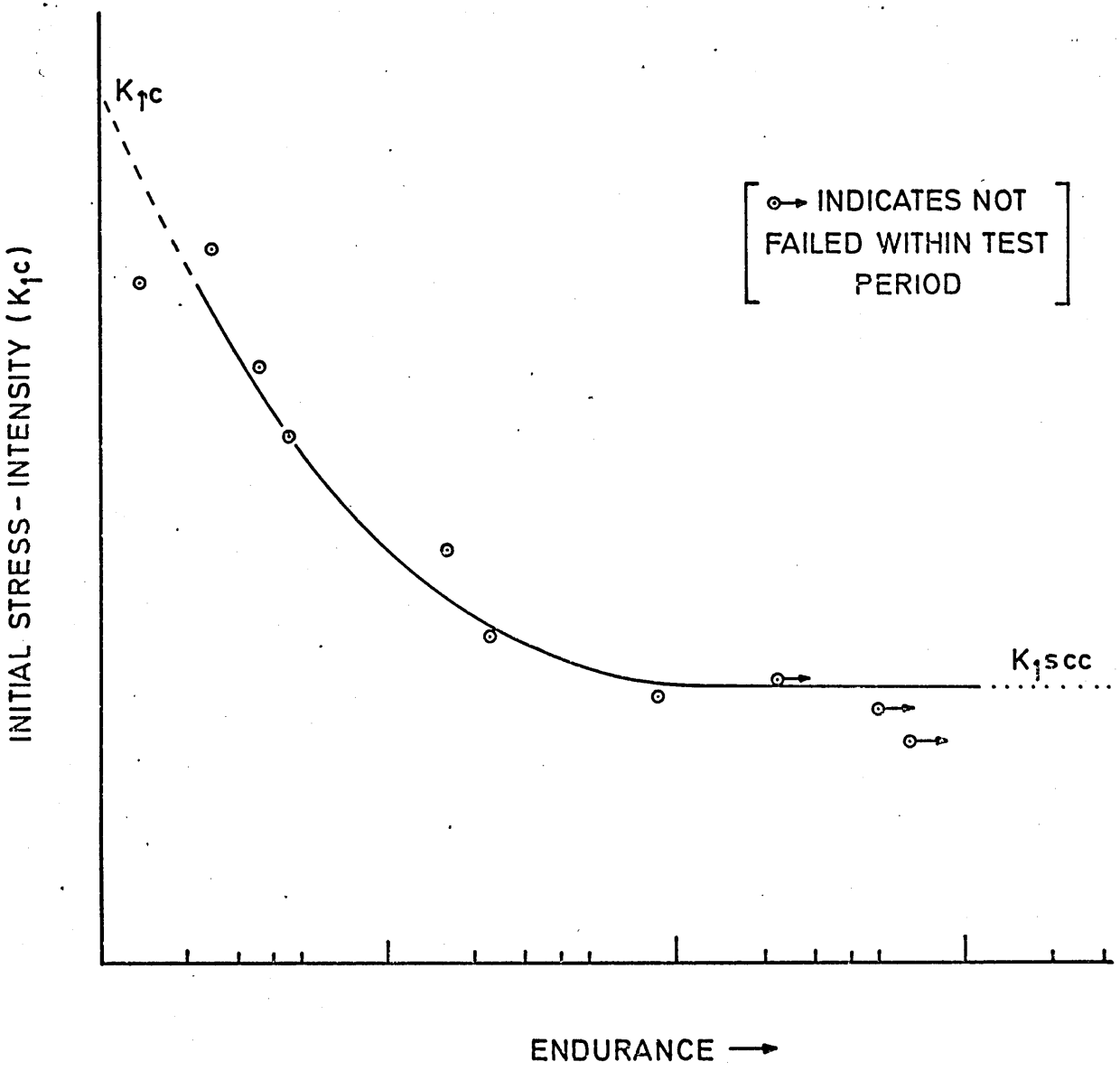

FIG. 4 SCHEMATIC DEPENDENCE OF ENDURANCE ON INITIAL STRESS-INTENSITY

such ductile materials as mild steel, so that machining costs become excessive, and test-rigs become bulky. Furthermore, although single cracks are initiated by fatigue, subsequent environmental growth is frequently branched, so that the stress conditions, once the test is underway, are problematical. Lastly, tests based on fracture mechanics provide a macroscale assessment of environmental performance which is much affected by microstructure, despite its claimed independence in fracture toughness determinations.

When welding is introduced as a further complication, the difficulties are multiplied by specimen location, residual stress and by microstructural heterogeneity, so that the validity of results becomes questionable. Nevertheless, Gooch et al[59] have described the application of a combined fracture mechanics and potentiometric technique to the problem of cracking in welded structures, and concluded that it is suitable for susceptibility determination in ferritic steels and aluminium alloys. In recent work, Gooch[60] has studied the behaviour of several welded high-strength steels including a maraging variety, by using specimens welded in such a manner as to give a planar H.A.Z. Cracks were therefore propagated through more or less uniform microstructures. By combining these results with three-point bend tests on fillet welds, it was possible to categorise material behaviour in terms of a defect tolerance parameter (D.T.P.).

Because of the imponderable effects of residual stress, changing microstructure and in some cases specimen thicknesses insufficient to maintain plane-strain conditions, results for welds are frequently reported as K_Q or K_{QSCC}, indicating their unknown validity.

3.5 FRACTURE MECHANICS AND ITS APPLICATION TO ENVIRONMENTAL CRACKING

The well-known Griffith approach to fracture in brittle materials was based on the work involved in creating new surfaces during fracture. Cracks spread if the additional surface energy required was just less than the associated decrease in elastic strain energy in the region of the crack. Metals and alloys however show appreciable plastic deformation even when fracturing in an apparently brittle manner, and this led Irwin[61] and Orowan[62] independently to suggest a modification to Griffith's original equation by including a term P to account for the work done in plastic deformation. Thus

$$\sigma_F = \frac{2E(\gamma + P)}{a} \qquad (1)$$

in which the fracture stress σ_F is a function of Youngs Modulus E, internal crack length 2a, surface energy γ and work during plastic deformation P. In practice, the latter term greatly exceeds the surface energy term and accounts for the varied fracture toughness of different alloys.

Considering the work done during crack extension, Irwin[63] subsequently defined the concentration of stress at the crack tip by a stress-intensity term K. For an elliptical crack, length 2a in an infinite solid, the value of K was given by:

$$K = \sigma_{app}\sqrt{\pi a}$$ where σ_{app} is the applied stress.

The failure criterion could now be found by equating work done during extension of the crack tip stress-field to that involved in creating new crack surfaces.

Two approaches may be considered, namely those of energy release during cracking, and of the stress-intensities responsible for crack extension. In plane strain conditions, the two are related by:

$$G_{1c} = \frac{K_{1c}^2(1 - \nu^2)}{E} \qquad (2)$$

where G_{1c} is the rate of strain-energy release per unit extension of the crack, K is the stress-intensity at its root and ν is Poisson's ratio. The subscript 1c refers to the critical stage in plane-strain conditions when crack extension becomes unstable. Both G and K can be referred to as fracture toughness, but the stress-intensity approach is most commonly used, since the K_{1c} values can be conveniently and directly related to applied stress and crack length for a given specimen geometry.

Since metals are not purely elastic solids, the values of K_{1c} calculated on this basis are in error if the plastic

zone size at the crack tip exceeds an agreed figure. Deformation effectively blunts the crack tip and increases the work necessary for crack propagation.

The value of fracture mechanics lies in the stipulation of specimen thicknesses which ensure that the plastic zone size is restricted, so that fracture toughness becomes independent of thickness. K_{1c} is then a characteristic of material and environment only.

Practically, fracture toughness is measured by observing the fracture stress of a standard test-piece containing a sharp crack of known length. Before the size of cracks which may cause catastrophic failure may be calculated, however, knowledge of the operative stress systems is required. Essentially, the stress systems at crack tips may be calculated by linear stress analysis[64] or measured experimentally by compliance methods.[65]

Consider a single edge-notched specimen as shown in Figure 5. The experiment consists of repeated measurements of specimen compliance for a series of crack depths ranging from 0.1W to 0.7W, where W is the specimen width. The compliance C is given by:

$$C = \frac{d}{P} \qquad (3)$$

where d is the specimen displacement at the mid-length under the load P. In the subsequent load-displacement graphs for each crack length, the gradient will be $\frac{d}{C}$, which is a decreasing function of a. From the changes in compliance

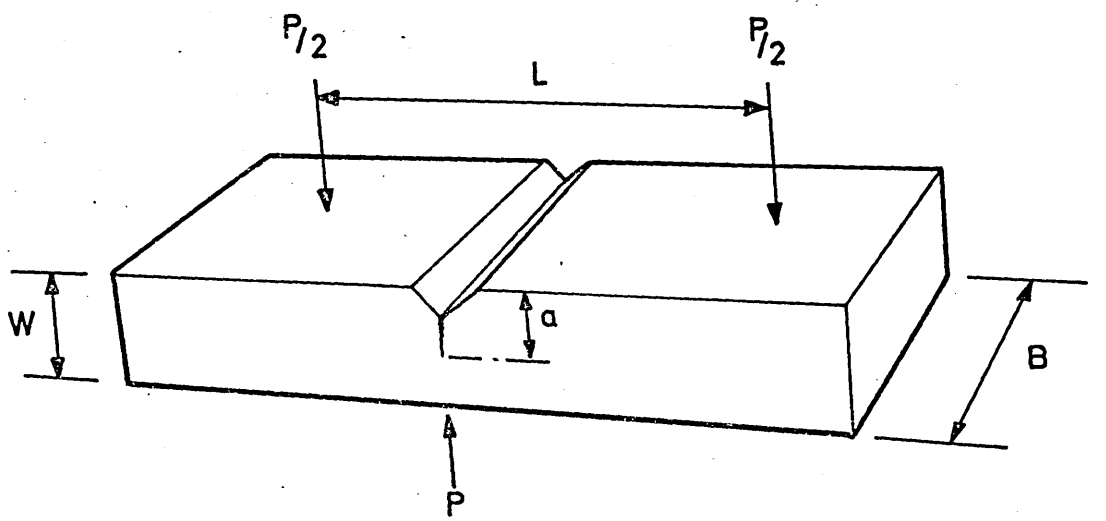

1. Crack lengh $(\frac{a}{W}) \neq 0{\cdot}6$
2. Width $B = W \rightarrow \frac{W}{8}$
3. Lengh $L = 4W$
4. Overall lengh $> 5W$

FIG. 5 Critical dimensions of single edge notched 3 point bend specimen.

with a, the energy loss per unit of plate thickness B is given by:

$$G = \frac{P^2}{2B}\left(\frac{dc}{da}\right) \qquad (4)$$

from which the expression involving stress-intensity K appears as:

$$K^2 = \frac{P^2 Y}{2WB^2} \qquad (5)$$

In this expression, Y is the modified compliance function similar to those available in tables[66] for particular specimen geometries and crack lengths $(\frac{a}{W})$, although these were derived by the more accurate technique of boundary collocation analysis.[67,68,]

For a single edge-notched bend specimen, of the type used in the present work:

$$Y = 1.93\left(\frac{a}{W}\right)^{\frac{1}{2}} - 3.07\left(\frac{a}{W}\right)^{3/2} + 14.53\left(\frac{a}{W}\right)^{5/2} - 25.11\left(\frac{a}{W}\right)^{7/2} + 25.8\left(\frac{a}{W}\right)^{9/2} \qquad (6)$$

is valid for values of $(\frac{a}{W})$ up to 0.7. Techniques are becoming available[69] for extending the range of this calibration to $(\frac{a}{W})$ values of up to 0.96, which is useful in calculating cracking velocities near the end of specimen life. Thus, given standard specimens each containing a sharp crack generated by pre-fatiguing, the cracks may be extended by slowly increasing the load up to the point at which unstable fracture occurs. Generally, growth is monitored by observing the voltage change across a clip-gauge, which varies with the crack-opening

displacement at the specimen surface, and hence with the crack length.

Depending on the type of load-displacement curve obtained,[70] the load P_Q at which instability occurs is substituted into a form of equation (5). Thus for single edge-notched bend tests (S.E.N.):

$$K_Q = \frac{6P_Q Y}{BW^{\frac{1}{2}}} \qquad (7)$$

which provides the provisional value K_Q. After examination of the crack-front profile, and measurements of probable size of the plastic zone at the crack-tip, based on:

$$(a,W) \geqslant 2.5\left(\frac{K_Q}{\sigma_y}\right)^2 \qquad (8)$$

the value of K_Q can be assumed a valid measurement of K_{1C} or otherwise, in which case specimen geometry may require modification before further testing.

3.5.1 Environmental Testing with Pre-cracked Specimens

Pre-cracked specimens may have a wide range of different geometries depending on the nature of the test carried out and on the availability of material. Essentially, tests can be classified according to whether the stress-intensity is made to increase, decrease, or to remain constant as the cracks extend. Most laboratory tests employ conditions of increasing intensity.

It is important that any index of cracking behaviour such as K_{1SCC}, should be independent of specimen type or dimensions under the conditions of testing. For fracture

toughness testing, which is carried out in air, the validity criterion of eq. (8) is usually sufficient to ensure that the crack-front plastic zone is small compared with other specimen dimensions. In the case of aggressive environments, however, it is possible that this criterion may be over-stringent in view of the increasingly brittle behaviour associated with stress-corrosion cracking. The acceptable, possibly reduced, criteria remain to be established.

A number of investigations[71,72,73] support the use of stress-intensity factors rather than net-section stresses to describe cracking behaviour, and confirm that similar results are obtained for different specimen geometries and thicknesses. Thus, Novak and Rolfe[74] showed K_{1C} and K_{1SCC} to be independent of specimen size for a 250 grade 18%Ni maraging steel. It would appear overall, that although $(\frac{a}{W})$ values may well approach unity during environmental testing, the results are none the less valid.

It is usually considered that due to lack of constraint at the crack-tip, plane-stress regions are more resistant to environmental cracking than are plane-strain regions. However, extension of cracks preferentially along the side surfaces of specimens has been observed by Carter,[75] while mid-section cracking lagged. It will later be shown that similar behaviour occurred in the present work. Nevertheless, particular care is usually taken to reduce

side shear to a minimum, so that some test-pieces are grooved on all four sides.

3.5.2 Threshold Stress-Intensities

The usual objective of pre-cracked specimen tests is to establish the stress-intensity below which crack propagation is negligeable within practical time limits. The endurances of specimens exposed at different initial intensities K_{1i} are then graphed as illustrated in Figure 4.

Threshold stress-intensities are then defined as the assymptotic stress-intensity to which the results tend. Because the assymptote is often not clear, some opinions would support the view that the actual threshold obtained depends more on the patience of the investigator than on the material concerned. Thus, different maximum exposure times are recommended for various alloy-environmental combinations. For low-alloy steels, 100 hours is normal, whereas with maraging steels 1000 hours is common, especially in mild environments.

3.5.3 Crack Growth Rates

Carter[76] has suggested that the shape of the K_{1i} versus endurance curve can provide qualitative information concerning the relationship between stress-intensity and crack growth rate. Thus, of the two curves illustrated in Figure 6, one suggests a strong dependence of growth rate on stress-intensities, while the other shows little dependence.

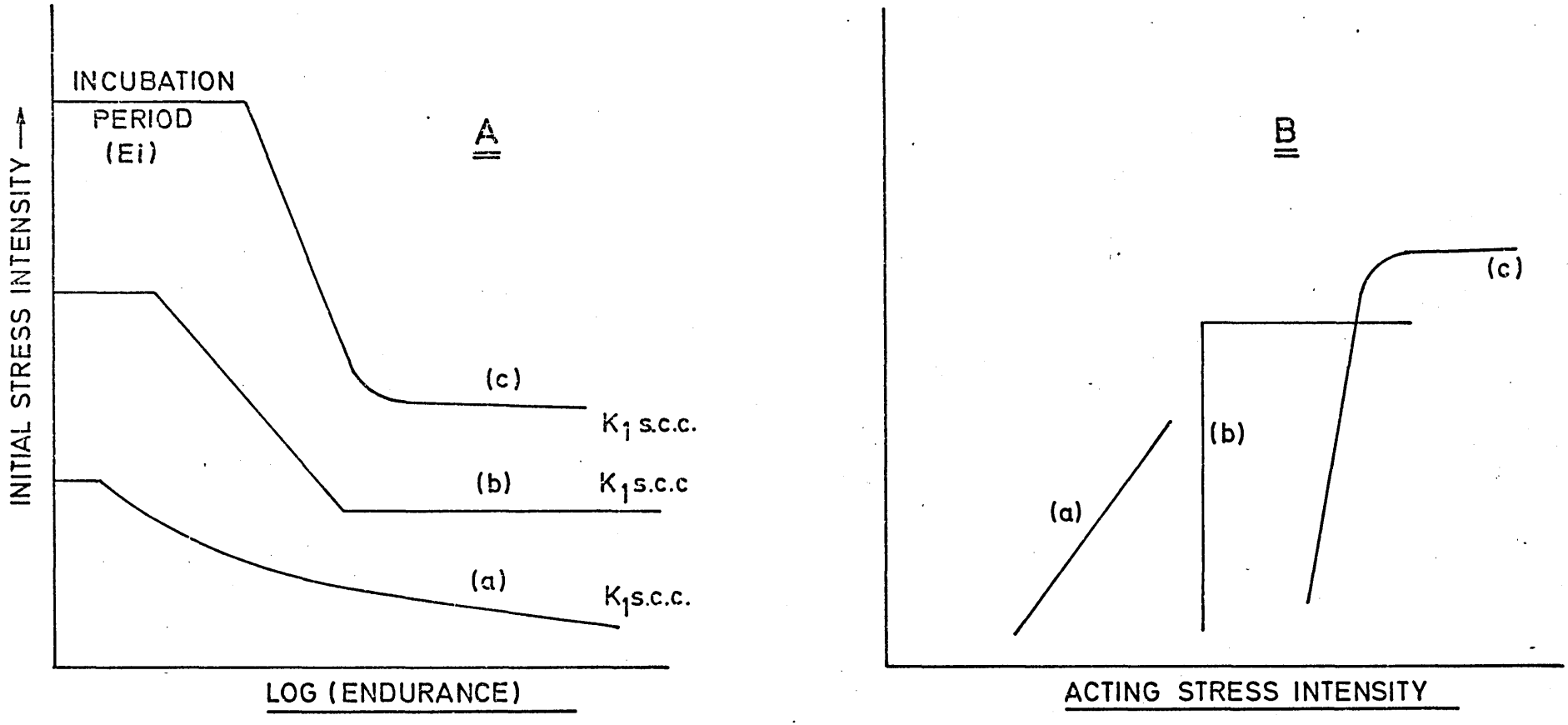

FIG.6 SCHEMATIC ENDURANCE CURVES (A) AND THEIR DERIVED FORM OF CRACK VELOCITY DEPENDENCE (B)

When cracking rates are plotted as logarithmic functions of K_{1i}, is is often found[76,77] that growth is independent of K_i over a wide range, but strongly dependent outside it. Such behaviour is illustrated in Figure 6. Accordingly, three stages of crack growth have been suggested. In the first stage, growth rate is strongly dependent on intensity, although growth may eventually cease in reducing stress type tests, indicating K_{1SCC}. Stage II, where growth is constant, occurs at some intermediate stress-intensity where the velocity is limited by rate-controlling mechanisms in the cracking process. In Stage III, growth again becomes strongly stress-intensity dependent, eventually leading to the K_{1C} value.

In some high-strength steels, however, crack velocity appeared to be linearly related to the applied stress-intesity as found by Carter[75] in 350 grade maraging steel. Although in titanium and aluminium alloys the activation energies for Stage I appear similar, the rate-controlling step is controversial. Scully[78] has noted that electro-chemical potential, environment, alloy composition and heat treatment all influence the velocity during Stage I cracking. Interestingly, it appears that if no corrosion occurs beforehand, such as with titanium in sea water, then Stage I is absent.[79]

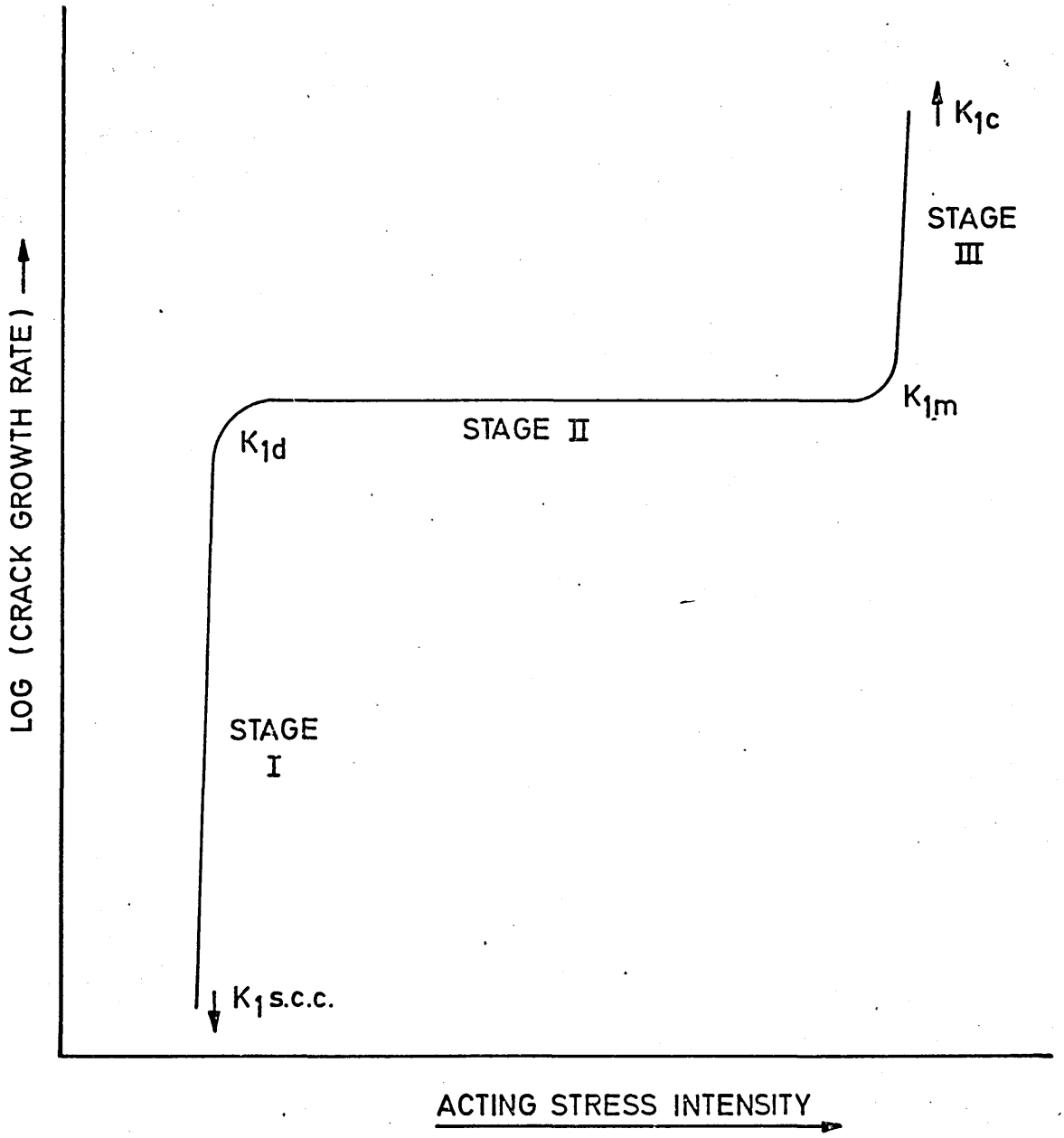

FIG. 7 GENERAL FORM OF CRACK VELOCITY DEPENDENCE ON STRESS INTENSITY (SCHEMATIC)

Among several models which have been suggested to explain the relationship between cracking rates and stress-intensity, that of Liu[80] appears to be most relevant to the present case of high-strength steels. The basis of this model is that of stress-enhanced diffusion of damaging species to the crack tip region, for which an exponential relationship can be derived.[81] Other models include those of stress-dependent dissolution which could sharpen a previously blunt crack,[82] and of increased density of dissolution sites at the crack tip making crack progression strain-dependent.[83]

Although Stage II cracking occurs at rates independent of stress-intensity for any particular material, plateau values differ considerably between different materials.[84] Scully[78] suggests that under such conditions, the rate controlling step is that of diffusion within the highly localised environment at the crack tip. Such environments can differ markedly from the main environment in which the tests are carried out.[85]

The constant velocity of Stage II is deemed a necessary criterion for crack branching to occur[76,86] and a critical stress-intensity is also required.[87]

There has been little discussion of Stage III cracking which is observed mainly in highly susceptible alloys,[78] and therefore of less practical importance.

3.6 ENVIRONMENTAL CRACKING OF MARAGING STEELS

As judged by threshold-stress values, there is no doubt that maraging steels afford a measure of safety greater than other comparable high-strength steels. The differences in behaviour stem from their higher initial fracture toughness and from their slower crack propagation rates once environmental cracks have initiated. Attempts to improve on yield stress values of approximately 2000 MN/m^2 by alloy development however, seem to be possible only if threshold stress-intensities below 10 $MN/m^{3/2}$ are permitted, so that it is likely that a limiting yield stress for the 18%Ni steels has been reached.

Overall, threshold-stresses appear to be mainly related to yield-stress, and to vary very little either in aqueous or gaseous environments, which suggests some common mechanism for cracking. The characteristic feature of stress-corrosion, namely the specificity of ion action, shows itself in the sensitivity of cracking rates to ions which affect hydrogen ingress. Thus, greatly differing endurances are found between specimens exposed to hydrogen sulphide and those exposed to sodium chloride solutions, although the eventual thresholds are similar. Most of the tests carried out on maraging steels have used salt-based solutions, although these are by no means the most aggressive of environments.

Within particular environments, behavioural differences due to composition, processing, and heat-treatment have been generally examined and assessed, although the sensitivity of the test methods used is often doubtful. The value of some early data is therefore purely qualitative. The results of Hayden and Floreen[88] highlight the optimistic assessments obtained from tests on smooth specimens, which provided threshold stresses varying from 1870 to 270 MN/m^2, depending upon the mode of stressing. The lowest values were obtained from pre-cracked samples.

A recent exhaustive review by Dautovich and Floreen[89] has provided a detailed summary of cracking studies prior to 1973, and includes many industrial laboratory data, access to which is restricted in the United Kingdom. Only few references are made, however, to welded test-pieces, and none to tests in hydrogen sulphide, although the gas itself was examined as a potentially harmful medium.

3.6.1 Threshold Stress-intensities in Sodium Chloride Solutions

Distinctions between the performances of maraging and other high-strength steels can conveniently be made on the basis of threshold stress and its variation with yield-stress. Several authors[89,90,91] have reviewed the inverse relationships which exists between these factors derived from tests in sodium chloride solutions. Results for maraging steels only are reproduced in Figure 8, which

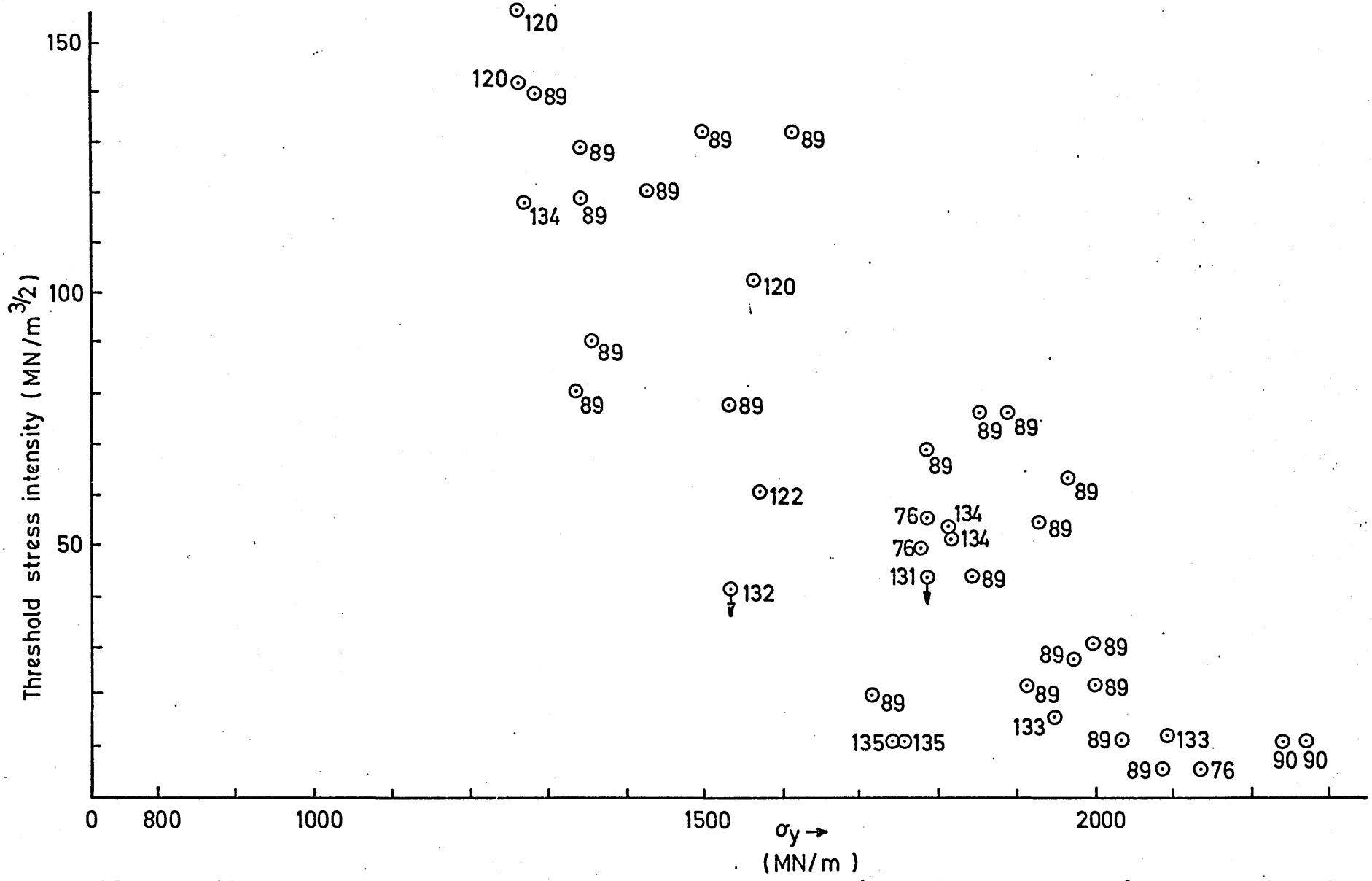

FIG. 8 Yield - stress dependence of threshold stress - intensity for maraging steels in salt solutions. (Subscripts denote references)

illustrates the wide scatter band obtained even when the test method and environment are closely specified.

As expected, scatter increases with yield-stress, but the absence of any obvious levelling out of threshold above 2000 MN/m^2 yield-stress points to a probable limit in the development of this particular composition type.

Within the range of yield-stresses normally experienced in 250 grade material, the K_{1SCC} values vary between 70 and 10 $MN/m^{3/2}$ with a mean of $\sim 45\ MN/m^{3/2}$.

Despite this scatter, other varieties of high-strength steels have proved significantly inferior to maraging steels in salt solutions,[90] and it is likely that their invidious comparison obtains in other environments.

3.6.2 Smooth Specimen Data in Salt Solutions

Dean and Copson[92] were among the first to examine behaviour in sea water of various grades and types of maraging steels, mainly by U-bend tests. Although the method of loading took no account of yield-stress variations, the superior behaviour of 18% nickel alloys compared with other grades was obvious, as shown in Table 5.

Of several disturbing features in these tests however, one is the disparity found by Dean and Copson between endurances of commercial 18% nickel alloys of the same nominal composition as those in Table 5, and tested similarly. This effect was ascribed to processing differences, and is characteristic of the stage of development reached by 1964.

%Ni	Mean Yield Stress (MN/m^2)	Test Type	Environment	Mean Endurance (days)
18	1280-1420	U	Nat. Seawater	> 677
18	1700	U	Nat. Seawater	> 677
18	1615-1870	U	Art. Seawater	42
18	1690	3pt. bend	Art. Seawater	> 185
20	1720	U	Nat. Seawater	3
25	1610-1710	3pt. bend	Art. Seawater	> 60
25	1720	U	Nat. Seawater	0.1

Table 5: Effect of Alloy Type on Endurance in Seawater of Maraging Steels (after Dean and Copson[92])

Leckie and Loginow[93] also carried out U-bend tests in seawater but found neither 12%Ni or 18%Ni steels to fail during 750 days exposure. With pre-cracked tests, however, a threshold stress of 0.25 σ_y was obtained for 18%Ni (250 grade) in natural seawater compared with 0.4 σ_y in artificial seawater.

The insensitivity of U-bend tests was also demonstrated by Kirk et al[94] in tests on 18%Ni maraging steels and on 4340 low-alloy steel. Samples of 200 grade 18%Ni steel remained uncracked after 1100 days exposure, and 250 grade steel was similarly uncracked after 540 days. By comparison, 4340 steel failed under the same conditions after only 6 days. Inexplicably, some 18%Ni steels tested as U-bends

in the marine atmosphere at Kure Beach had begun to fail after 82-402 days, depending on the yield stress.

3.6.3 Tests in Other Environments (excluding sulphides)

Some three years after the introduction of maraging steels, Setterlund[95] reported the results of bend tests in a variety of environments including atmospheric, distilled water at several different temperatures, and some organic fluids as well as seawater. Cracking occurred in comparatively innocuous environments such as distilled water or trichloroethylene. General factors which lowered the endurance measured at 0.75 σ_y included high strength levels, welding and increased environment temperatures. An interesting conclusion was that aerated water was the least aggressive media.

Tests in distilled water also reported by Yamatoto and Fujita[96] and by Reuter and Hartblower,[97] although neither set of results was presented in a form directly comparable with that of Setterlund.

With pre-cracked specimens, Stavros and Paxton[98] found no difference in threshold-stress for 300 grade 18%Ni steel in either distilled water or salt solutions.

3.6.4 Influence of Minor Compositional Variations

There is general agreement that of various nickel content maraging steels, the 18% nickel variety provides the optimum stress-corrosion resistance overall. Within this class, residual elements should be kept as low as possible,

probably from fracture toughness considerations.

Nevertheless, investigations of the effects of minor compositional variations have been very few. Proctor and Paxton[99] found slight beneficial effects when the carbon and phosphorus levels were increased from 0.005 to 0.062 wt% and 0.002 to 0.030 wt% respectively, whereas small additions of chromium were detrimental. The overall threshold stress-intensities were all of the order of 10 $MN/m^{3/2}$ however, so that scope for substantial effects was restricted.

Larger variations in residual elements do affect stress corrosion resistance. Dautovich[100] showed that low carbon and especially low sulphur contents improved the performance of 18%Ni steels in salt solutions, behaviour which could be expressed as:

$$K_{1SCC} = 363 - \frac{2.48 \times 10^5}{\sigma_y} + \frac{4.01 \times 10^7}{(\sigma_y)^2} + \frac{80.9}{C} + \frac{542}{S}$$

where K_{1SCC} is given in Ksi $\sqrt{in}$, σ_y in Ksi, with C and S in p.p.m. On this basis, Proctor and Paxton with sulphur levels of ~30 p.p.m. would have found its effect insignificant. The relationship quoted is very sensitive to composition and predicts K_{1SCC} values of ~30 Ksi $\sqrt{in}$ (~33 $MN/m^{3/2}$) for alloys similar to Proctor and Paxton's.

Both sulphur and carbon form compounds which precipitate at prior-austenite grain boundaries, so that their effect on intergranular cracking is not suprising. It is

doubtful however, whether control of residual elements to less than 30 p.p.m. is worthwhile purely from a stress-corrosion viewpoint.

3.6.5 Heat-Treatment Effects

Conventionally, solution-treatment of 18%Ni maraging steels is carried out at 815°C for 1 hour, followed by ageing for 3 hours at 480°C. Variations in these heat treatment conditions or procedures normally have a marked effect on susceptibility to cracking, especially in age-hardenable alloys. Solution-treatment temperatures are of direct relevance to grain size development which, in turn should govern the extent of subsequent grain-boundary precipitation.

However, grain size per se has proved an enigmatic factor as far as maraging steels are concerned, especially when judged on K_{1SCC} values. It would appear overall, that in higher strength materials, the thresholds are too low for grain size effects to be significant, but that for lower strength steels, large grain sizes resulting from excessively high solution-treatment temperatures are detrimental.

Thus Stavros and Paxton[98] found no difference between the K_{1SCC} of 300 grade material given either a single 815°C or a duplex 1275° + 930°C solution-treatment before ageing, although they produced a wide range of grain sizes and toughness. This was also confirmed by Carter[75] on

similar materials. The duplex treatment gave maximum tensile properties, but had no effect on toughness or on threshold stress-intensity.

In 250 grade materials, Parkins and Haney[101], Castagne[102] and Dean and Copson[92] found less resistance to chloride environments after solution-treatment at 1075°C, compared with 815°C. Unfortunately, these results were inconsistent, possibly because some of the materials had already been austenised conventionally before treatment at the higher temperature.[101]

Work by Dautovich, unpublished, but quoted in his survey,[89] refers to tests on 200 and on a 270 grade material. In these, the former was definitely harmed by treatment at 1210°C, while the 270 grade material was unaffected either by low or excessively high solution-treatment temperatures.

While the influence of solution-treatment temperature is therefore debatable, the conditions during subsequent ageing strongly affect cracking behaviour. Ageing temperatures normally range from 400°C to 580°C for times varying between 3 and 16 hours, with practices aimed at obtaining the maximum yield stresses for each alloy. Generally, underageing increases the rate of crack propogation and in some cases the K_{1SCC} also, whereas the opposite beneficial effects accrue from overageing. However, endurance is a function of incubation period as

well as cracking rate, so that behaviour judged by one factor only may be misleading. Thus, Carter,[90] using a modified 300 grade steel in salt solution, found that the K_{1SCC} values of approximately 10 Ksi $\sqrt{in}$ were independent of ageing time or temperature. Cracking rates meanwhile decreased with ageing temperature, but extended endurances resulted mainly from greatly increased incubation periods. A summary of Carter's data is reproduced below:

Ageing Treatment	Average Crack Velocity (mm/sec)	Stress-Intensity Range of Measurement ($MN/m^{3/2}$)
3 hrs at 460°C	60×10^{-5}	15 - 43
8 hrs at 475°C	12×10^{-5}	27 - 55
3 hrs at 575°C	2.9×10^{-5}	27 - 87

Table 6: Effect of Ageing Conditions on Cracking of 300 grade Material, After Carter[73]

The velocities quoted are averaged over measurements at 3 - 4 different stress-intensities.

In earlier work on a 350 grade material,[75] the same author again found an approximately constant K_{1SCC} of 11 $MN/m^{3/2}$, and that endurance increased with ageing temperature, again as a result of increased incubation periods. Cracking was intergranular, regardless of the heat-treatment used.

An interesting feature of work by Dautovich[99] was a change from transgranular to intergranular cracking consequent on underageing 270 grade material.

Overall, most experimental evidence indicates that ageing for 3 hours at 475 - 480°C results in both optimum tensile properties and cracking resistance.

3.6.6 Sulphide Environments

The additional hazard represented by sulphide ions in salt solutions was first recognised in petroleum plant.[103] Severe cracking problems occurred principally with martensitic steels in sour oil-wells. In consequence, many field and laboratory studies have been made in attempts to improve material performance. Extensive surveys have been made by Smialowski,[104] and most recently by Greer,[105] both of whom conclude that the mechanism of sulphide cracking in high-strength steels relies on hydrogen embrittlement.

To correlate with sour oil-well experience, much work has been carried out in salt solutions containing hydrogen sulphide, to which additions of acetic acid were sometimes made and which represents an extremely potent environment.

Although a wide variety of alloy steels are known to be susceptible, the great majority of studies have concerned low-alloy steels. As far as these alloys are concerned therefore, the principal effects only are reviewed.

3.6.6.1 Strength and Microstructural Effects

In view of the wide range of steels tested, cracking behaviour has often been related to hardness or yield stress. There is general agreement now however, that of the two parameters, hardness gives a better indication of susceptibility.

Hudgins et al[106] determined a quasi-threshold between 15 and 25 Rockwell C hardness below which no cracking was observed, although the actual endurances above the threshold depended very strongly on sulphide concentrations.

For 4130 steel containing 0.3%C, 1.0%Cr, 0.2%Mo and 0.5%Mn, Swanson and Tralmer[107] suggested a threshold hardness of approximately 20 R_c.

In practice, service failures have been notably few in steels with hardnesses less than 22 R_c and this figure has therefore been used as a design value much akin to the 10J, (15 ft.lb.) brittle-fracture criterion for low temperature service.

Although Frazer[108] deduced from the evidence of some 104 different alloys that composition was a statistically significant factor in sulphide cracking, this conclusion has since been questioned, and microstructure rather than composition is now thought to be the major factor. Typical of many tests on martensitic low-alloy steels in sulphide saturated solutions are those by Kim and Loginow.[109]

Simple tension samples of a 3%Ni, 1.6%Cr, 0.5%Mo steel containing 0.13% carbon showed thresholds at $0.15\,\sigma_{UTS}$ and $0.18\,\sigma_{UTS}$ after tempering at 560 and 700°C. Judged either by endurance or cracking rate, resistance in these experiments improved with tempering temperature, an effect which could be related to reduced yield-stress. It was concluded that susceptibility depended upon the amount of corrosion-generated hydrogen trapped within the lattice, perhaps at carbide/matrix interfaces or at dislocation tangles. Certainly, a clear linear relationship existed between yield-stress and hydrogen uptake during exposure. One possibility is that polarisation by sulphide ions prevents escape of surface hydrogen.

3.6.6.2 Environmental Influences

Although hydrogen sulphide is acknowledged as a potent cracking agent, especially in combination with other corrosive species, its modus operandi is not clear. Hydrogen sulphide solutions are themselves sufficiently corrosive to generate cathodic hydrogen, but their influence as cracking media can be either enhanced or completely prevented by changes in pH. Hudgins et al,[106] Treeder and Swanson,[110] and Dvoracek[111] all found a marked increase in the liklehood of failure as pH values decreased below 5, although the effect also depended on sulphide concentration.

Concentration effects per se have been shown to be significant,[106,112,113] with endurance increasing as

sulphide amounts decrease. However, there appears to be no limit below which sulphide concentrations can be neglected, and general opinion is that even at the lowest detectable levels, sulphide ions are harmful.

More recently, McIntyre and Priest[114,115] have performed tests in dry hydrogen sulphide, in dry hydrogen atmospheres and in salt solutions and found that the K_{1SCC} values for a variety of steels are almost identical in each environment. The actual rates of cracking in the stage II plateau however, were some four orders of magnitude greater for hydrogen sulphide than in salt solutions. These results confirmed earlier similar work by the same authors for two low-alloy steels,[116] and the two findings suggest that cracking of high-strength steels operates under the same aegis - that of hydrogen control. The actual values appear dependent upon the properties of the martensites or bainites involved and hence correlate with their yield stresses. Meanwhile, the principal effect of various environments may be to restrict the supply of nascent hydrogen either by actually controlling the corrosion rate, by change of electrode-potential, or by poisoning, as in the case of hydrogen sulphide.

3.6.7. Maraging Steels in Sulphide Environments

Few data concerning maraging steels in sulphide containing environments have been published, but those available all confirm their marked susceptibility. Thus

Snape,[117] using sulphide-saturated acidified salt solutions, compared the resistances of two low-alloy steels with a 12Ni, 5Cr, 3Mo maraging steel. For the latter, K_{1SCC} values of $\sim 26 MN/m^{3/2}$ were obtained compared with 11 - 15 $MN/m^{3/2}$ for the two low-alloy steels. Moreover, the incubation periods were considerably greater for maraging steel, and its crack propagation slower than those in low-alloy steels.

The only other published data are contained in a letter by Scharfstein[118] concerning smooth specimen tests in hydrogen sulphide saturated 5% acetic acid. For a 250 grade 18%Ni steel stressed at 0.6 σ_y, the endurance was only some 0.4 - 0.9 hours compared with 15 - 42.2 hours in 6%NaCl + chromate solution. Significantly, unaged material also failed rapidly (3 - 11 hours) in the sulphide test, but remained unbroken after 215 hours in the salt-chromate solution.

Unpublished work by Horsman[119] on precracked samples in a 1% ammonium sulphide solution suggested a K_{1SCC} value of $\sim 23 MN/m^{3/2}$ for conventionally aged 250 grade material, but a slightly higher value of $\sim 27 MN/m^{3/2}$ for material heat-treated to simulate a weld H.A.Z. structure. A point of interest in this work is that ammonium sulphide solutions develop a pH of ~9 during exposure, so that the aggressive nature of the sulphide ions would be offset by the low availability of hydrogen ions.

3.7 ENVIRONMENTAL CRACKING OF MARAGING STEEL WELDMENTS

Cracking is particularly likely at welded joints, by reason of enhanced stress levels and detrimental changes in microstructure. Furthermore, geometrical factors associated with joint design permit concentration of aggressive chemical species in the danger areas. In high-strength steels, residual tensile stresses of yield-point magnitude can occur after welding, and the risks of micro-cracking during solidification or subsequently by hydrogen assisted cold cracking are considerable. Even when stress-relief has been carried out, local concentrations of stress will usually remain, so that initial weld defects grow under environmental influences, especially those which encourage hydrogen formation.

Despite a general appreciation of these factors, a dearth of published information exists regarding the performance of welded high-strength steels. In this respect, maraging steels are no exception, and no data have been located on their behaviour when welded and exposed to hydrogen sulphide.

Early papers covering the resistance of maraging alloys to chlorides and atmospheric environments generally, however, have included brief references to welded joints. In all cases, the results suggested that welding was a detrimental factor, but regrettably, the value of these data is little more than qualitative since reproductibility and experimental

detail are almost non-existent. Principal omissions in reports of tensile and U-bend tests are:

(i) the presence or absence of reinforcement,
(ii) the filler compositions used, and
(iii) the heat inputs.

In consequence, the relative susceptibilities of weld metals and heat-affected zones are either ignored or occasion no comment.

3.7.1 Smooth Specimen Data

Setterlund[95] found that TIG welding substantially reduced both the strength and cracking resistance of 18 and 20%Ni steels in water to levels below those of low-alloy steels similarly exposed. By extrapolation of his results, the endurance of 250 grade TIG welds would have been ~200 hours at 0.75 σ_y compared with ~9000 hours for parent metal.

Dean and Copson[92] also referred to TIG welding as detrimental to resistance in chlorides and a variety of atmospheres, and noted that major cracks occurred in the heat-affected zones.

In a more detailed paper, Kenyon, Kirk and Van Rooyen[120] assessed the behaviour of 180 and 200 grade maraging steels in 3½%NaCl and in sea water. Multipass TIG and MIG welds were used with matching fillers and average heat inputs of 0.5 and 1.4 KJ/mm per pass respectively. While parent 200 grade material remained unbroken after 3 years, both TIG

and MIG welds failed in times ranging from 2-18 months, with MIG welds being marginally the less resistant. By comparison, TIG welds in 180 grade material proved as resistant as the parent metal.

With TIG and MIG welds showing similar endurances in spite of microstructural differences, further bend-tests were carried out on 200 grade material to examine the influence of post-welded heat-treatments. Resolution for 1 hour at 816°C after welding produced a marked improvement in resistance, but single higher temperature solution treatments were detrimental. This effect was attributed to coarse grain sizes which developed in both weld and parent metal, yet strangely, resistance could be restored by further solution treatments at 593°C and 816°C. The effect could not be related to changes in mechanical properties which were similar after each treatment.

By coupling welded samples to zinc, the effects of cathodic protection were found to be negligible on TIG welded 180 grade alloy, but slightly greater on the 200 grade. An decrease in cathodic potential to -1.25V S.C.E. proved disastorous for 200 grade material with all the welded specimens failing in less than 50 days. This indicated the danger of surface hydrogen in the higher strength materials.

3.7.2 Results From Precracked Specimens

The previous authors[120] also used fracture mechanics type cantilever-bend specimens to determine the K_{1SCC} values of parent and TIG welded alloys. Their results are summarised in Table 7 below.

Alloy (grade)	Parent Metal	TIG Weld
180	142 153	134 -
200	101	76

Table 7: K_{1SCC} Values in $MN/m^{3/2}$ for Welds and Parent Metals in Chloride Solutions (after Kenyon et al[120])

Slight differences were noted between sea-water and 3½NaCl solutions, but more substantial reductions occurred on coupling to zinc or by using impressed current (-0.85V S.C.E.). This concurs with similar behaviour in bend tests, and Kenyon stresses the additional hazard posed by hydrogen embrittlement of welds resulting from cathodic protection.

Delayed failures of TIG welds in both air and in pentaborane were reported by Toy and Phillips,[121] although no K_{1SCC} or cracking rate data were presented. Failure in air was shown to be associated with cathodic hydrogen in both 250 and 300 grade materials by the technique of evaporating neodymium onto the specimen surface. Black neodymium hydride then formed from hydrogen released from

retained austenite in the weldment. Failure in pentaborane could not be identified as either chemical or electrochemical in nature, but it is possible that the single high level test stress of 0.9 K_{1C} caused some of the rapid failures to occur simply by overload.

From 6 mm thickness 250 grade plate, Freedman[122] used precracked tensile test pieces to determine the K_{1SCC} values of both TIG welds and of the heat-affected zones as reproduced by a 'Gleeble' weld simulator. The results for a marine atmosphere and 200 g/l NaCl laboratory tests were as follows:

MATERIAL	K_{1C} ($MN/m^{3/2}$)	K_{1SCC} ($MN/m^{3/2}$)	
		NaCl Solution	Marine Atmosphere
Parent	115	80 ± 4	58 ± 8
TIG Weld	59	25.5 ± 5	30 ± 8
HAZ(1460°C)	126	44 ± 8	-
(Simulated): (810°C)	100	42 ± 4	-
(730°C)	124	67 ± 9	59

Table 8: Limiting Stress Intensities for TIG Welded 250 Grade Material[122]

Noting that the K_{1SCC} values for simulated heat-affected zone material were similar to that of parent metal, Freedman concluded that in 18%Ni alloys, the susceptibility of the weldment was controlled by the low K_{1SCC} of weld

metal. Of the actual data quoted, the validity of K_{1C} values may be questionable since fractured samples showed considerable shear-lip formation, although the threshold values appear acceptable.

Apart from the Freedman data, work carried out by Gooch[123] at the Welding Institute has, to date, provided the most detailed and practical assessment of weld behaviour in 3%NaCl solutions. In comparing 180 grade maraging steel with other high-strength alloy steels, cracked samples cut from welds made with a K edge-preparation (double-bevel-groove joint) were used, so that planar fusion boundaries and heat-affected zones were obtained normal to the plate surface. Particular regions could then be examined by appropriate siting of the prefatigue notch. Gooch's results are summarised in Table 9 below:

WELDING PROCESS	CRACK PROPOGATION THROUGH					
	PARENT METAL		WELD METAL		Tr.H.A.Z.	
	K_Q	K_{QSCC}	K_Q	K_{QSCC}	K_Q	K_{QSCC}
Metal Arc	111	68	55	44	-	-
MIG	"	"	-	70	115	88
Electron-Beam	"	"	66	43	-	-

Table 9: Critical Stress-Intensities ($MN/m^{3/2}$) for 180 Grade Maraging Steel Welded by Various Processes[123]

In addition to the precracked tests, butt-welded samples were tested in 3-point bending, with one face ground flush for loading but leaving the reinforcement intact on the other, thus providing a stress-concentration. Nominal stress levels of 0.67 and 0.85 σ_y were used as representative of design and proof-test loadings respectively. At 0.67 σ_y, MIG welded material remained intact after 3000 hours, but at 0.85 σ_y, cracks eventually appeared in the HAZ and propogated into the weld metal after 5000 hours. By comparison, similarly tested electron-beam welds failed in the weld metal after only 0.01 hours at 0.67 σ_y. From both types of test, Gooch derived 'defect-tolerance parameters', defined as:

$$\text{D.T.P.} = \left(\frac{K_Q}{\sigma_y}\right)^2 \quad \text{, or} \quad \text{D.T.P.} = \left(\frac{K_{QSCC}}{\sigma_y}\right)^2 \qquad (9)$$

where σ_y is the base metal yield stress. Obviously, the values based on stress-corrosion conditions will be smaller than those in air. Plain welds were shown to behave much as would have been predicted from fracture-mechanics tests, with greatest endurances from welds having the highest D.T.P.'s. Values for maraging steel ranged from 1.55 mm to 5.11 mm for weld metal and heat-affected zones exposed to salt solutions. Based on plain weld tests, D.T.P. values were 3.28 mm for MIG weld metal and 1.28 for electron-beam weld metal. Generally, the relation between D.T.P. and hardness was inversely linear, judged on results for all

the 5 steels tested. It was concluded that 180 grade maraging steel afforded as high a resistance to environmental cracking as the best of those steels.

In discussing his results, Gooch makes the interesting observation that high cracking resistance may result from the beneficial presence of retained austenite, rather than this phase being the cause of poor resistance. This suggestion was made on the grounds that metal-arc weld metal ought to have had a very low K_{1SCC} on view of its austenite content, and yet this was not the case. Toy and Phillips[121] austenite hydrogen sources are possibly, therefore, an effect of environmental cracking rather than a cause.

4. EXPERIMENTAL TECHNIQUES

4.1 INTRODUCTION

At the outset of the present work, the intention was to examine crack-propagation rates in thin sheet materials. The advantages of such an approach lay in economics, ease of welding, and in loading requirements, bearing in mind the limitations of the stress-corrosion testing machines available. Some stress/endurance data were subsequently obtained on TIG welded samples of 0.9 mm thickness sheet, but attempts to obtain valid crack propagation rates were frustrated by their multipoint initiation and branching development.

Meanwhile, references to specimens precracked in fatigue and later stress-corroded had begun to appear in the literature, and it was decided at this stage to change the emphasis of the work to thicker materials capable of sustaining the required plane-strain conditions during tests. With the increased material thickness, it was also advisable to change to a more industrially applicable method of welding, viz. submerged-arc. Whilst a multi-run TIG welding technique could have been used, the heat-inputs and the risk of including defects in the weld would have been considerable.

Unexpected difficulties now arose with hitherto simple metallurgical operations, and more importantly,

despite the great care taken during submerged-arc welding, centreline defects still occurred which affected considerable lengths of all the material welded. The specimens eventually obtained, therefore, represented a compromise between test requirements, availability of material and the loading capacity of the testing apparatus.

4.2 MATERIALS

The preliminary trials were carried out on 0.9 mm material supplied as-welded, in the cold-rolled and solution treated condition, by Bristol Aerojet Ltd. Both mechanised TIG welded, and electron-beam welded sheets were included in these tests together with plain material.

For the major part of the experimental work, however, plate, kindly provided by Firth Brown Ltd., Sheffield, was used. This material was initially supplied as vacuum-remelted and forged billets 100 x 100 x 600 mm in dimensions. Subsequently, these were further forged and hot-rolled, and then cut transverse to the final rolling direction to produce plates 400 mm length by 150 mm x 17 mm in cross-section. Some cross-rolling was involved in supplementing the lateral extension during forging to obtain the width necessary for welding.

Both the filler wires used were manufactured by Telcon Metals Ltd., to compositions which matched or slightly overmatched those of the parent materials. They had been degreased before reeling.

The submerged-arc welding flux was a basic alumina-chalk agglomerated type containing ferro-titanium, which was manufactured by Metrode Ltd., Chertsey, Surrey, following the composition described by Wilson and Wildman.[39]

4.2.1 Compositions

Chemical analyses of each material, as determined by standard wet methods, are given in Tables 10,11 and 12. Having a significantly higher cobalt content, the sheet material corresponded to the 2000 MN/m^2 grade of maraging steels, while the plate was of the 1700 MN/m^2 grade, these figures being nominal commercially expected yield stress values, equivalent to 300 and 250 Ksi respectively.

It would be expected that weld compositions derived from each combination of materials would be similar to those of the parent metals. In the first instance, the recovery of elements in both the TIG and submerged-arc methods approaches 100%, with any losses of titanium to the flux in the latter method offset by additions of ferro-titanium. Secondly, dilutions of the filler by parent metals as calculated from transverse macro-sections of the welds, were of the order 60-80% with the joint geometries used. The actual composition of a typical plate weld is given in Table 13 and confirms the similarity between parent and weld metals.

Material	Origin	C	Mn	Si	S	P	Ni	Co	Mo	Ti	Al
250 grade Sheet	Bristol Aerojet Ltd.	0.030	0.04	0.08	0.002	0.002	18.7	9.2	5.12	0.45	0.09
1.6 mm dia. filler wire	Telcon Metals Ltd.	0.070	0.03	0.07	0.006	0.005	18.6	9.1	5.2	0.07	0.06

Table 10: Compositions (in wt.%) of Sheet Material

Material	Origin	C	Mn	Si	S	P	Ni	Co	Mo	Ti	Al
250 grade plate	Firth-Brown Ltd.	0.026	0.035	0.12	0.008	0.003	18.35	8.0	5.2	0.56	0.15
2.4 mm dia. filler wire	Telcon Metals Ltd.	0.020	0.050	0.03	0.005	0.003	19.7	8.94	4.85	0.61	n.d.

Table 11: Compositions (in wt.%) of Plate Material

Material	Origin	Al_2O_3	$CaCO_3$	CaF_2	Fe-Ti (45%Ti5%Al)	MgO	$Na_2O(SiO_2)_3$	$K_2O(SiO_2)_3$
Agglomerated Flux	Metrode Products Ltd.	35.0	26.4	14.1	5.7	13.3	1.8	3.7

Table 12: Composition (in wt.%) of Submerged Arc Welding Flux

Material	C	Mn	Si	S	P	Ni	Co	Mo	Ti	Al
Plate Weld Metal	0.022	0.037	0.21	0.011	0.004	18.30	8.20	5.16	0.17	0.13

Table 13: Composition (in wt.%) of Submerged-Arc Weld Metal

4.3 HEAT TREATMENTS

Generally, maraging steels are supplied in the solution-treated and air-cooled condition after reduction to the required thickness, so that stresses required for any further mechanical treatments are minimised. Ageing is then a final operation, taking advantage of the minimal dimensional changes which occur.

For the present work, sheet material was solution-treated in air for 1 hour at 820°C, followed by air-cooling to room temperature. Surface oxide was then removed by acid-pickling prior to welding. All these operations were carried out by Bristol Aerojet Ltd.

The plate material was solution-treated under the same temperature/time conditions in a resistance furnace at British Steel Corporation, River Don Works, Sheffield, and subsequently air-cooled. In this instance, surface oxide was not removed prior to welding since a machined edge-preparation was required later. After welding, specimens were cut and machined to final dimensions from the welded test-plates, and then aged in air at 480°C for 3 hours. Oxide formed during this treatment was removed from sheet specimens by light abrasion, but it was not necessary to remove such oxide from plate specimens since subsequent machining on all specimen surfaces was required.

4.4 WELDING

4.4.1 TIG Welding Procedure

At Bristol Aerojet Ltd., mechanised TIG welding of pairs of sheets enabled test samples measuring 400 mm x 300 mm x 0.9 mm with a central longitudinal weld to be made. Electron-beam welding was also carried out on further sets of plates, but no tests were attempted on these as the welds were offset due to distortion.

The conditions used for TIG welding were those given in Table 14. Abutting sheet edges were wire-brushed and degreased in white spirit before being clamped together on a stainless steel backing-bar.

Since no records of arc voltage were made, calculation of heat input to the TIG welds is impossible, but assuming an arc voltage of 15 and an arc efficiency of 30%, the heat input would have been of the order of 0.1 KJ/mm or less.

4.4.2 Submerged-Arc Welding Procedure

Pairs of plates cut to 400 mm length were edge-prepared with a shaper to produce a double-Vee, 70^{o} included-angle joint-geometry with a 4.8 mm land.

Before attempting welds on the limited number of maraging plates available, trial runs at Bristol Aerojet Ltd., were made on similarly dimensioned mild-steel plates, so that optimum heat inputs and welding speeds could be determined. Using one pass from each side, these trials showed that adequate interpenetration of the two passes

Edge Preparation	Shielding gas	No. of Passes	Polarity	Current (amps)	Arc Volts	Arc Travel Speed (mm/sec)	Wire Feed Speed (mm/sec)
Square, close-butt	Argon	1	DC negative	35-40	n.d.	2.1	9.0

Table 14: TIG Welding Conditions: Sheet Material

Edge Preparation	No. of Passes	Current (amps)	Arc Volts	Arc Travel Speed (mm/sec)	Wire Feed Speed (mm/sec)	Wire. Diam. (mm)
Double Vee 80° inc. angle 4.8mm land 3.2mm gap	1	480	41	3.3	6	2.4
	2R	475	40	3.3	6	2.4

Table 15: Submerged-Arc Welding Procedure: Plate Material

could only just be obtained at the maximum current (450 amps) available from the power source, at speeds which produced an acceptable weld profile.

An approach was therefore made to E.S.A.B. Ltd., Sittingbourne, where a larger power source with a A6 type welding head was available. Experiments at this company unfortunately limited by time, suggested that currents of the order of 465-475 amps were sufficient to ensure inter-penetration. It was also found that the edge-preparation required slight modification to include (i) an 80^{o} angle, and (ii) a 3.2 mm root gap between the faces achieved by stainless steel inserts at each end of the joint. Immediately before welding, the joint edges were wire-brushed and degreased with white spirit. The final joint geometry is shown schemetically in Figure 9.

Mild steel run-off and run-on plates were attached beforehand by MIG welding, while two tack welds within the joint proper were deposited by submerged-arc to minimise distortion. The average welding conditions finally arrived at are shown in Table 15.

Using flux prebaked to remove moisture, the first runs were completed and allowed to cool to approximately $25^{o}C$, before thoroughly removing oxide and slag from the weld root by hand-grinding with an abrasive disc. After further wire-brushing, the second passes were then completed.

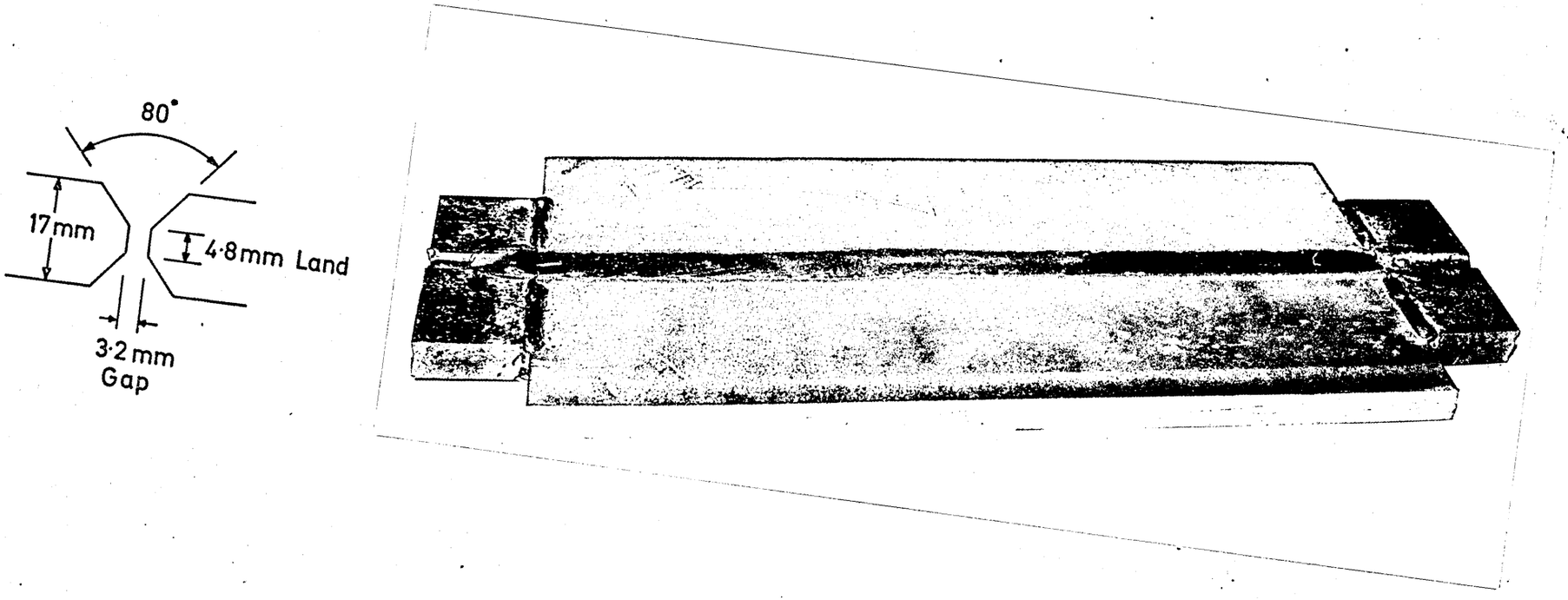

FIG. 9 Completed submerged arc-weld and prior edge preparation.

Welds on six pairs of plates were produced using the conditions of Table 6 in which the currents and arc voltages are average values, each having fluctuated some 5% during runs.

Assuming a value of 95% for arc efficiency, the heat input per pass during submerged-arc welding was approximately 5.7 KJ/mm.

Generally, the welds produced were of good shape although their surfaces has the roughness characterisitic of basic fluxes (Figure 10). A point of interest was the occurance of hot-cracking at the craters and at run-off plate junctions (Figure 11). This may have been due to the sulphur pick-up from the mild steel combined with excessive strain during welding. In addition, a certain degree of angular distortion occurred, leading to a displacement of approximately 5^{o} between one side of the weld and the other.

In view of the care taken during welding, it was extremely disappointing to find, revealed by radiography (Figure 12), appreciable lack of fusion in the major portions of all the plates welded. This was later confirmed by sectioning, and it consequently forced the change in specimen dimensions described in section 4.5.2.

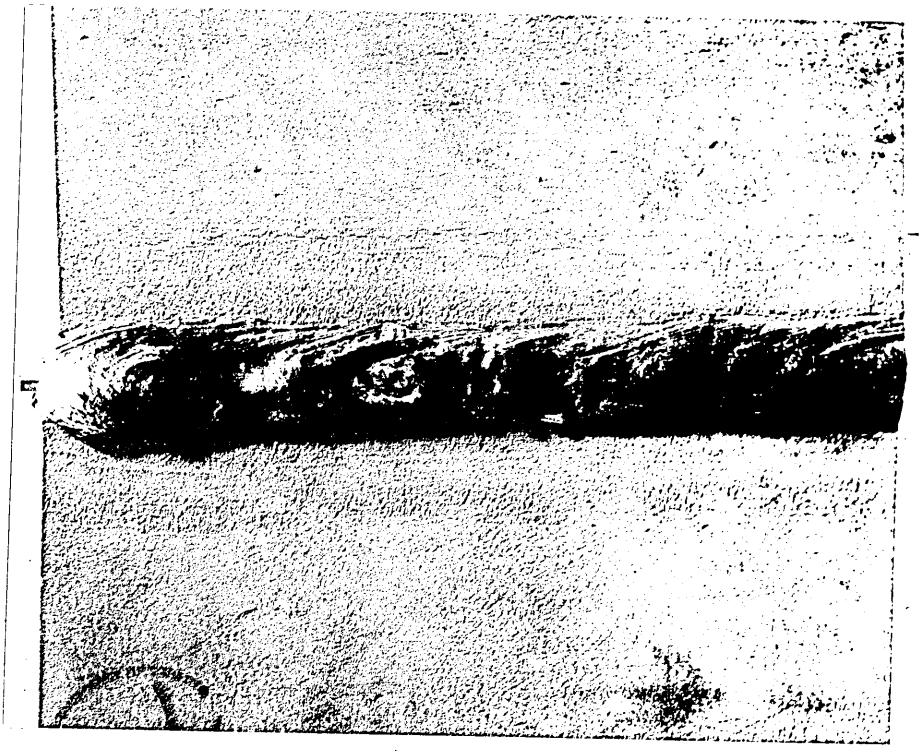

x ¾ approx

Figure 10: Surface Appearance of Submerged-Arc Welded Plate

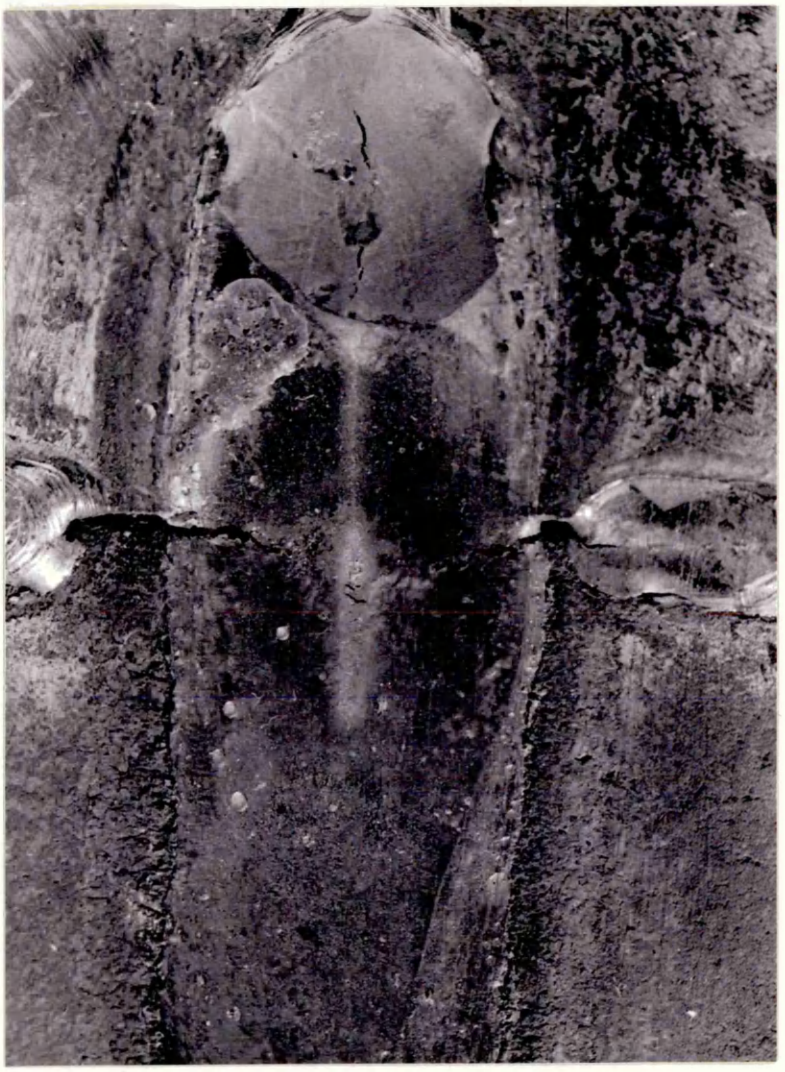

x 2½ approx

Figure 11: Hot-Cracking in Weld Crater and at Run-Off Plate Junction on Submerged-Arc Welded Plate

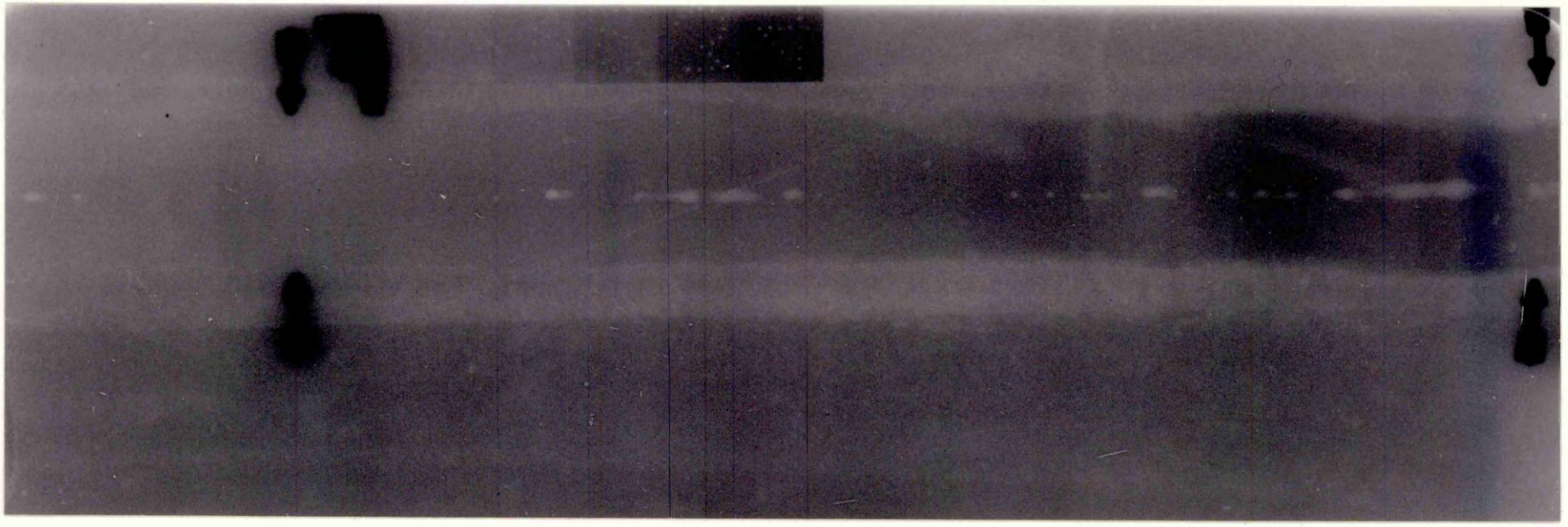

Figure 12: Lack of Fusion Revealed by Radiography

4.5 TEST-PIECE PREPARATION

4.5.1 TIG Welded Material

Substandard sheet tensile test-pieces were milled from parallel sided blanks cut transverse to the weld, from unaged material and leaving the weld reinforcement intact. In order to fit the testing chamber, one shoulder was made twice the length of the other, with the weld positioned in the centre of the gauge-length. This form of test-piece was also used to determine the tensile properties of the welded material. The thin oxide film which formed on subsequent ageing of each test-piece, was removed by light abrasion with emery paper before exposure.

4.5.2 Submerged-Arc Welded Material

To produce single-edge-notched specimens, test-piece blanks were first cut by sawing from welded material transverse to the weld and at a slow speed to minimise overheating. Edge and end effects were obviated by discarding the first and last 40 mm of each welded plate. From each such plate, some 19 test blanks approximately 17 mm x 17 mm in cross-section were ultimately prepared.

The weld reinforcement was next removed from both sides of each blank by milling or shaping. Using one side of the weld joint as a reference plane, this operation reduced the thickness of the other side somewhat due to its angular distortion, but allowed the now parallel sided blanks to be subsequently gripped and machined in small groups.

Prior to notching, the top surface and one side of each blank was surface-ground using water-cooling, and then macro-etched to show the weld position. Aiming at set distances from the weld interface proved difficult, so that lines marking the intended notch positions were scribed at a random series of distances from the parent metal-weld metal interface and measured later. The direction of subsequent crack propagation was therefore parallel to the welding direction.

After cutting to length (75 mm) with a fine, water-cooled slitting disc, specimens were notched with a shaper to produce the notch-geometry shown in Figure 13. It was originally intended to test specimens approximately 10 mm x 10 mm in cross-section, but with the presence of a crack-like defect at the specimen mid-width, it was decided to slit each specimen along the defect plane despite the consequent reduction in effective specimen thickness. A further small loss in thickness resulted from surface grinding to correct the non-square cutting action of the disc. It was of course essential to ensure rectangularity in order that crack propogation would occur evenly across the specimen cross-section.

At this stage, the specimens were finally aged.

4.5.3 Macro-Etching

All SEN test-pieces were macro-etched before ageing in a 50% solution in water of a mixed acid etch comprising

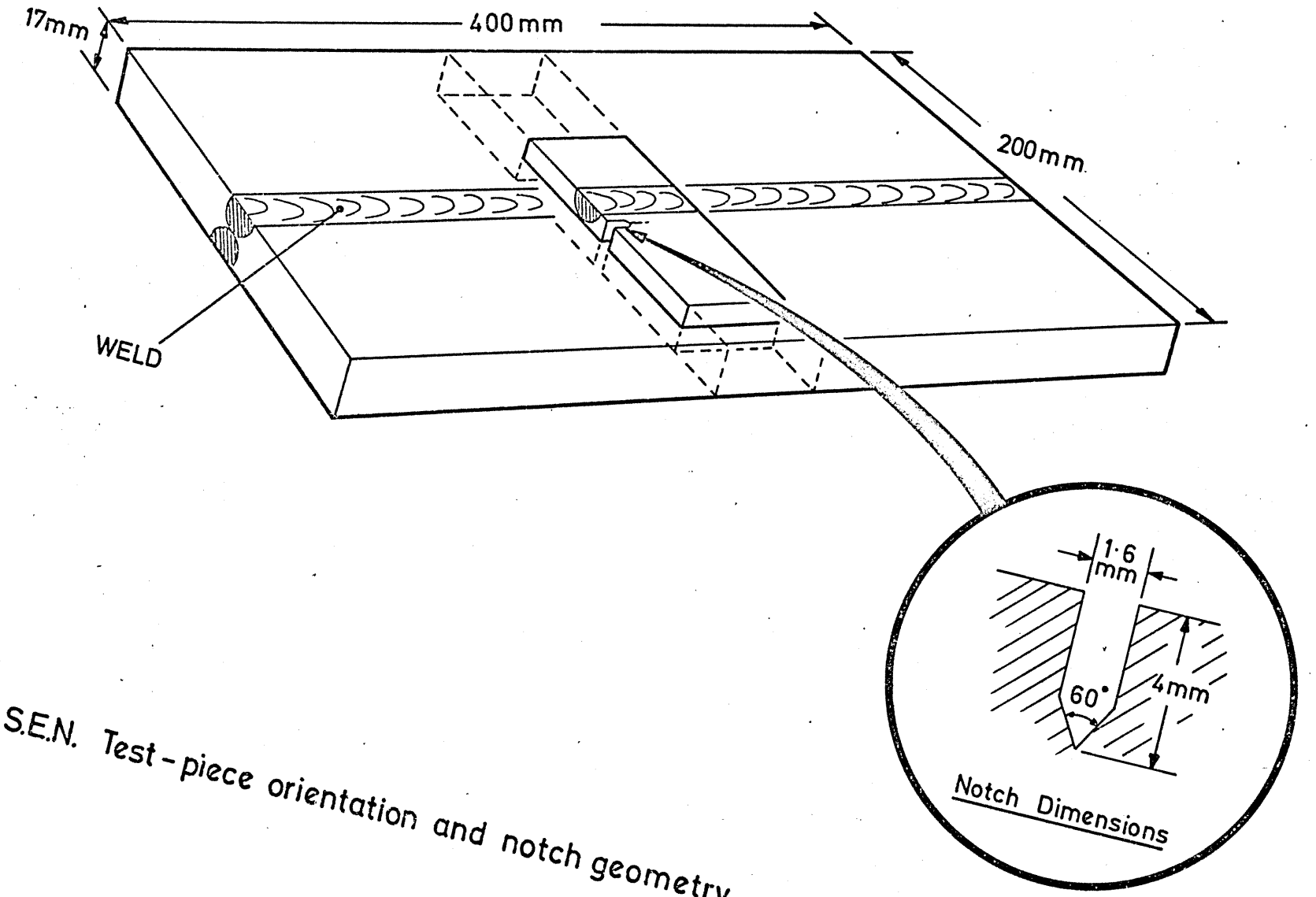

FIG. 13 S.E.N. Test-piece orientation and notch geometry.

60% concentrated sulphuric acid, 20% concentrated hydrochloric acid and 20% concentrated nitric acids, The initially cold solution gained heat rapidly during use, and provided a satisfactory macro-etch within 1 minute. However, the etched surface became simultaneously covered with a tenacious black film, presumably of nickel oxide. This required subsequent removal in a concentrated nitric acid dip, in which the film dissolved within 5-10 seconds before passivation. Patience was necessary to obtain a satisfactory etch, since washing with water after the acid dip frequently depassivated the metal and reformed the black film, unless treatment was rapid.

A similar black film formed during contact with the hydrogen sulphide used for cracking tests. This proved even more difficult to remove and was a constant problem when fractography was required, since its removal in acid damaged the fracture surface. Provided samples were removed from the corrodent immediately after failure, those samples with endurances of less than 3 hours could be scrubbed sufficiently clean using detergent. Otherwise the black film remained to partially obscure surface features in light and electron fractography.

4.5.4 Definition of Notch Position

Taking the weld interface as the origin, notch positions were defined as the mean distance to the plane of the notch

measured over the specimen width, with negative values indicating weld metal. Distances from the weld to the dark-etching band were also measured in order to provide an estimate of peak temperature in the crack regions. Minimum values were recorded, since in many cases the dark band resulting from the second welding pass occurred at a slightly different position from the first.

By grouping specimens according to distance from the interface, it was later convenient to produce approximate stress-endurance curves characteristic of the following regions:

	DISTANCE FROM WELD INTERFACE (mm)			
	(-8.0 - -2.0)	(-2.1 - +4.0)	(+4.1 - +8.0)	(+8.1 - +25)
Region	Weld Metal	Interfacial Zone	Dark etching band	Remote Parent Metal

Table 16: Definition of Weld Regions

SEN specimens were precracked in fatigue by reverse three-point bending on an Amsler Vibrophore machine, employing a 0.3 MN dynamometer at a positive mean-stress, and at a frequency of 4500 Hz. Progress of each crack was monitored using a telescope mounted horizontally some 500 mm from one side of the specimen under fatigue, and was stopped when the crack length reached an equivalent $(\frac{a}{w})$ value of 0.5. During crack initiation, a starting load of

2.3 ±1.3 KN was used which was reduced normally to 1.3 ±1.0 KN as soon as initiation was observed. Propagation at the lowest practical stress is necessary in order to restrict the size of the plastically deformed region at the crack-tip.

In the present work, less than 20,000 cycles at the higher stress was necessary for initiation, with propagation complete after an additional 70,000 cycles at the lower stress.

4.6 ENVIRONMENTAL TESTING

4.6.1 Environments

At the outset, testing of TIG welded material was carried out in the ubiquitous 3% sodium chloride solution with or without polarisation to accelerate cracking.

On the decision to adopt a fracture mechanics approach, it was thought profitable to change the environment to one containing sulphide ions. As described earlier, this ion is a potent cracking agent in contact with high-strength steels, and can cause rapid failures in industrial applications.

Some previous environmental tests on pre-cracked samples were conducted in a 1% solution of ammonium sulphide, and produced interesting but variable results.[124] There were difficulties however in obtaining and keeping chemically pure ammonium sulphide, which decomposes continually into a series of complex polysulphides and precipitates free colloidal sulphur.

In the present work, sodium sulphide solutions were initially tried without success, the main problem being the development of high pH values due to dissociated sodium ions. Specimens exposed to this solution either cracked instantly at high stress-insensities or remained uncracked at lower intensities.

The environment finally adopted was an ice-cold saturated solution of hydrogen sulphide in distilled water. Although near zero when produced, its temperature rose to approximately $10^{o}C$ on contact with the test-rig, so that excess hydrogen sulphide formed on all exposed surfaces including the test piece within the solution. Bubbles so formed remained for some 4 hours or more depending upon conditions. At the time, it was assumed that during the 4 hour period, the total sulphide content in solution would remain reasonably constant, and this was subsequently confirmed by tests using a sulphide selective electrode. As illustrated in Figure 14, loss of sulphide ions became appreciable after 3-4 hrs, so that as a precaution, solutions in contact with test pieces for more than 3 hours were either replenished or completely renewed.

In view of the constant release of toxic fumes, the whole environmental chamber was totally enclosed in a polythene chamber from which excess hydrogen sulphide was continually extracted by an electric fan. This arrangement is illustrated in Figure 15.

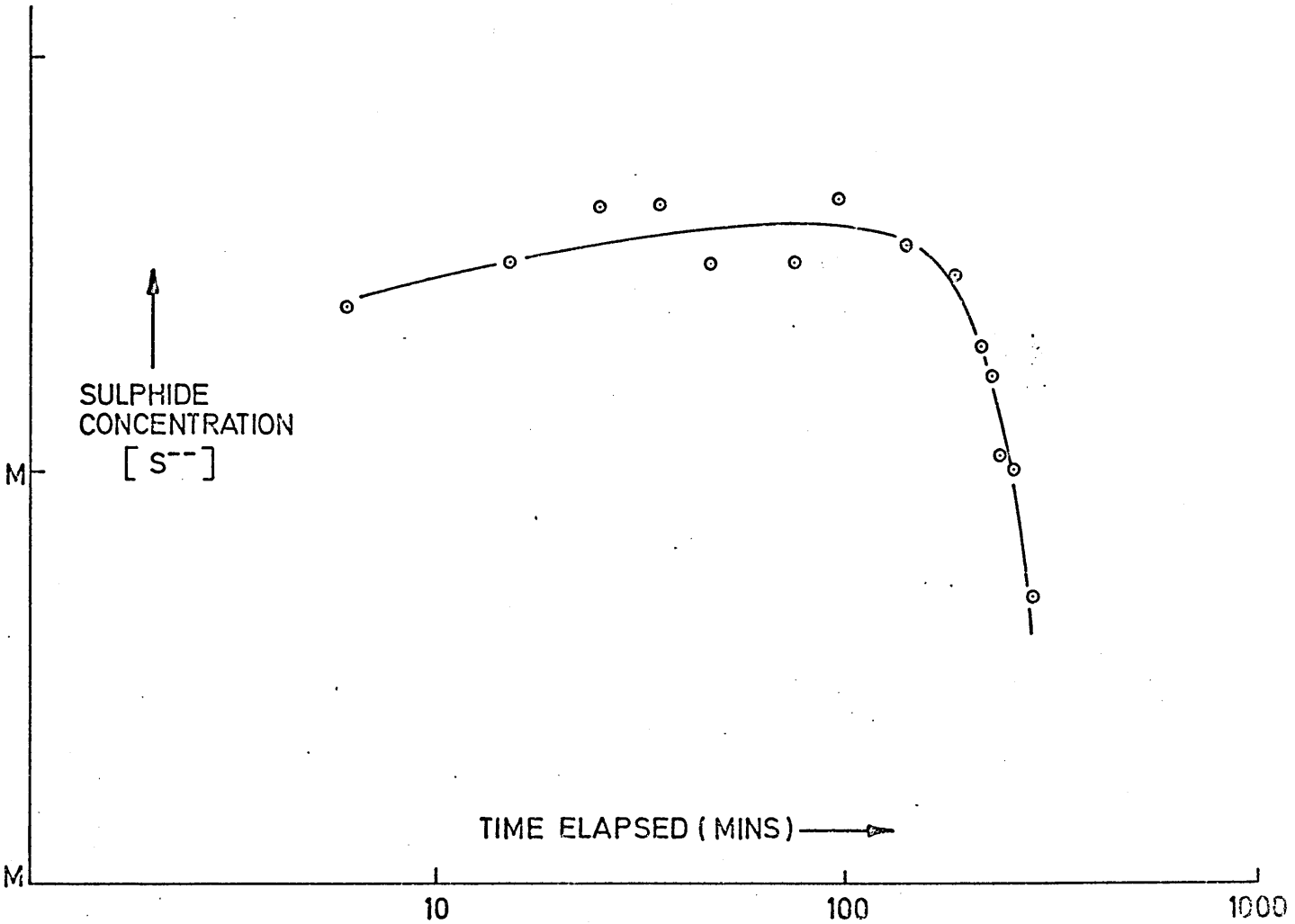

FIG. 14 Change of sulphide concentration in H_2S saturated water with time.

$\times \frac{1}{20}$ approx

Figure 15: General View of Test-Rig, showing chamber from which excess hydrogen sulphide was extracted by an internal fan

4.6.2 Constant-Load Rupture Tests

Using a constant-load Denison creep machine, TIG welded sheet specimens were simply loaded in direct tension via 18%Cr stainless steel shackles. The corrodent was contained in a cylindrical tuffnol cell which surrounded the specimen. Complete waxing of both the cell bottom and the specimen shoulders allowed a known surface area to be exposed when using galvanostatic conditions. Endurances were recorded automatically when the descending beam triggered a microswitch.

With the same Denison machine, the cell used for testing SEN specimens is shown in Figure 16. Two horizontal knife-edges were formed by spark machining rectangular holes in two 20 mm dia. stainless steel rods. These were screwed into the stainless steel base plate of the cell. Bending loads were applied to the specimen via an inverted saddle containing knife-edge, also made in stainless steel. Knowing its length, each specimen could, with set screws, be positioned accurately across the knife-edges with the saddle directly beneath the notch.

Loads were calculated from the relationship:

$$P = \eta \cdot \frac{K_q B \sqrt{W}}{10Y} \qquad (10)$$

in which the terms are as defined in section 3.5, and η was set between 0.1 and 0.6 to give the range of loads required for stress-intensity-endurance curves. In the first few tests, loads were applied after filling the cell with

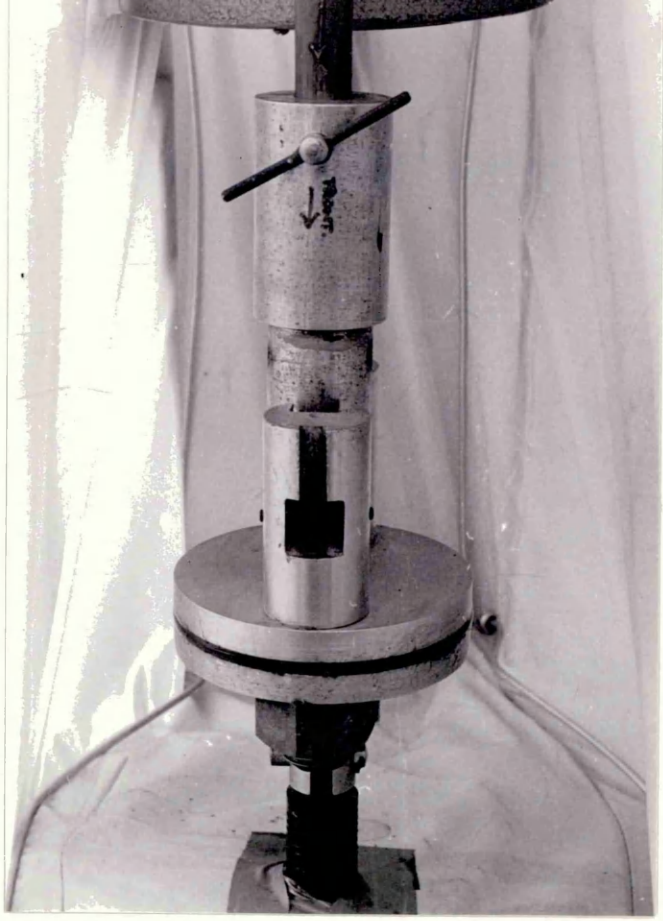

x ⅓ approx

(a) Knife edges and central saddle

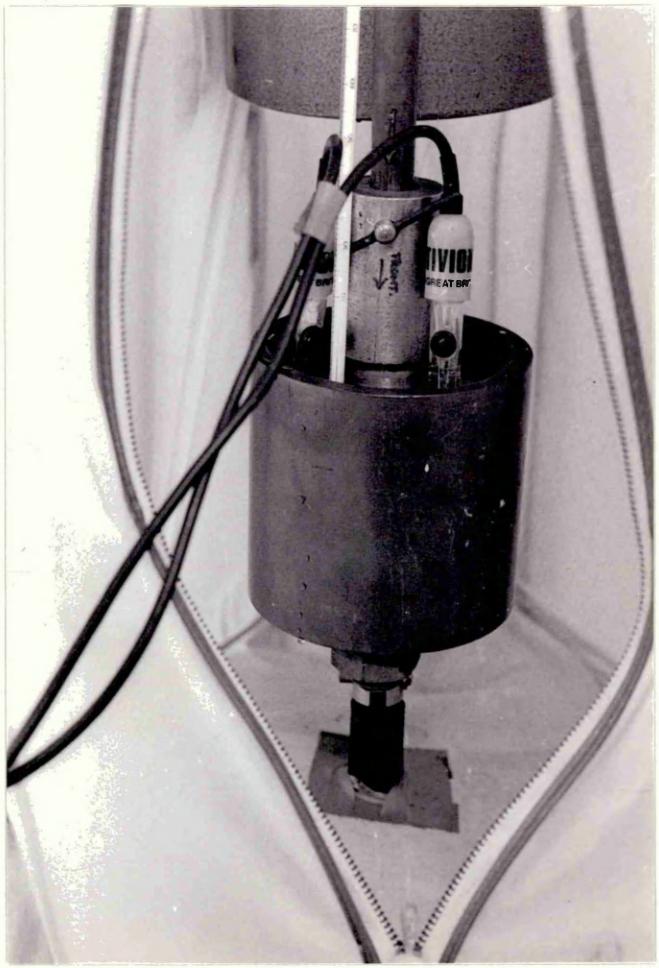

x ⅓ approx

(b) Cell in use, with monitoring electrodes

Figure 16: Loading Arrangements for SEN test sample

endurance measured from the time of introduction.

4.6.3 Crack Growth Rates

In air, changes in crack-opening displacement as measured by a clip-gauge, can be used to follow crack-growth. Methods based on specimen resistance,[125,126] accoustics,[127,128] eddy-currents[129] and ultrasonics[130] are also possible. The resistance technique was first introduced to study hydrogen embrittlement in sharply notched round specimens, and relies on the change of potential distribution which occurs as cracks elongate. Two substantial contacts soldered to the specimen ends enable currents of the order of 20 amps to be passed. Two further fine contacts are spot-welded or soldered either side of the notch, so that changes in crack length which cause potential changes across the notch can be monitored.

With specimens immersed in electrically conductive solutions however, it was thought that complications could arise, not only through conduction between the crack-faces, but because the potentials developed could affect the corrosion potential at the crack-tip, and hence influence the cracking processes.

In the present case, access to the notch was restricted by the central knife-edge saddle, which prevented the use of a clip-gauge. It was therefore decided to monitor crack-growth via the changes in specimen deflection as transmitted through the loading beam. Beam movement could

be conveniently detected by means of an Instron electro-magnetic extensometer which obviated contact either with the specimen or the loading mechanism, and whose output was recorded automatically throughout the life of each specimen. Typical beam displacement curves are shown in Figures 17 - 20.

Beam movement has been used on previous occasions to follow crack growth[131] and is a satisfactory method provided an adequate correlation can be obtained between crack length and beam position. The method relies on the three-point bending relationship:

$$D = \frac{5BWl^3}{384M} \qquad (11)$$

in which D is the deflection from the zero-stress equilibrium position, M is the bulk modulus and l is the specimen length between the outer knife-edges. A correlation for pre-cracked specimens is normally obtained by allowing environmental cracks to progress to various $(\frac{a}{w})$, but without fracture. The test-pieces are then removed from the corrodent and broken open to allow direct measurement of crack length.

In the present case, with insufficient specimens available for the above method, crack-length data was obtained from all the failed SEN specimens for which deflection records were available. The non-linear correlation obtained between crack length and recorded beam displacement is discussed in section 5.3.2.

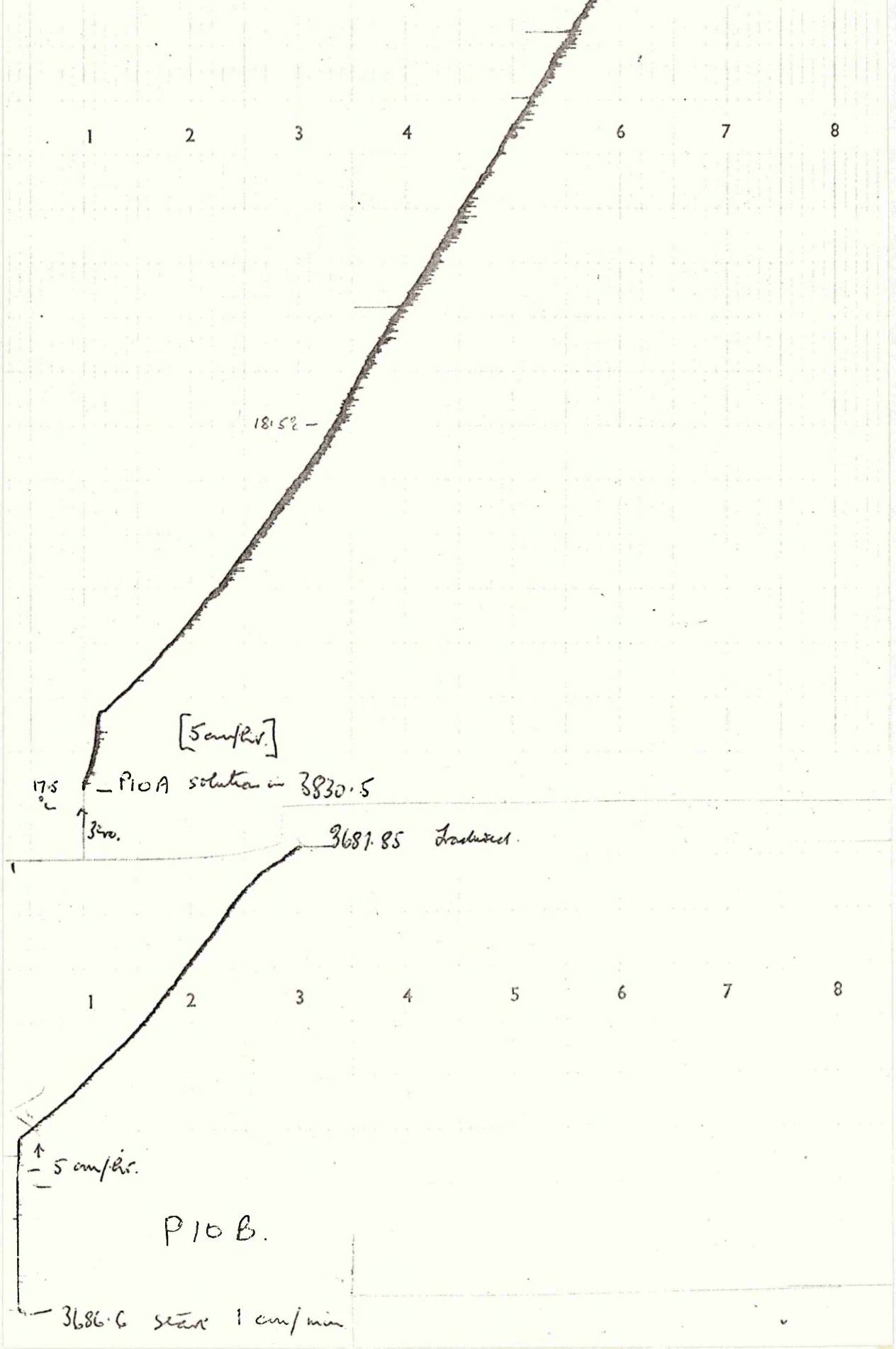

Figure 17: Load - displacement curves

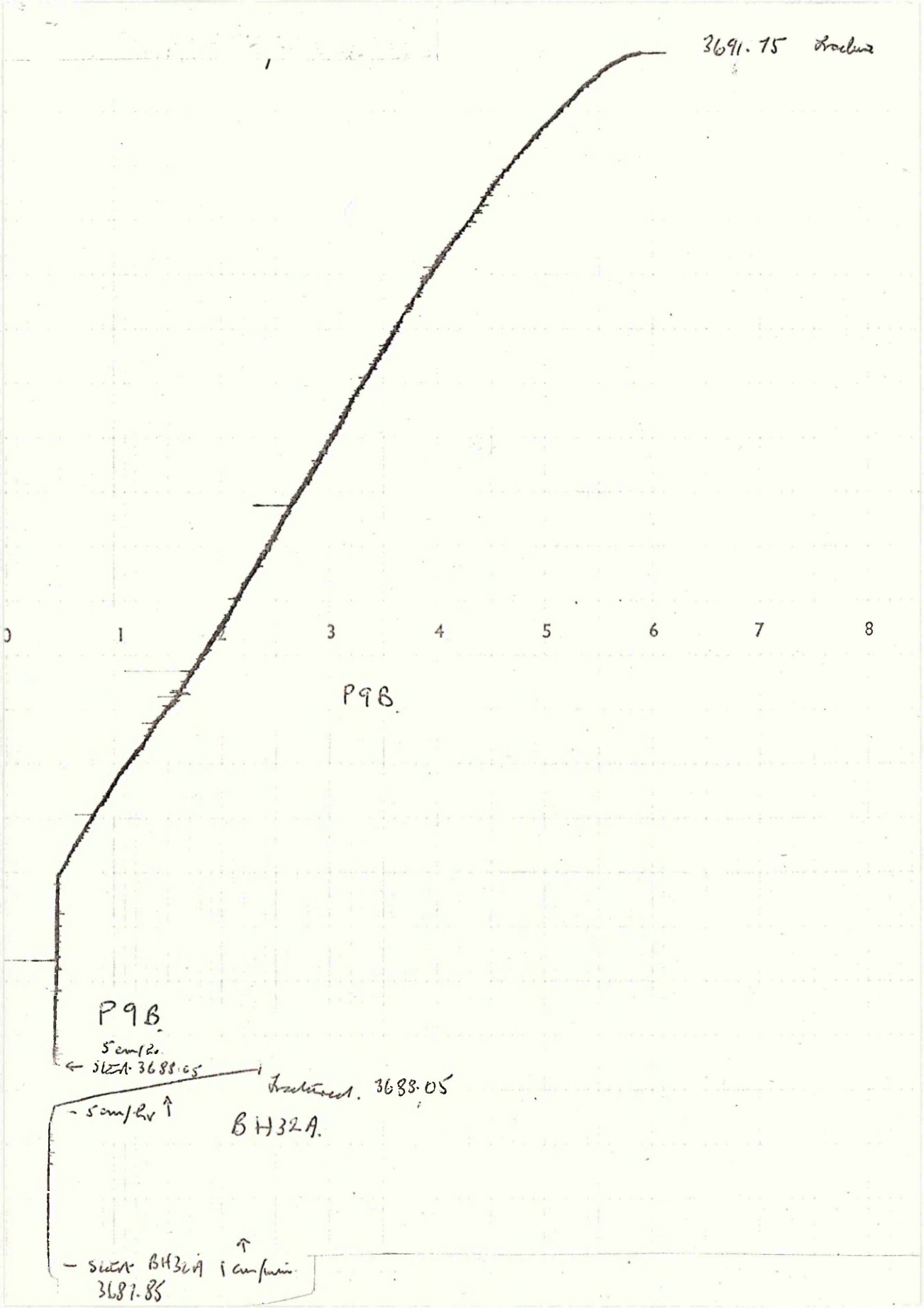

Figure 18: Load - displacement curves (cont.)

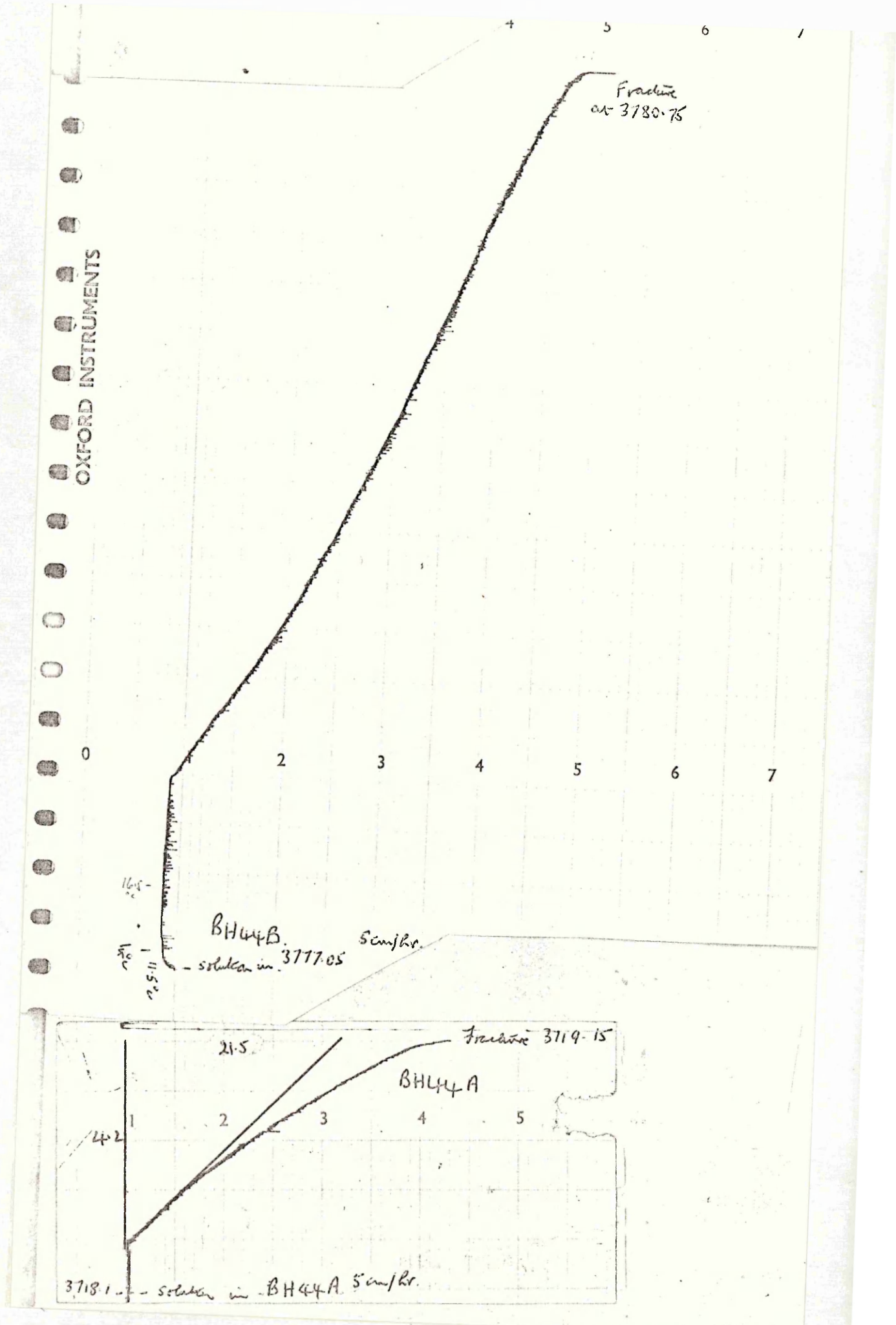

Figure 19: Load - displacement curves (cont.)

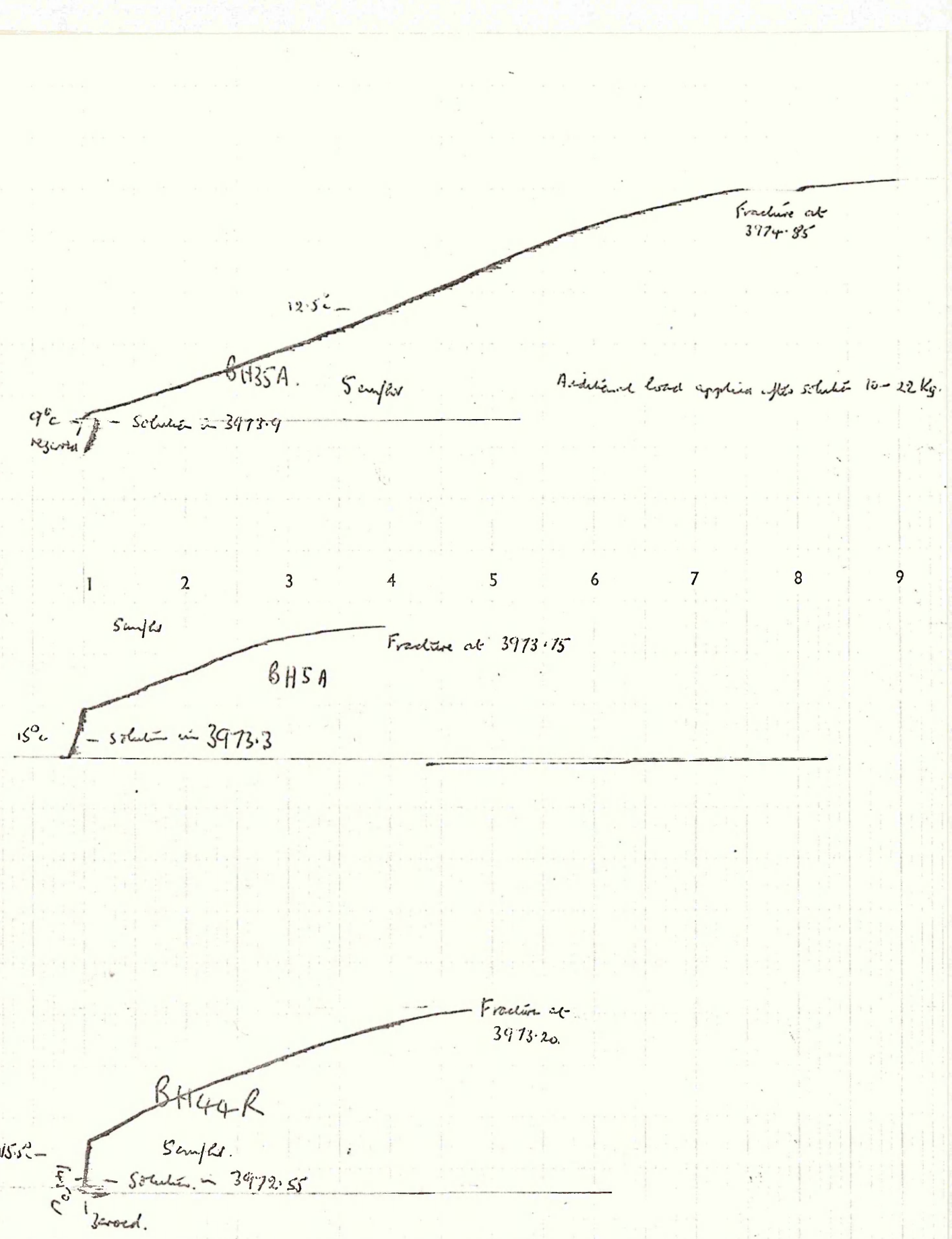

Figure 20: Load Displacement Curves (cont.)

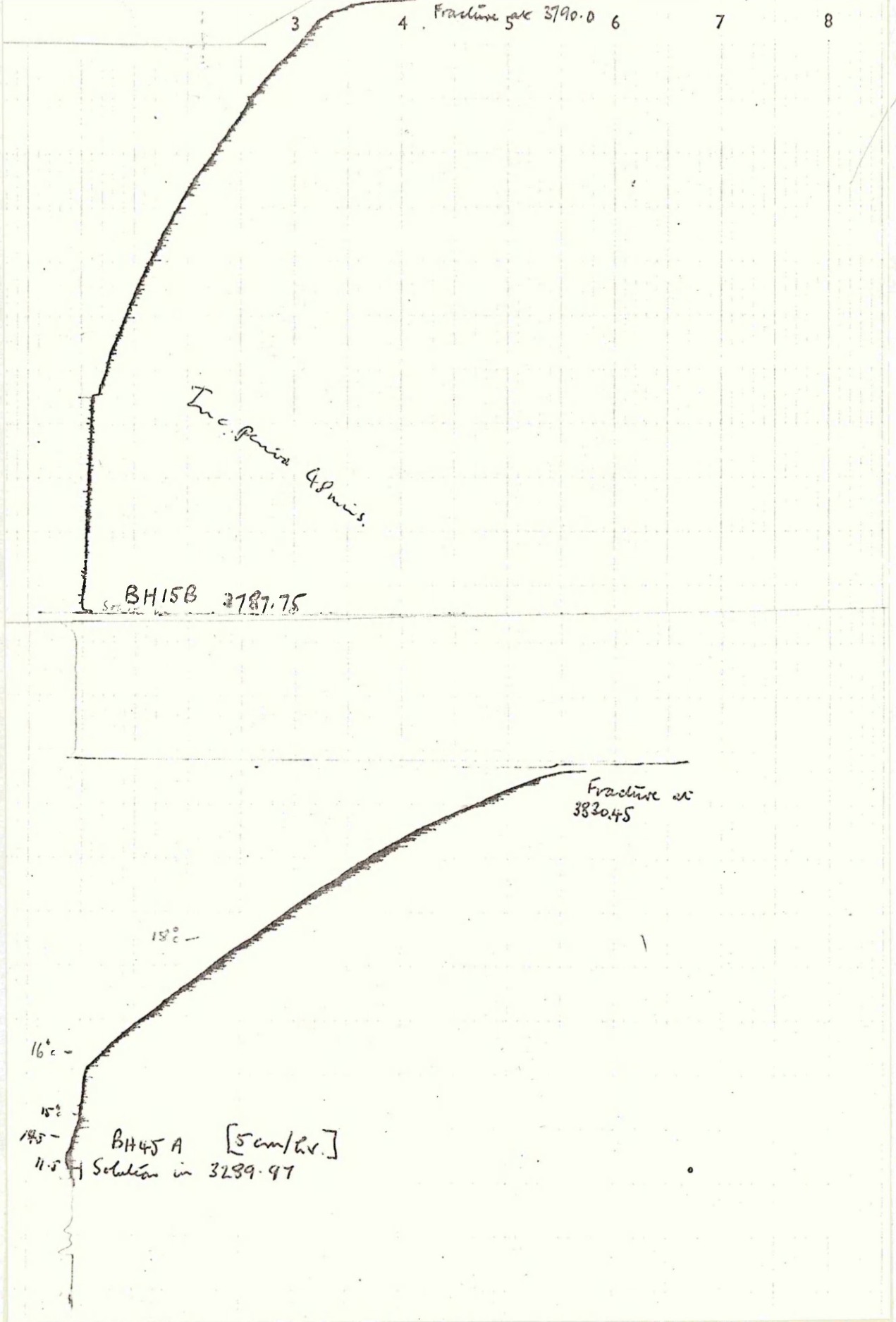

Figure 20: Load Displacement Curves (cont.)

To calculate average growth rates, chart deflections were extracted in pairs and the corresponding crack lengths obtained from the equation of best fit. Successive growth rates calculated from the record of any one specimen are likely to become progressively more inaccurate as growth proceeds, due to crack branching and changes in microstructure along the crack path.

4.7 DETERMINATION OF MECHANICAL PROPERTIES

4.7.1 Tensile Properties

Replicate sub-standard tensile test-pieces from sheet material were tested using a hard-beam, Instron testing machine at a crosshead speed of 2 mm/min.

It was however, impractical to test submerged-arc welded material in the same way. For any consideration of the validity of fracture-toughness measurements, yield-stress values for particular regions are required, but with the weld geometry used in the present work, the necessary consistent through-thickness microstructure cannot be obtained.

Recourse to hardness data is possible in order to obtain an estimate of tensile strength, using previously published correlations[126]. Hardness transverses were, therefore, carried out on each thickness of welded material in both the as-welded and aged conditions.

4.7.2 Fracture Toughness Testing

Fracture toughness measurements in air were made using precracked SEN specimens held in the same three-point bending jig as that used for cracking tests, and stressed in an Instron hard-beam testing machine. The recommended practice for Plane-Strain Fracture Toughness Testing[126] was followed except that no attempt could be made to follow crack-growth with a clip-gauge. Fortunately, the load/displacement records using the standard instrumentation were essentially linear with no 'pop-in' behaviour. This enabled estimates of toughness K_Q, to be made from the conventional relationship for SEN three-point bend specimens with L = 4W:

$$K_Q = \frac{P_Q Y}{B\sqrt{W}} \qquad (12)$$

in which P_Q is the maximum load attained during the test, and Y is the tabulated compliance function[66] for the particular $(\frac{a}{w})$ value of each specimen.

4.8 FRACTOGRAPHY

4.8.1 Optical Macroscopy

Macrophotographs were taken of all fracture surfaces after cracking in hydrogen sulphide, together with some after K_{1C} determinations in air. Any corrosion products were removed with detergent prior to examination. A magnification of approximately 7 proved sufficient both to reveal structural features such as coarse-grained regions prior to scanning microscopy, and enabled measurements of

crack area to be made. Irregular growth during cracking necessitated five replicate determinations by planimeter on photographs of each individual fatigue and environmental crack. Mean crack lengths could then be calculated from specimen thickness by division.

4.8.2 Scanning-Electron Microscopy

Selected areas of these fracture surfaces representative of stress corrosion cracking in the four basic weld structures were examined on Cambridge and Phillips stereoscan instruments. Attention was concentrated on regions where transition between different modes of cracking occurred. Whilst most of the areas were observed in two dimensions, interpretation of some was aided by the use of stereo-pairs, produced by taking two successive fractographs of each area with a 6^{o} difference in tilt between them. Subsequent examination through a binocular viewer provided a three-dimensional effect. This technique was particularly useful in observing stretch-zones which could occur at the onset of environmental cracking.

5. EXPERIMENTAL RESULTS

5.1 MICROSTRUCTURAL VARIATIONS

Microstructures representative of aged materials from each basic zone are shown in Figures 21 to 24.

Remote material unaffected by welding consisted of massive martensite, Widmanstätten in appearance, formed from completely recrystallised prior-austenite. A few small islands of retained austenite were prominent in both sheet and plate materials, as were particles of titanium carbonitride and titanium sulphide, although positive identification of these was not attempted. The unaffected plate structure was much coarser than that of sheet material, and in the former, at a magnification of $^{x}500$, thin boundaries of untransformed austenite were evidently separating some martensite colonies (Figure 21(a)).

The visible limit of each heat-affected zone was defined by the macroscopically dark etching band characteristic of the 650^{o}C peak temperature isotherm in welded maraging steels. Only thin bands, some 0.2 mm wide, were formed during the single pass welds, but in plate, duplex bands approximately 4 mm wide occurred by virtue of reheating from the second passes which originated from slightly differing arc positions. Coleman and Jordan[43] have, by X-ray analysis, shown the structure of dark bands to be diffuse martensite containing fine reverted austenite,

x500
Etched in
Mixed Acids

Figure 21(a): Retained Austenite at Prior Grain Boundaries in Parent Metal

x100
Etched in
Mixed Acids

Figure 21(b): General Microstructure of Parent Plate: Widmanstatten Martensite

giving the overall mottled appearance shown in Figures 22(a) and 22(b).

Approaching the weld interface, the progressive development in grain-size with peak temperature resulted in increasingly acicular martensite plates. The interface itself was distinguished by a linear vein of reverted austenite with associated cell boundary austenite together forming a single grain width band. Figures 23(a), 23(b) and 27 illustrate this feature, together with the sudden appearance also of retained austenite, whose coarseness exceeded that found in the weld centres.

Both TIG and submerged-arc weld metals consisted of martensite originating from cored equiaxed grains and containing interdendritic pools of retained austenite, as depicted in Figures 24(b), 25 and 26. The main difference between the weld structures lay in the size and frequency of such pools, both statistics being slightly greater in TIG weld metal.

Despite the hot-cracking observed at the plate run-off region, neither plate nor sheet test-pieces showed any evidence of hot-shortness such as grain boundary liquation. With porosity also absent, no defects were found which could have markedly influenced subsequent cracking behaviour.

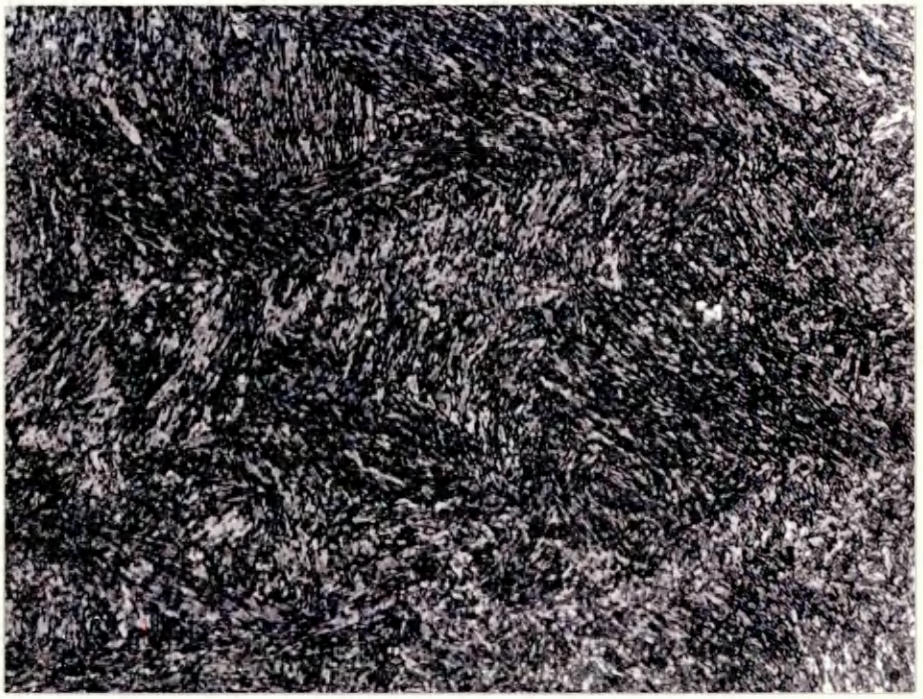

x500
Etched in
Mixed Acids

Figure 22(a): Dark-Etching Band: Submerged-Arc Weld Showing Fine Dispersion of Retained Austenite

x100
Etched in
Mixed Acids

Figure 22(b): Dark-Etching Band: Submerged-Arc Weld General Appearance

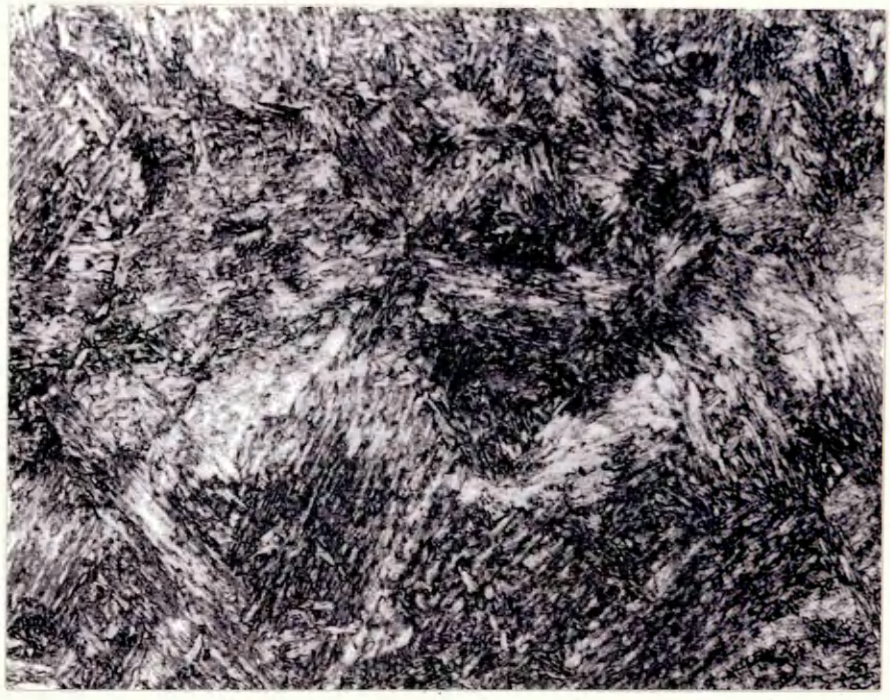

x500
Etched in
Mixed Acids

Figure 23(a): Prior-Austenite Grain Boundaries at Interface of Submerged-Arc Weld

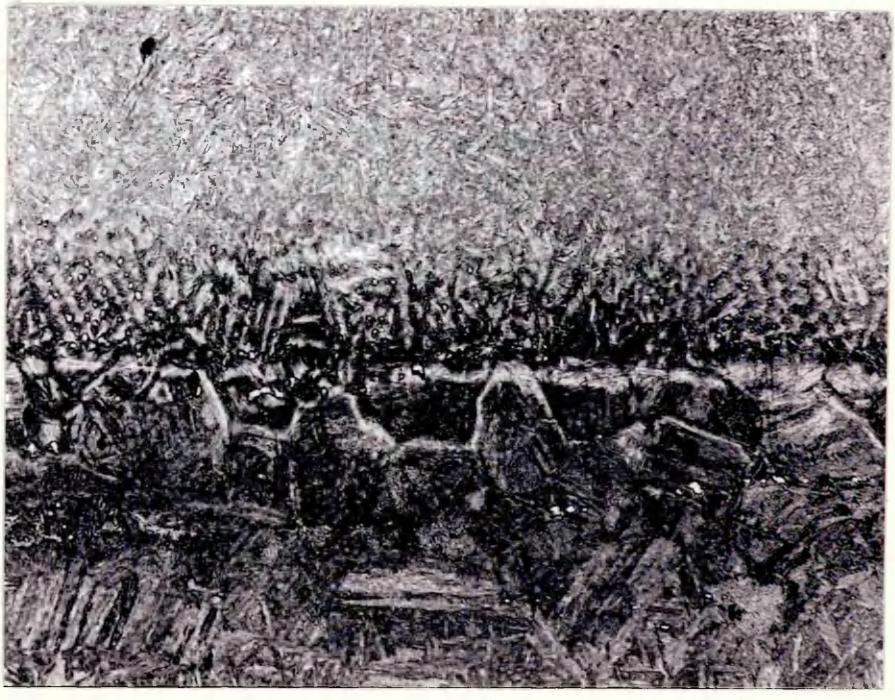

A.Z.

RFACE

LD
TAL

x100
Etched in
Mixed Acids

Figure 23(b): Interface between Submerged-Arc Weld and H.A.Z., showing Increase in Retained Austenite Coarseness

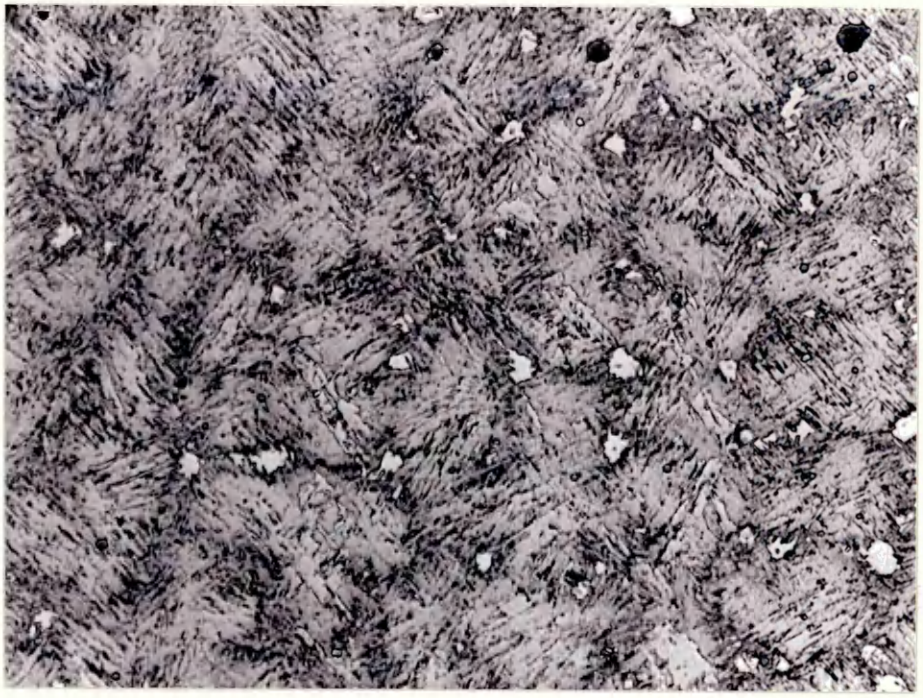

x500
Etched in
Mixed Acids

Figure 24(a): Pools of Retained Austenite in Submerged-Arc Weld Metal

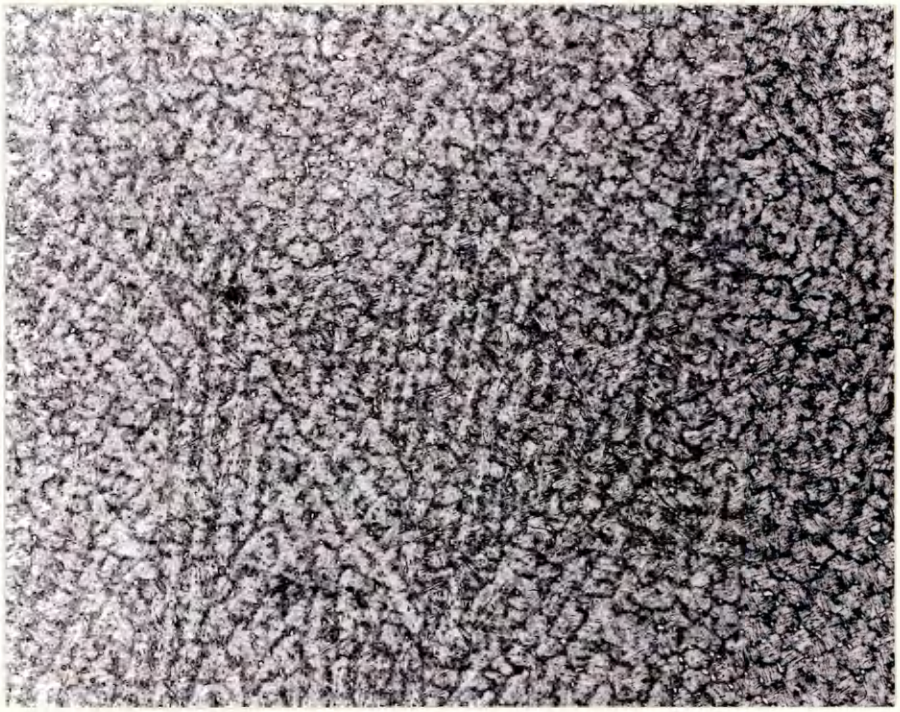

x100
Etched in
Mixed Acids

Figure 24(b): General Structure of Submerged-Arc Weld showing Equiaxial Grains at Weld Centre

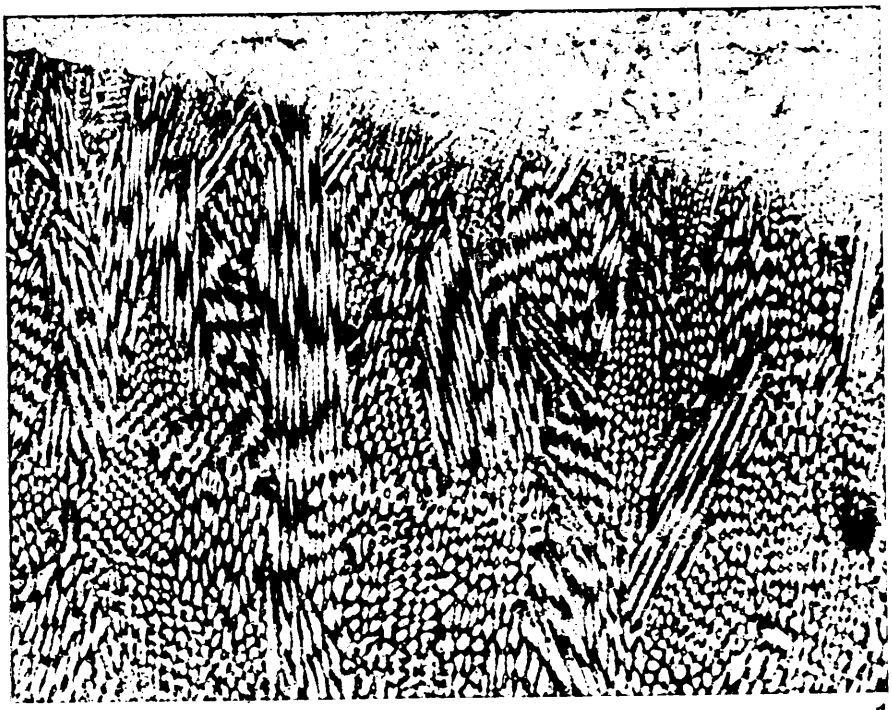

x100
Etched in
Mixed Acids

Figure 25: Feathery Dendrites near Interface of TIG Weld Metal

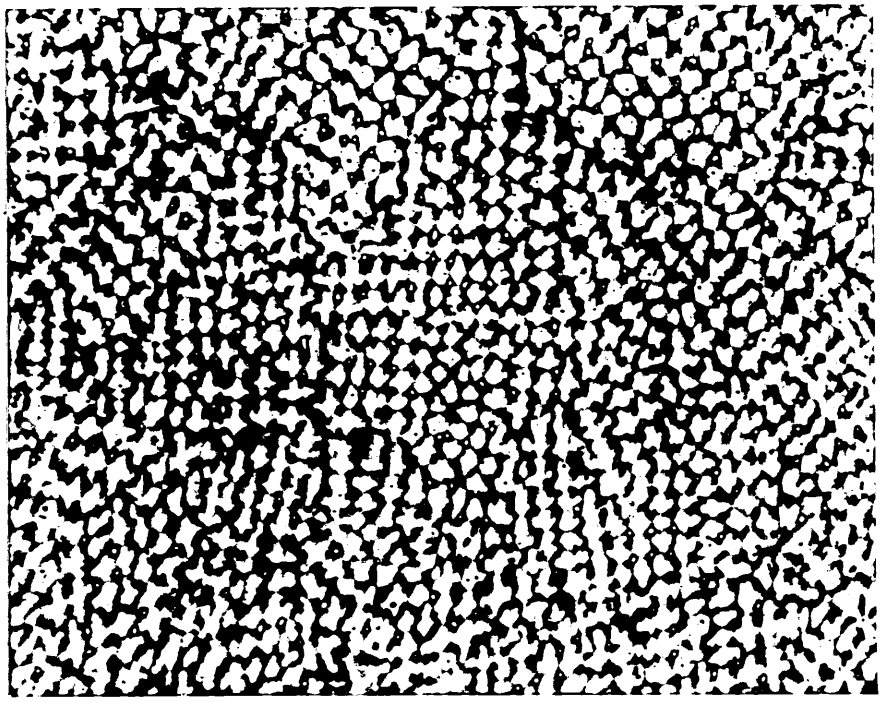

x250
Etched in
Mixed Acids

Figure 26: Structure of TIG Weld Metal, showing Pools of Retained Austenite

Weld Metal H.A.Z.

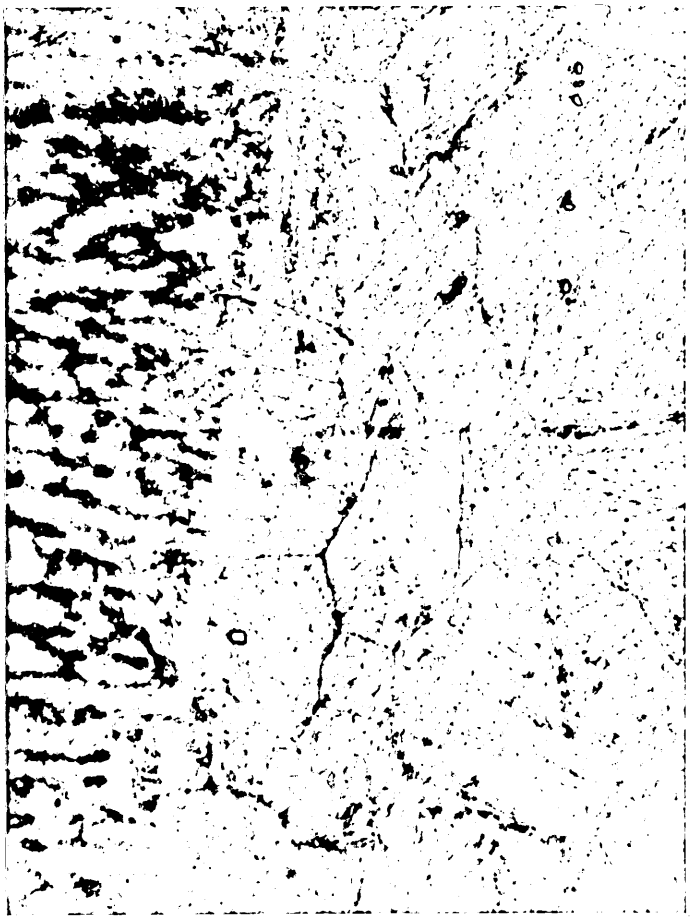

x500
Etched in
Mixed Acids

Figure 27: Interface Structure of TIG Weld, showing Parallel Ghost Band at Actual Interface

5.2 MECHANICAL PROPERTIES

5.2.1 Hardness

Hardness traverses across materials both as-welded and after ageing are shown in Figures 28(a) and 28(b), which display the conventional variations with peak temperature in the H.A.Z. Maximum hardness of ~530 V.P.N. in as-welded plate occurred 7 mm from the interface, compared with 4 mm for the TIG welded sheet. On ageing, previous hardness maxima became minima and vice versa, in the dark-etching zone and interface regions respectively. The distinct reduction in hardness in the dark-etching zones near submerged-arc welds occurred in two adjacent bands each some 0.5 mm wide, and indicated an overageing effect in material already subjected to a peak temperature of ~650°C.

Comparison between sheet and plate material, aged after welding, showed only marginal differences between them in either remote regions or weld metal, with plate material the hardest in each case:

Material	Weld ($V.P.N._{30}$)	Remote ($V.P.N._{30}$)
Sheet	537	586
Plate	555	600

(Means of 5 measurements)

Table 17: Comparative Hardness of Sheet and Plate Materials

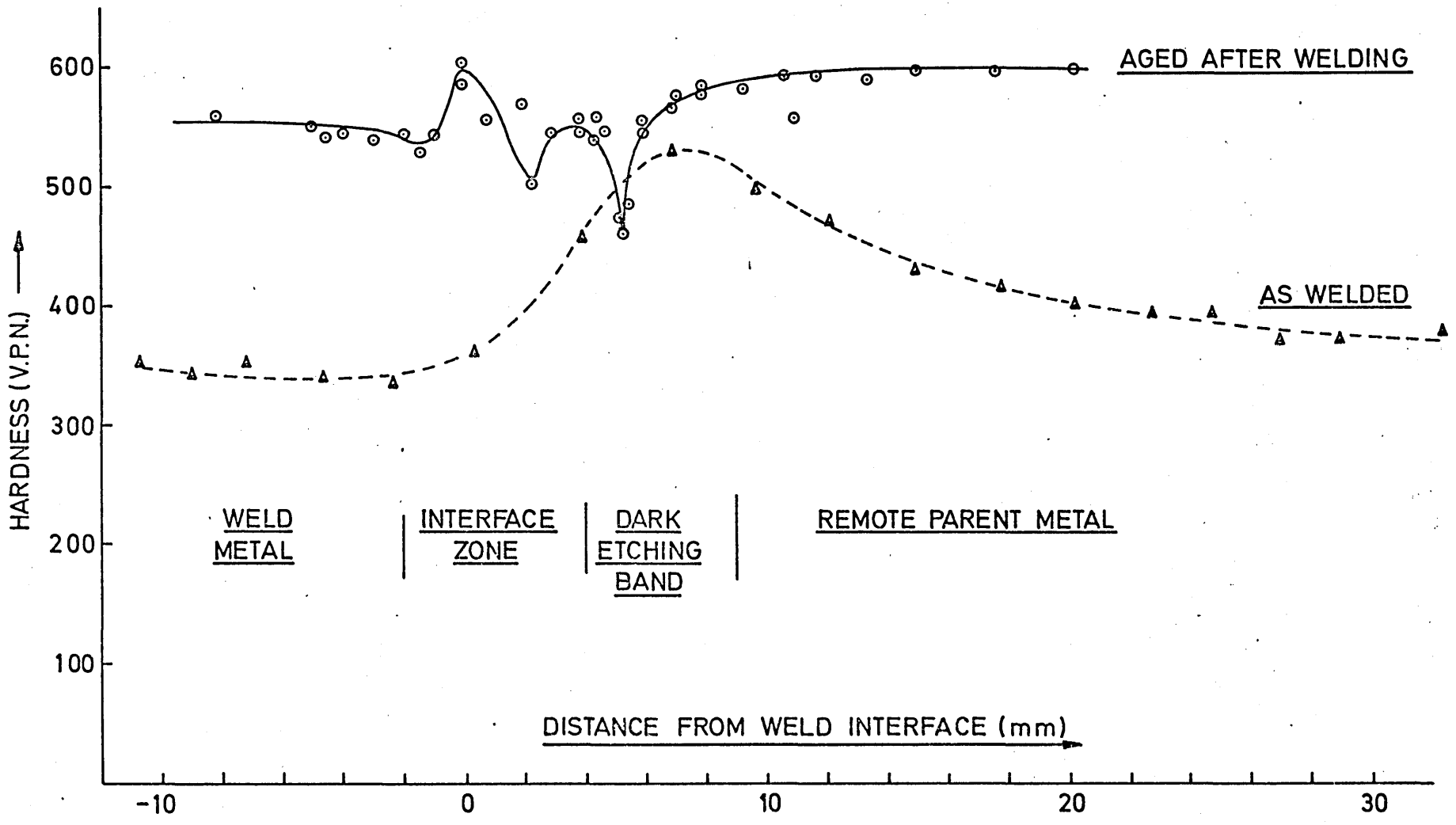

FIG. 67 Hardness variation across submerged-arc weld and heat-affected zone.

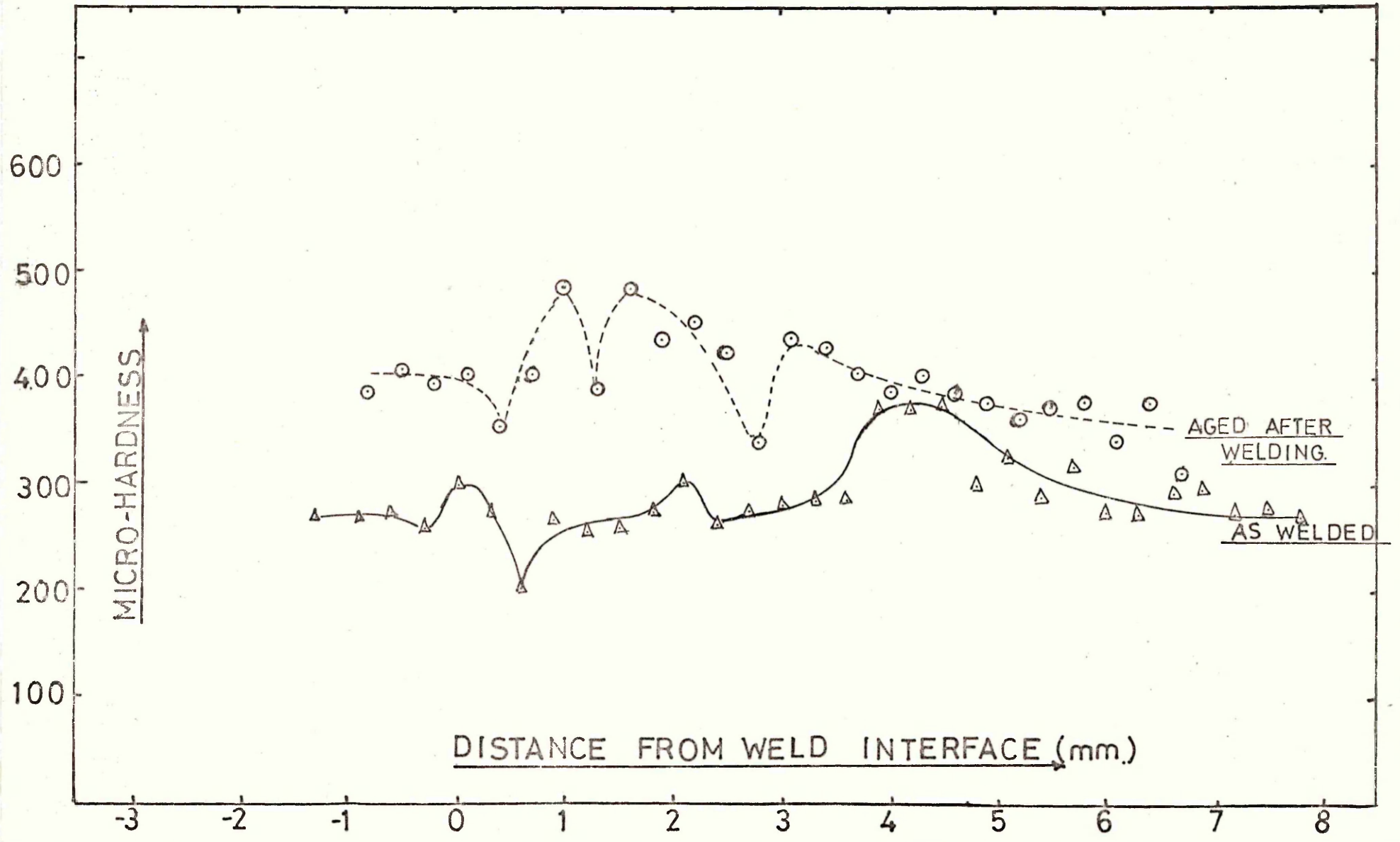

Figure 28(b): Micro-Hardness Transverse Across TIG Weld and HAZ

5.2.2 Fracture Toughness

Some 17 fracture toughness determinations on submerged-arc welded plate were carried out in air, using rising-load tests on specimens previously fatigue-cracked to $(\frac{a}{w})$ values of ~ 0.5.

The majority of load-displacement curves obtained were completely linear up to the point of fracture, as illustrated in the chart records reproduced in Figures 29(a) and 29(b). In the remainder, the pop-in values all occurred within 2% of the maximum load. In each case therefore, the maximum load achieved was used as the P_Q value from which K_Q was calculated.

Insufficient results were available to justify grouping into the four basic zones, but estimates of the toughness of each could be obtained from the overall variation in K_Q values with distance. Figure 30 shows the substantially lower toughness, ~ 80 MN/m$^{3/2}$, of weld metal compared with the remote metal value of 112 MN/m$^{3/2}$. The maximum toughness of 125 MN/m$^{3/2}$ however, occurred in the dark-etching bands.

In the absence of specific yield stress data for each zone, the validity of K_Q values judged on the criterion

$$(B,a) \geqslant 2.5 \left(\frac{K_Q}{\sigma_y}\right)^2 \qquad (13)$$

cannot be established. If a nominal yield stress of 1700 MN/m^2 is assumed, then only the weld metal toughnesses would

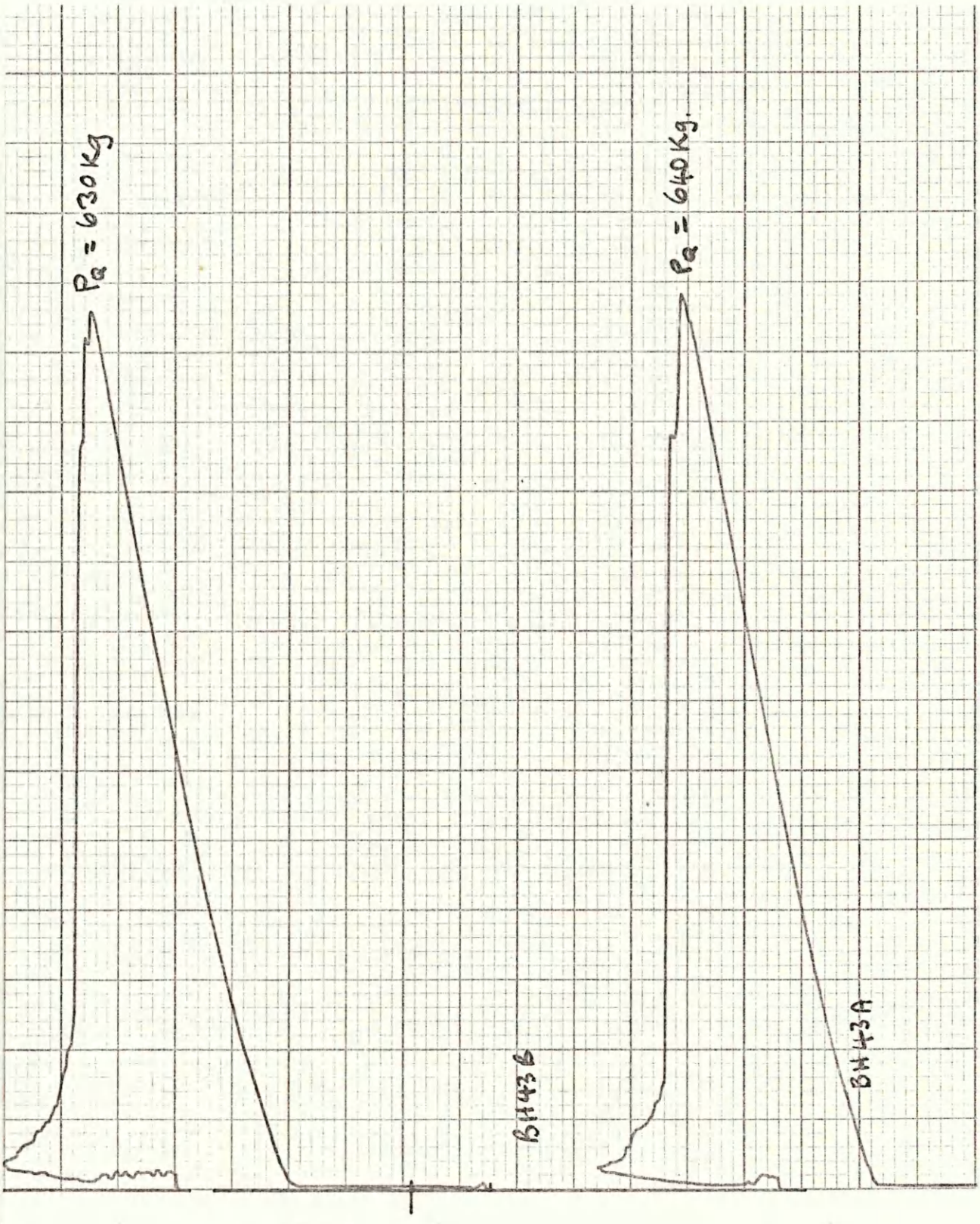

Figure 28: Load-Deflection Curves obtained during K_{1C} Determination, showing Linear Increase to P_Q

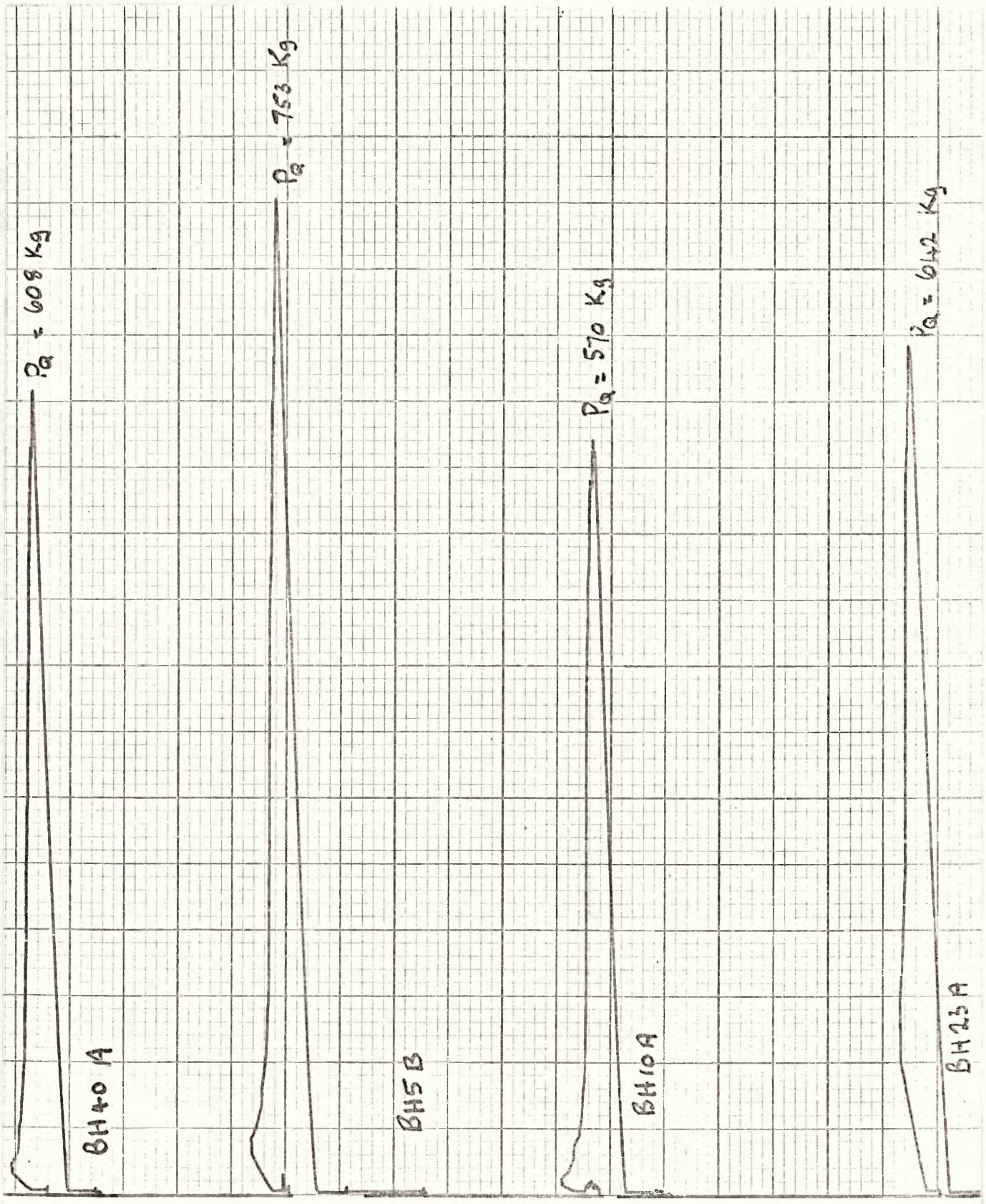

Figure29(b): Load-Deflection Curves (cont.)

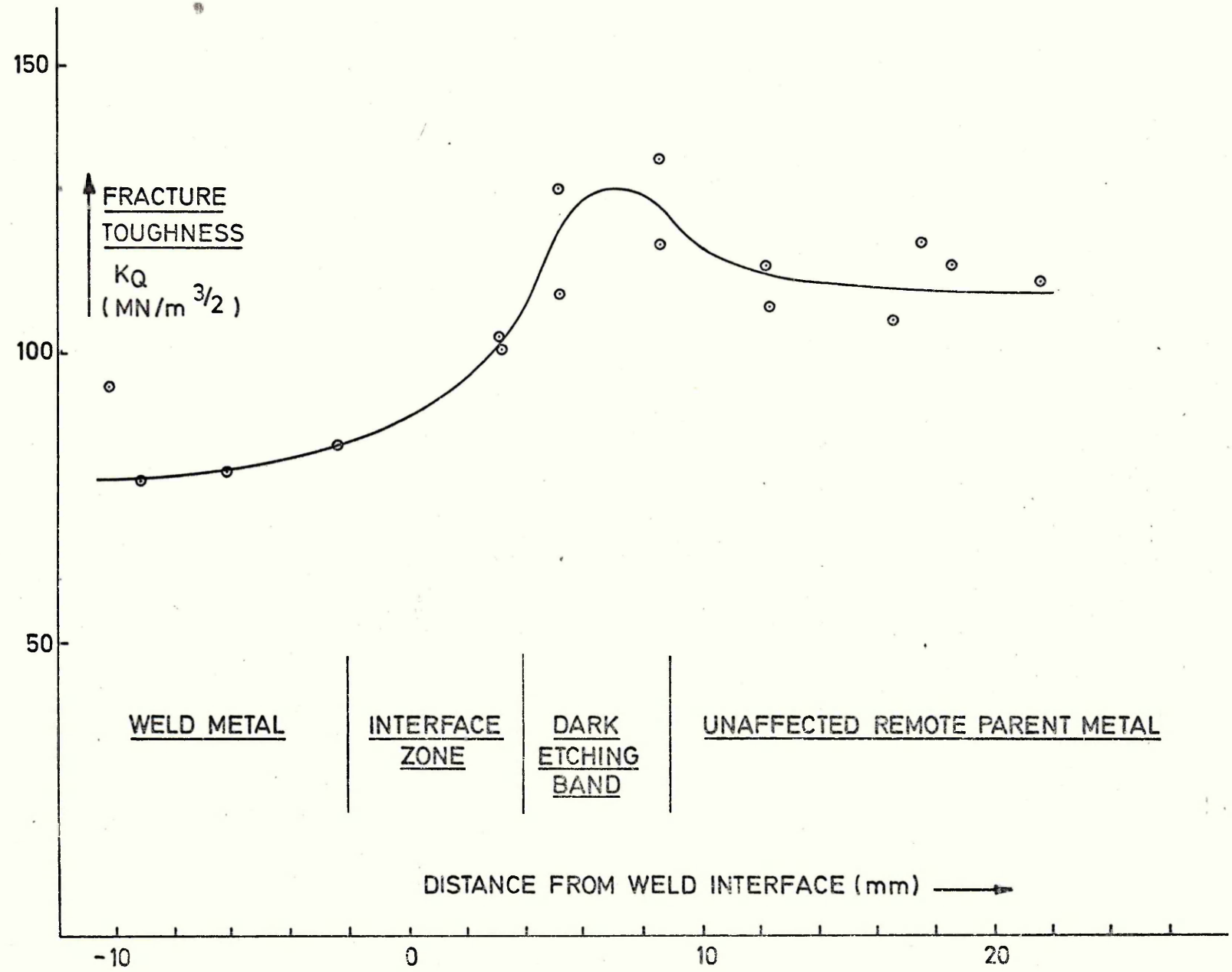

FIG. 30 Variation in fracture toughness across submerged-arc weld and heat-affected zone.

satisfy this condition, while parent metal values would not. In no case however did the shear lip area exceed 5% of the total fracture surface, so that conditions in all tests were certainly close to plane-strain.

5.3 ENVIRONMENTAL CRACKING

5.3.1 TIG Welded Sheet

Initial experiments were carried out with two objectives in mind. The first was to determine simple stress-endurance relationships for both unwelded and welded metal after ageing. Secondly, peak temperature effects were to be simulated by solution-treatment of plain material at excessive temperatures.

The results of anodic exposure at 6.3 ma/cm^2 in salt solution for welded and unwelded sheet are plotted in Figures 31 and 32. Suprisingly, with all conditions of material, rapid failures still occurred at stress levels as low as 10-20% of the nominal U.T.S. In addition, there was no significant departure from linearity in the stress-log (endurance) relationships, although limiting stress-intensities are a common feature of stress-corrosion data.

The endurances of welded material were substantially lower than those of plain sheet over the whole range of stresses examined. At the 50% U.T.S. level, a more than five-fold difference in endurance was evident between welded and unwelded material.

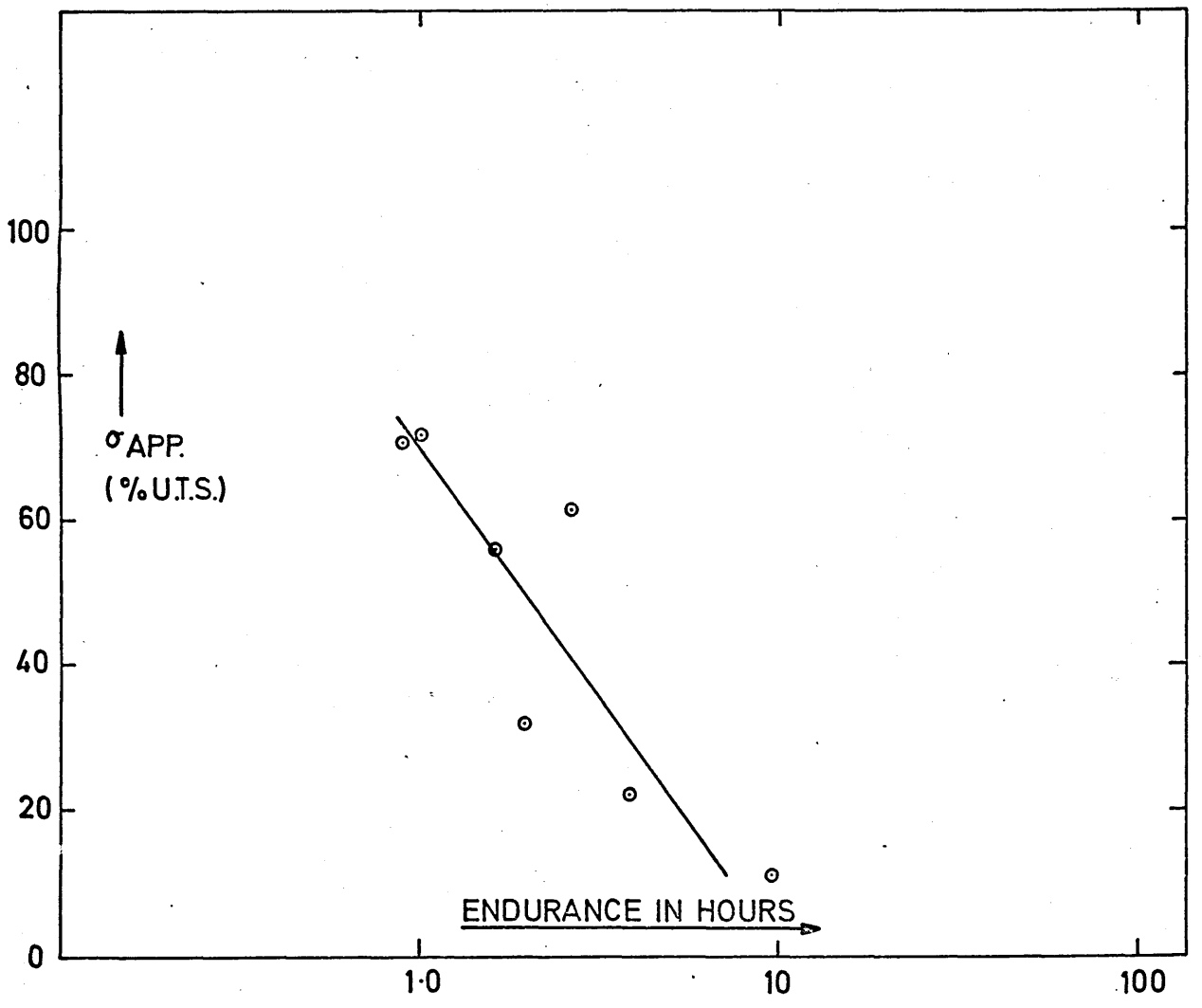

FIG. 31 Endurance of TIG welded maraging steel sheet under impressed current conditions in sodium chloride solution.

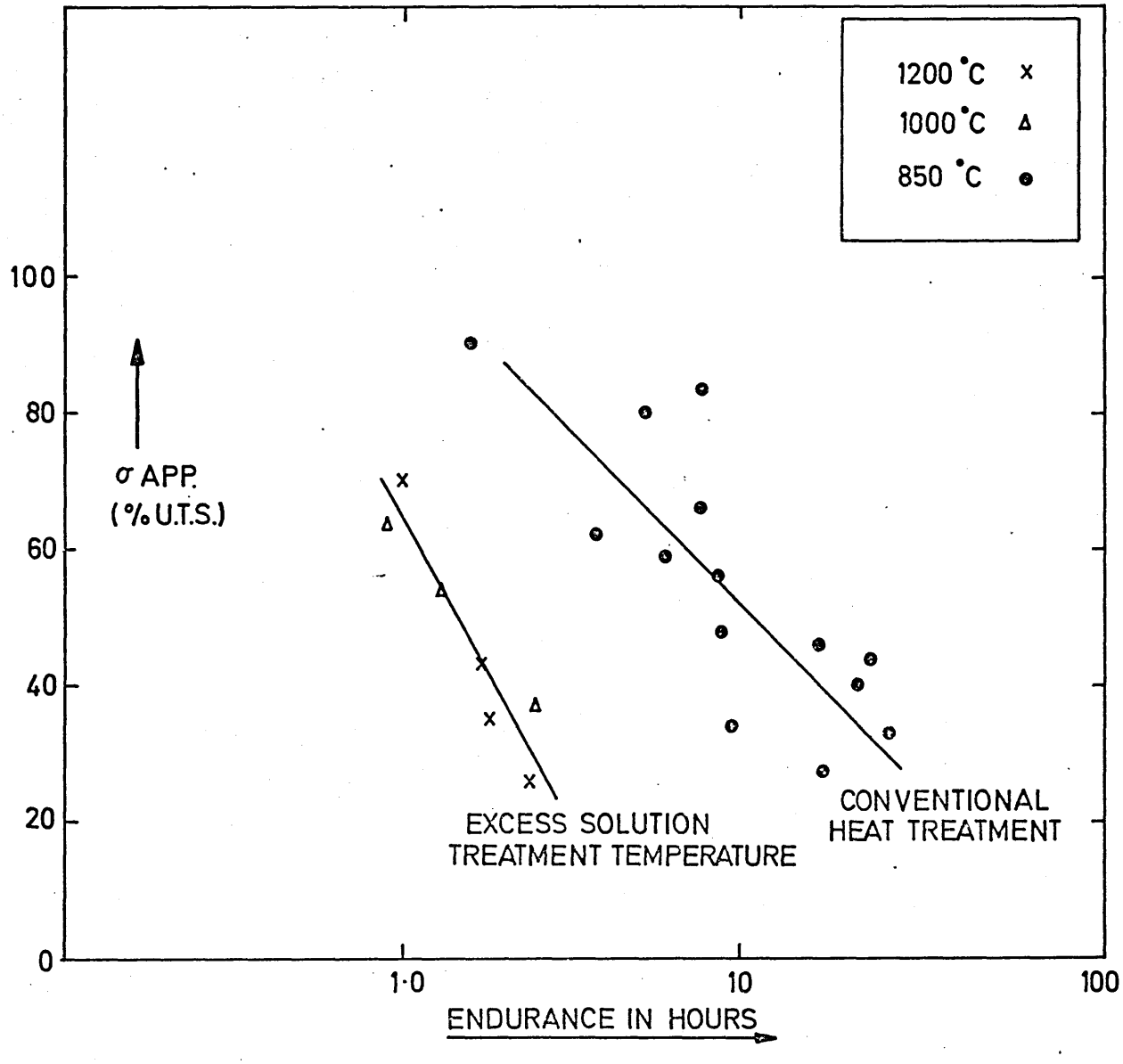

FIG.32 Effect of prior solution-treatment temperature on endurance of maraging steel sheet in impressed current tests (6·3 MA/cm^2)

In all the TIG welded samples tested, fracture occurred immediately adjacent to the weld bead, in the region of maximum grain-growth. Unwelded specimens solution-treated at 1200°C and at 1000°C were therefore used to simulate the grain growth region. Despite their different solution treatments however, there was insufficient evidence to distinguish between their endurances The results were therefore grouped for comparison with conventionally heat-treated material in Figure 32. Within the range of stresses used, endurance emerged as simple exponential functions of stress represented by:

$$E_{815} = 42.08 \exp(-0.028\ \sigma_{app}) \quad (14)$$

$$E_{1000,1200} = 4.57 \exp(-0.023\ \sigma_{app}) \quad (15)$$

$$E_{815+TIG} = 9.22 \exp(-0.030\ \sigma_{app}) \quad (16)$$

where the subscripts refer to solution treatment temperatures and to welding method respectively. The correlation coefficients obtained were all significant at better than the 0.02 level.

	RELATIONSHIP		
	E_{815}	$E_{1000,1200}$	$E_{815 + TIG}$
Correlation Coefficient	-0.799	-0.944	-0.858
Degrees of Freedom	17	5	5
Significance	0.01	0.001	0.02

Table 18: Significance of Stress-Log(Endurance) Relationships

The three most striking features of these results are, (i) the difference between conventional and excessive solution-treatment temperatures, (ii) the agreement between endurances of welded specimens and those having had excessive solution-treatment, and (iii) the similarity between the gradients of the stress-endurance relationships.

The extent to which stress-corrosion alone is responsible for eventual failure can be judged from unstressed control tests carried out under similar galvanostatic conditions. Figure 33 shows the linear variation between loss in U.T.S. and time obtained for unwelded samples exposed at 6.3 ma/cm^2, which lost strength at the rate of 2.5% per hour. Specimens with an endurance say of 10 hours when stressed at 50% U.T.S. would actually have lost only 30% of their strength by stress-corrosion alone.

Losses by stress-corrosion as opposed to electrochemical dissolution, were both current and polarity dependent, as shown in Figure 34, which emphasises the very short endurances to be expected from iron-nickel martensite under cathodic polarisation. Whilst applied currents of either polarity markedly increased cracking rates, the endurances under cathodic polarisation were at least an order of magnitude lower.

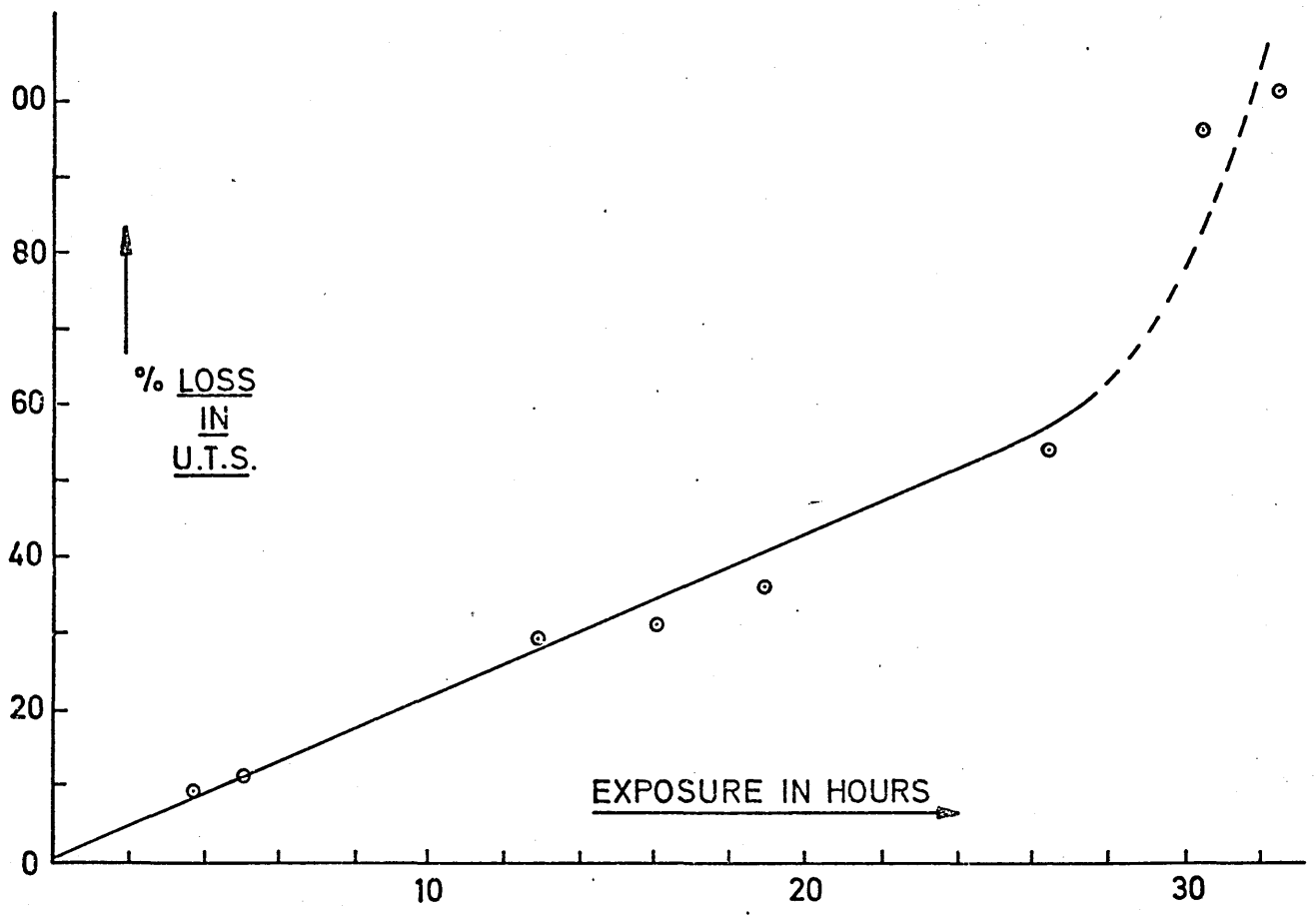

FIG. 33 Tensile losses in sheet maraging steel anodically exposed in sodium chloride at 6·3 MA/cm^2, unstressed.

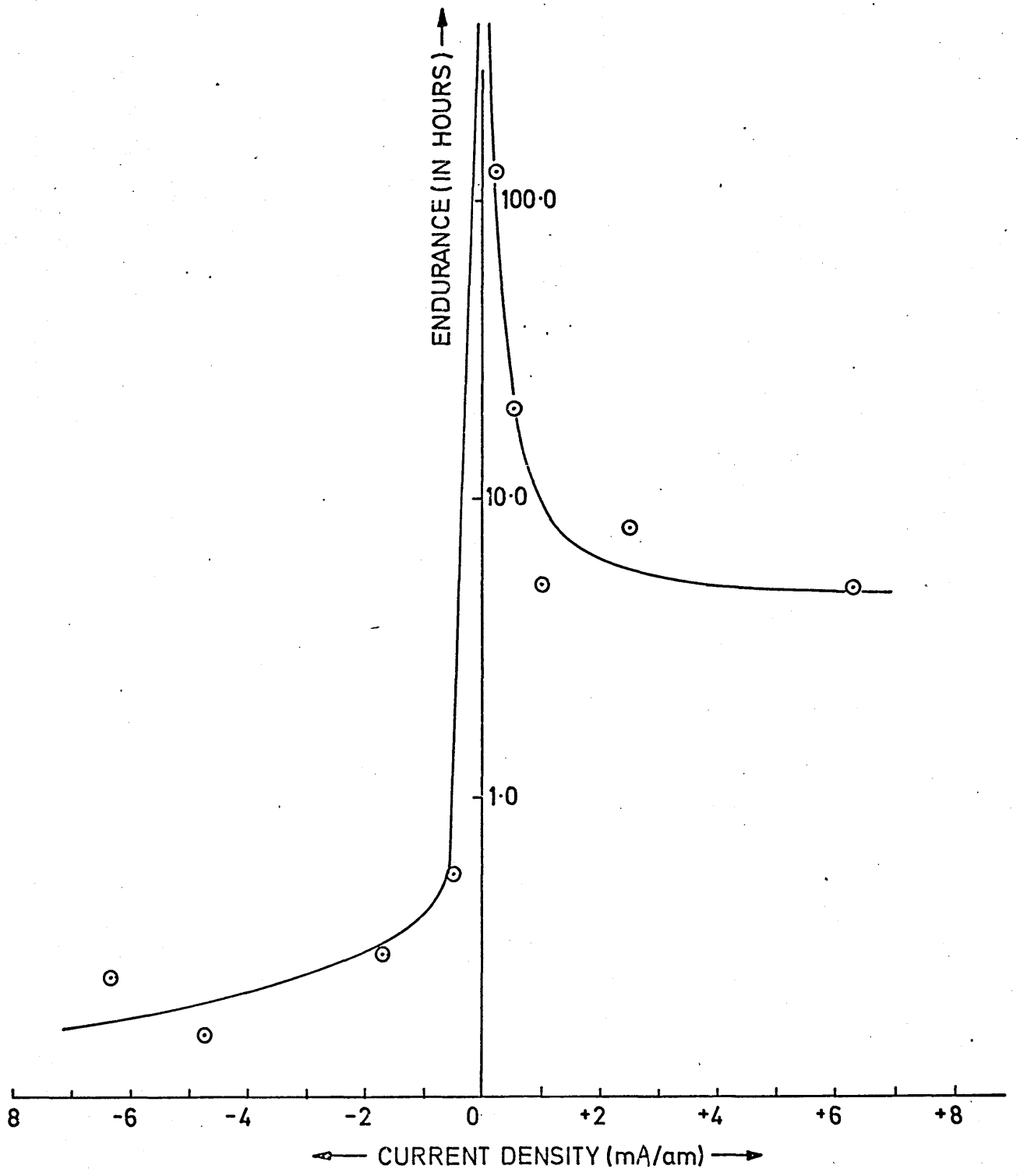

IG.34 Polarity effects on endurance of sheet maraging steel under impressed current conditions.

5.3.2 Submerged-Arc Welded Plate

A study of the behaviour in hydrogen sulphide of pre-cracked welded specimens formed the major part of the present work, in which some 60 samples were tested overall.

Having determined the variation of toughness K_Q with position about the weld interface, as described in Section 5.2, tests at various initial stress-intensities were carried out to establish conventional stress-intensity endurance curves for each of the basic regions. This procedure was adopted since it proved impossible to re-produce specimens which would crack through identical microstructural paths. The results, grouped for each region, are illustrated in Figures 35 to 38. In each of these cases, the endurances used are raw experimental values, i.e. no account has been taken of the incubation periods which proved to be a general feature of many tests.

Considering these results, four main features emerge. One is the marked sensitivity of endurance to initial stress intensity, it having proved impossible to exceed more than 65% of the dry air K_Q value without immediate fracture during loading. The second feature is the rapid increase of endurance at stress-intensities below approximately $0.4K_Q$, which suggested a K_{QSCC} value of 20 - 30 $MN/m^{3/2}$. Thirdly, the similarity between the

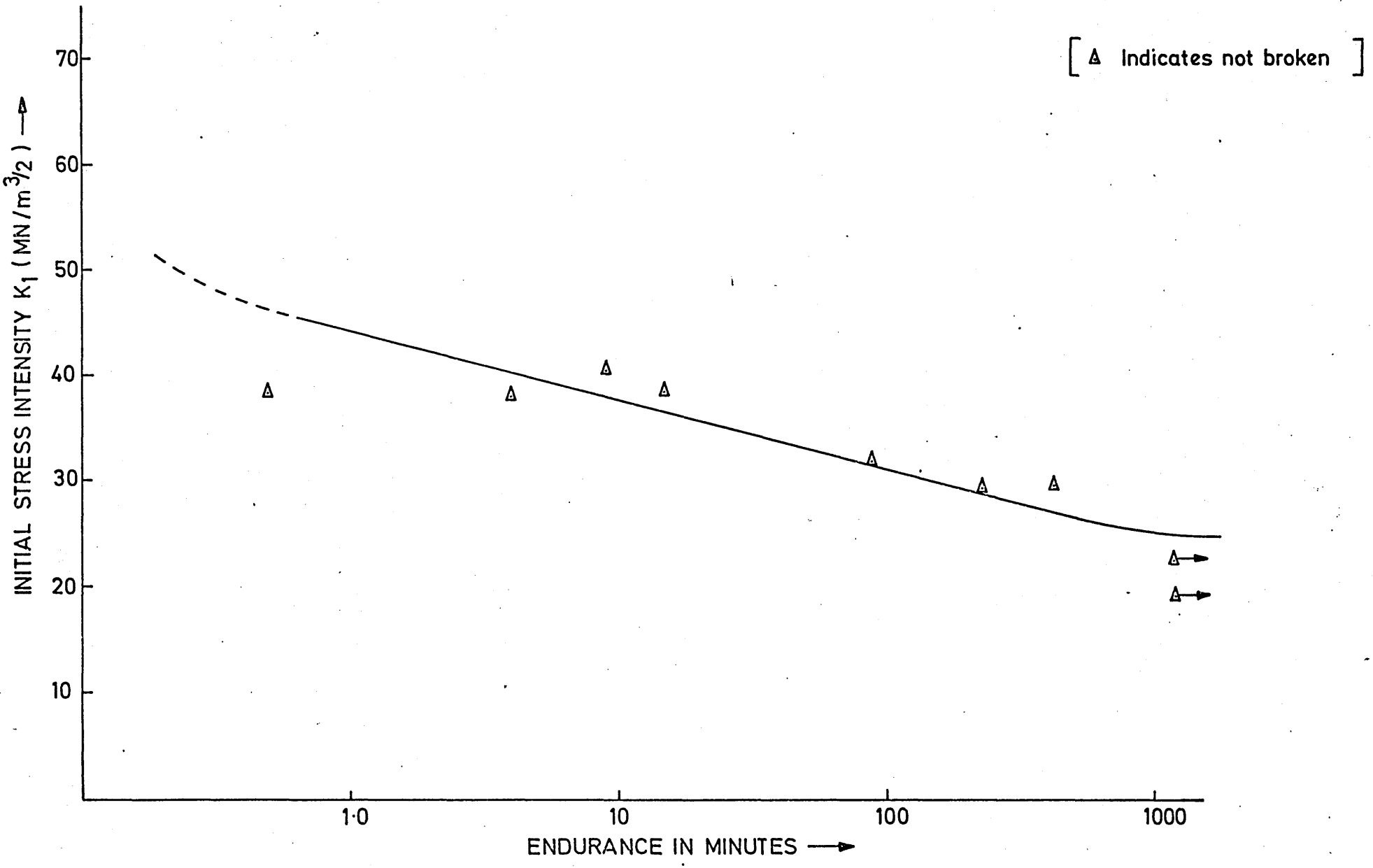

FIG. 35 BEHAVIOUR OF SUBMERGED-ARC WELD METAL IN HYDROGEN SULPHIDE SOLUTION.

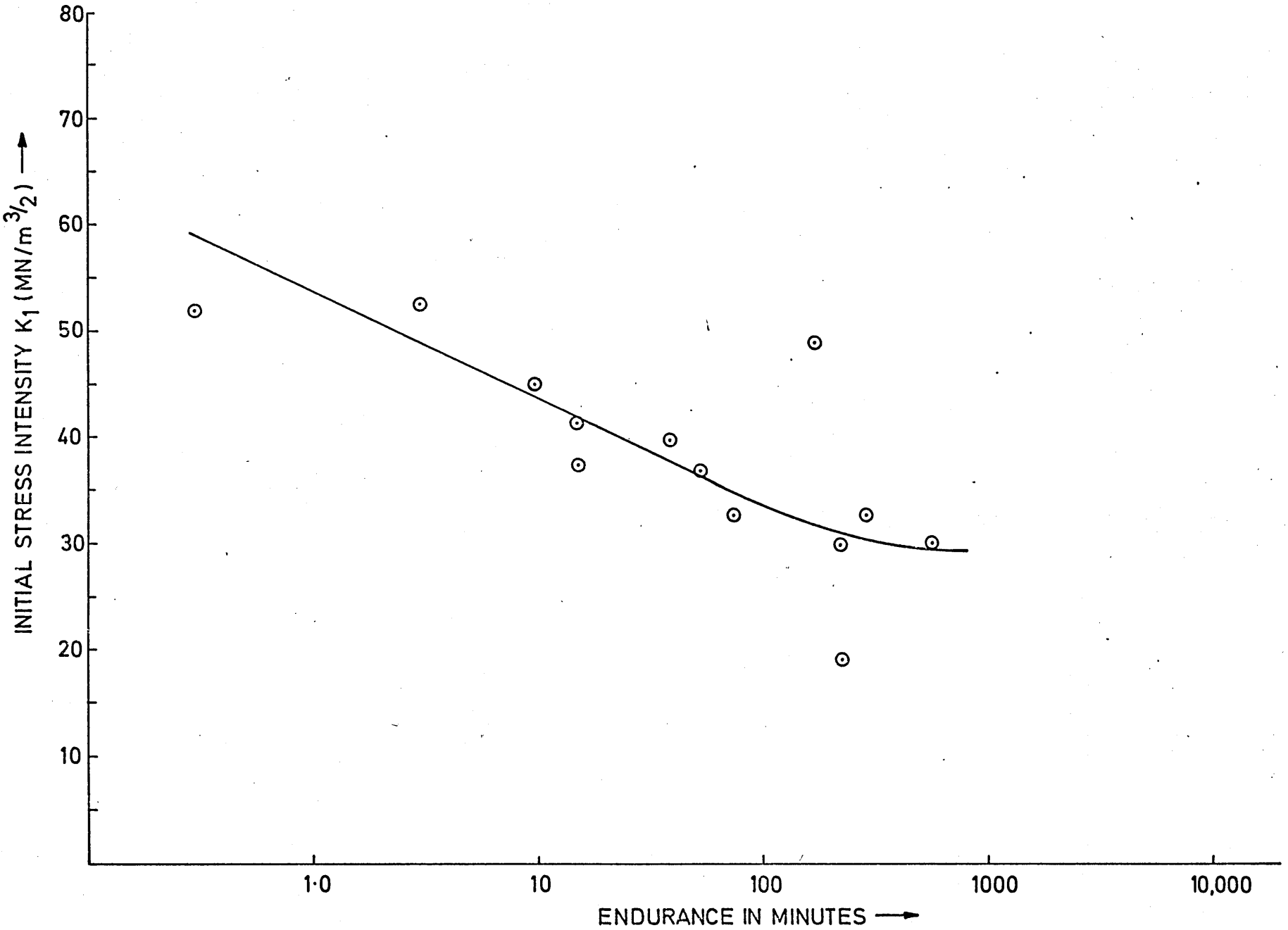

FIG. 36 Behaviour of parent maraging steel material in hydrogen sulphide solution.

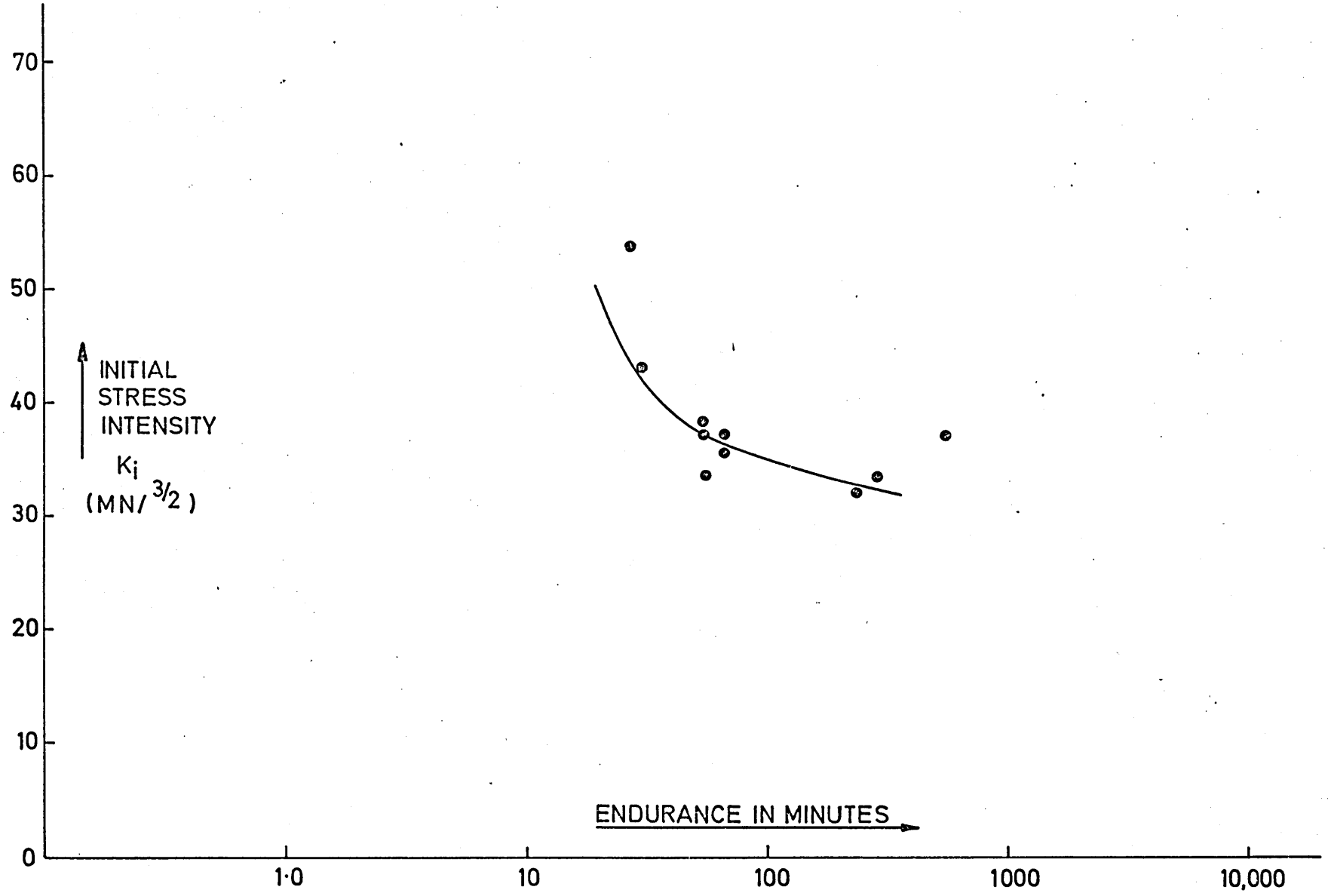

FIG. 37 Behaviour of interface region of welded maraging steel in hydrogen sulphide solution.

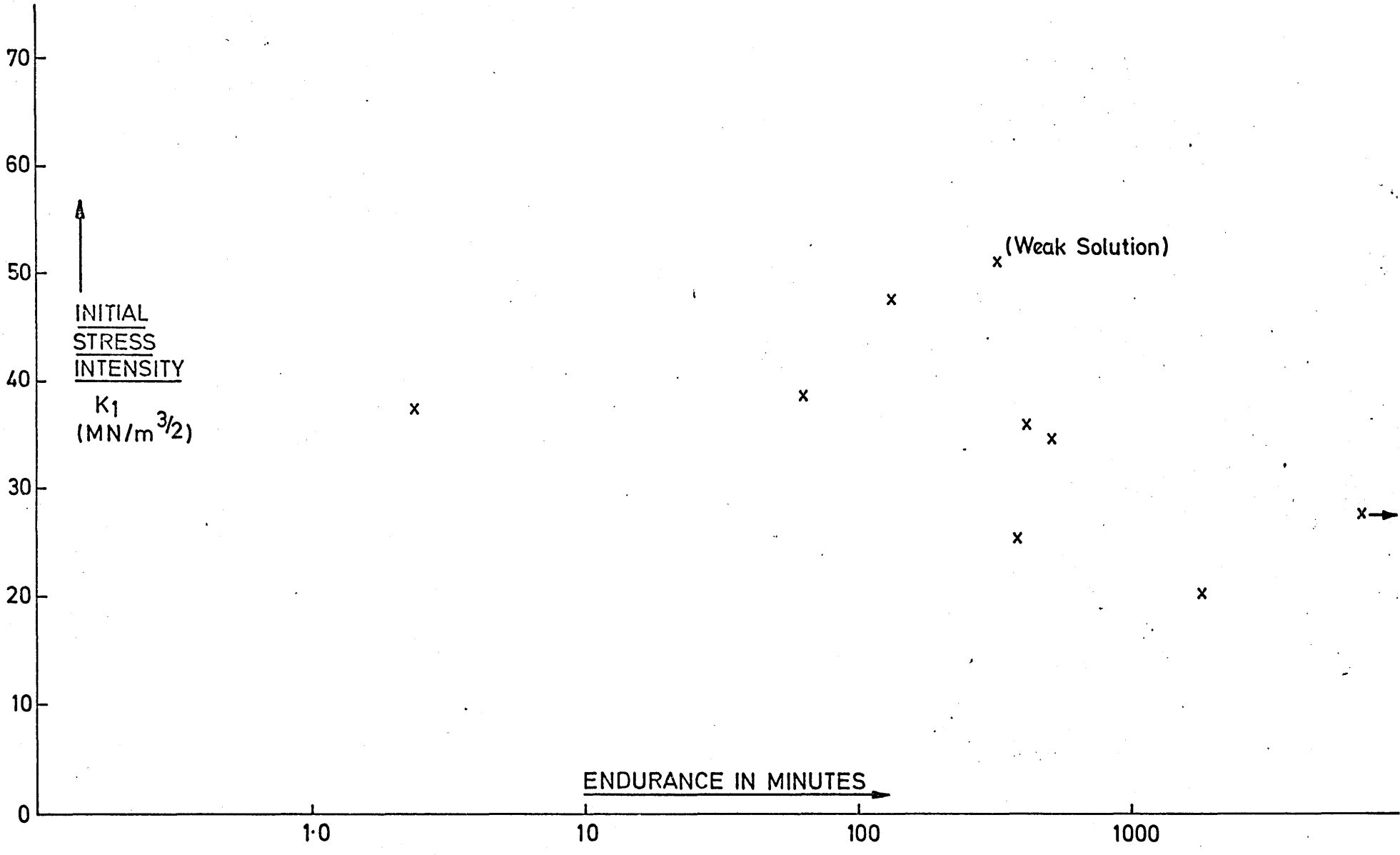

FIG. 38 Behaviour of heat-affected zone maraging steel (Omax - 650°C) in hydrogen sulphide solution

endurances of each basic region, which indicated only minor differences in cracking rates between the main structures. Lastly, the degree of scatter experienced which was disappointing, although scarcely suprising in view of the possible sources of variation within the test-pieces.

Movements of the test-rig beam, recorded automatically throughout each test, provided data both on crack propagation rates and the incubation periods. Typical recordings of beam movement are illustrated in Figures 17-20. Incubation periods proved to be a feature in many of the tests, and generally increased in length as the total endurances increased (Figure 39) although this feature was inconsistent.

Commencement of cracking was marked in the majority of cases by an easily discernible change in beam position, and only in very few instances was there any difficulty in detecting the onset of crack-growth. Once started, the growth rate generally decreased before then becoming more or less constant for much of the duration. Towards the end of most tests, however, growth-rate again increased with the change in effective stress-intensity, and terminated in sudden failure of the remaining ligament. This point was indicated on the recording by the hot-wire pen eventually moving too rapidly to affect the heat-sensitive

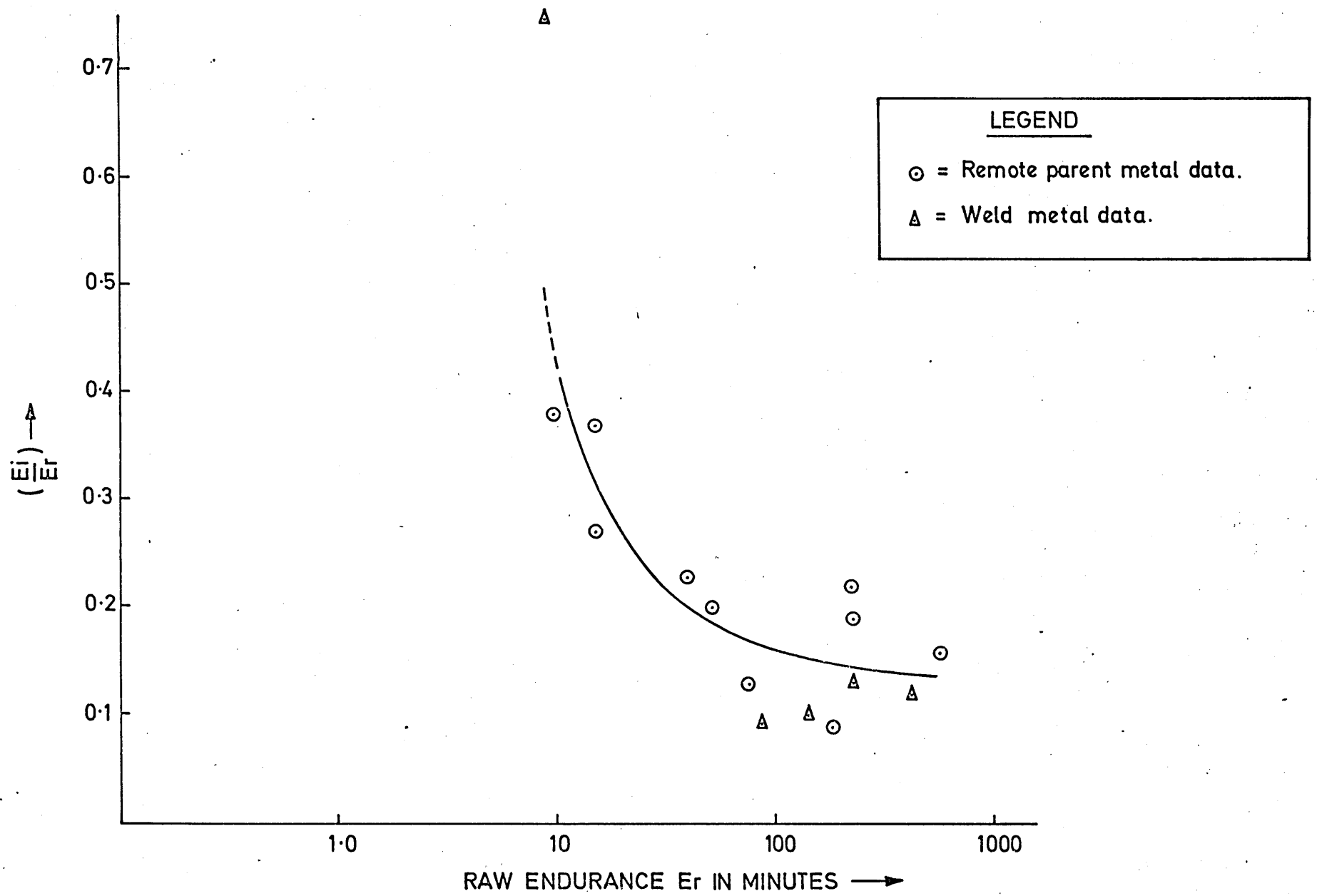

FIG 39 VARIATION OF INCUBATION PERIOD WITH RAW ENDURANCE.

chart paper. Although crude, no accuracy in timing was lost by this method of recording endurances, as they were in all cases confirmed by a separate timer triggered by the descending beam.

Final environmental crack lengths before rapid failure were then related to recorded beam-deflections in order to calculate approximate cracking rates. After allowing for specimen dimensions and load, this data is computer plotted in Figure 40, which illustrates the cubic relationship obtained. The curve should pass through the origin since beam displacement was zero at the start of each test. Assuming that only changes in crack length affect beam displacement, and that the modulus of each basic region is similar, an equation which provided the statistically best description of the data was found by computer analysis to be:

$$(\frac{B\sqrt{W}}{P}).C = 4801.6\bar{z}^3 + 1886.6\bar{z}^2 + 352.70\bar{z} + 34.048 \qquad (17)$$

In this equation, C is the recorded beam displacement, and $\bar{z} = (\frac{a}{W}) - 0.1875$.

Initial cracking velocities were then calculated from the beam displacements which occurred during the first 30 mins of each test.

The results obtained, plotted in Figures 41 and 42 show that for weld metal and parent metal at least, initial cracking velocities were of the order of 10^{-4} - 10^{-3} mm/sec at stress-

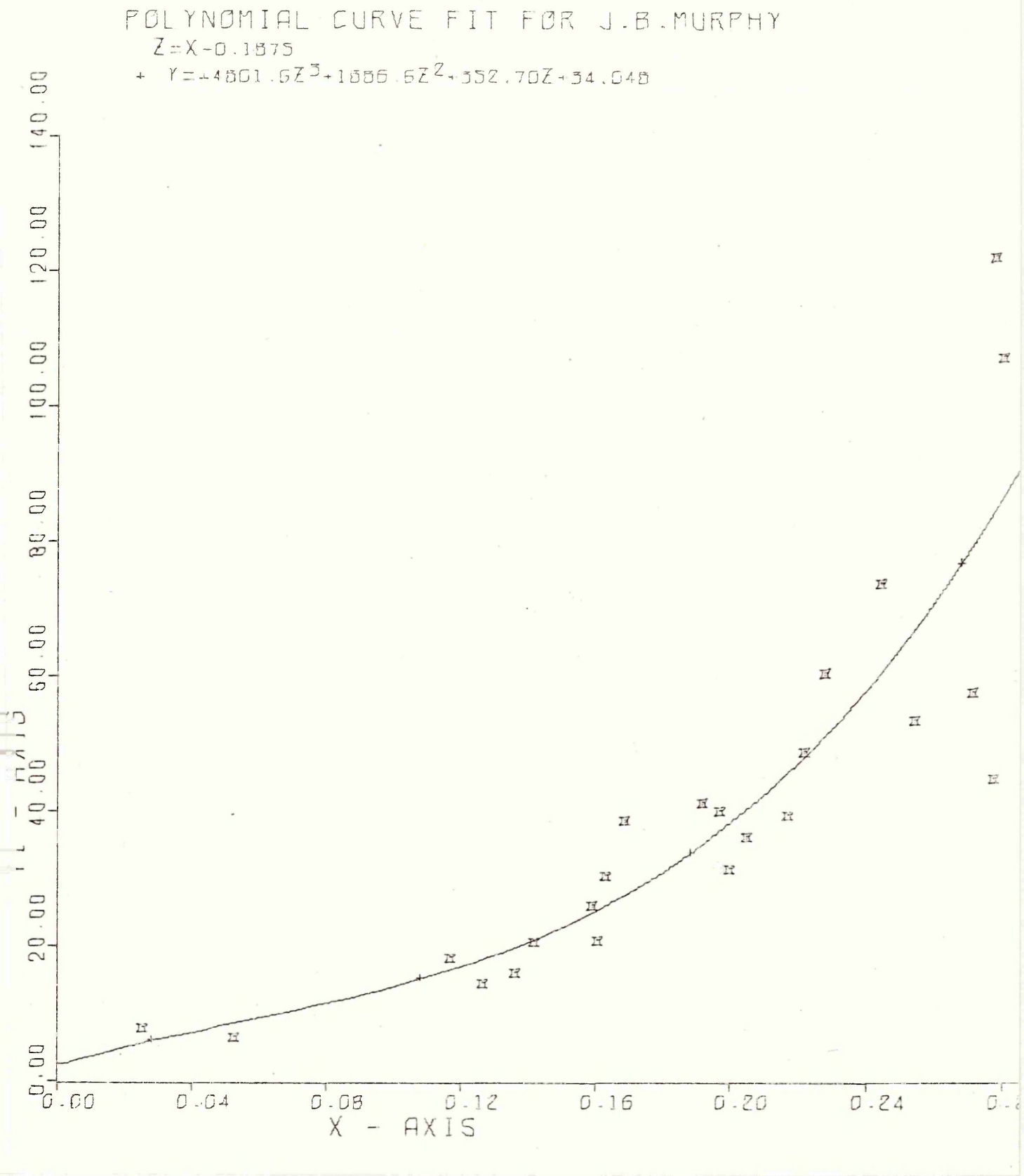

Figure 40: Beam Displacement as a Function of Mean Crack Length

($x = (\frac{a}{W})_{s.c.}$ and $y = (\frac{B\sqrt{W}}{p})c$, where c is the recorded beam displacement)

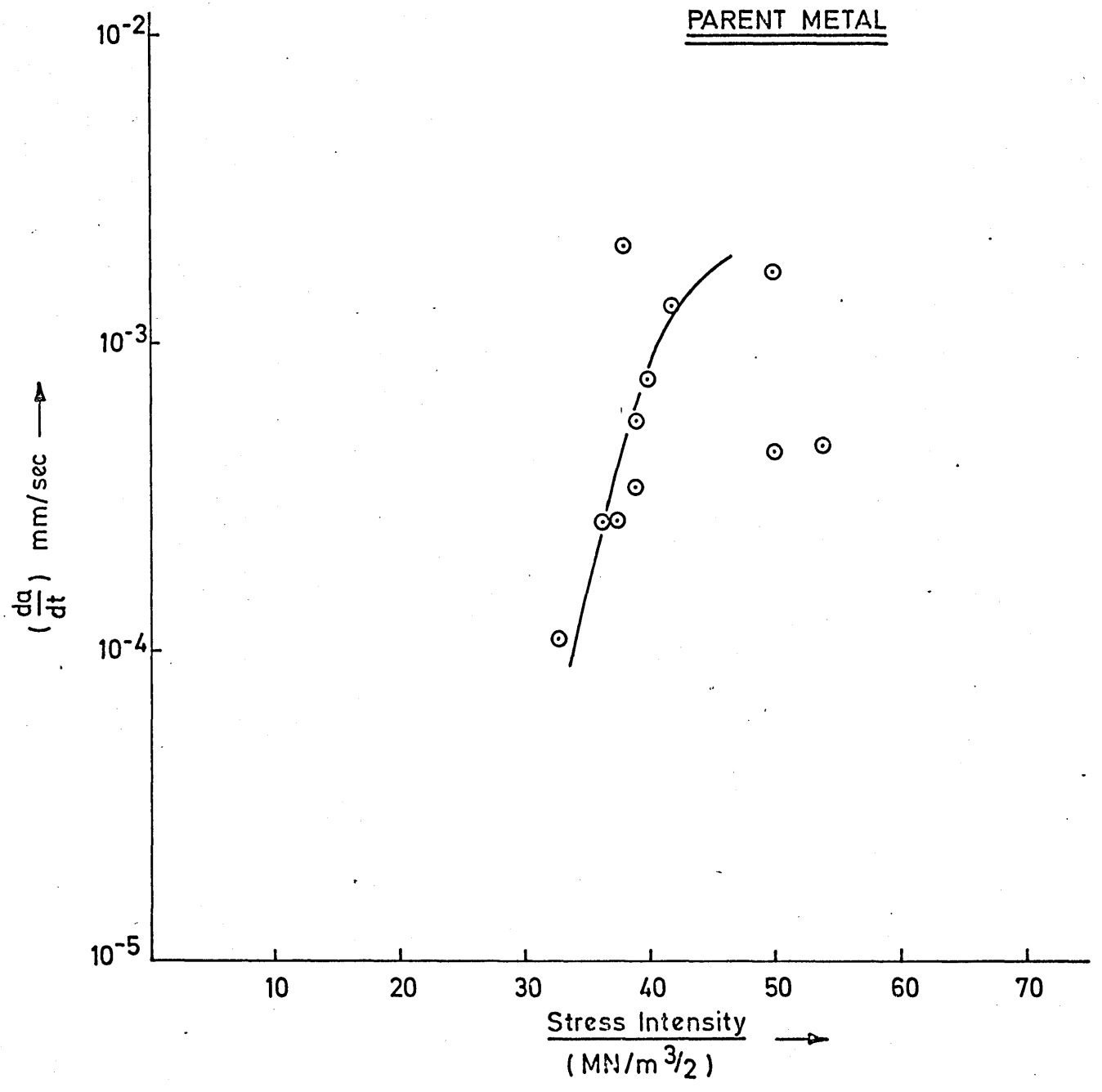

FIG. 41 Crack growth rates in maraging steel exposed to hydrogen sulphide.

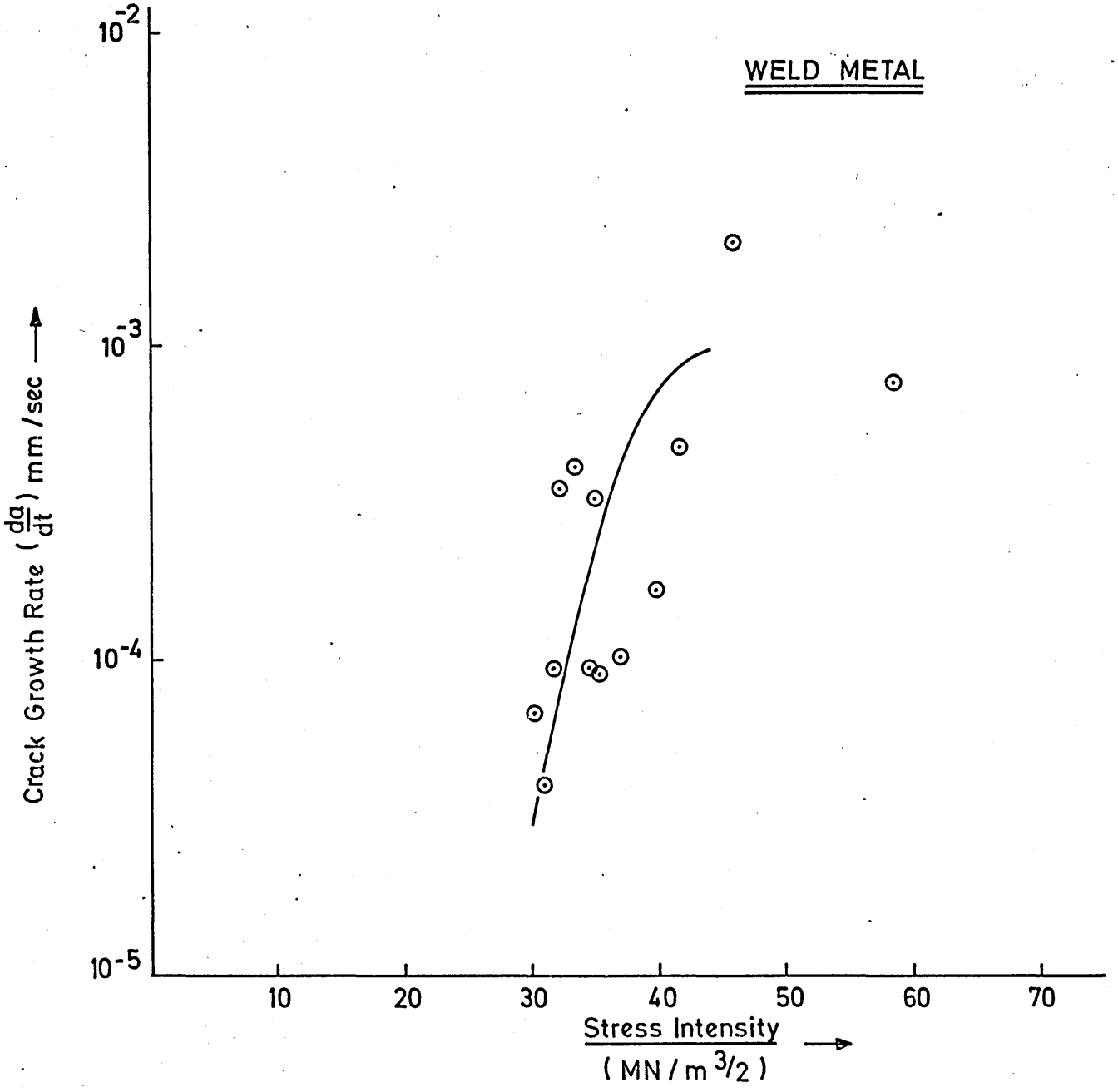

FIG. 42 Crack growth rates in submerged-arc weld metal exposed to hydrogen sulphide.

intensities of 30-40 $MN/m^{3/2}$. For weld metal, there was some slight evidence that Stage II crack growth was becoming operative at intensities greater than 40 $MN/m^{3/2}$.

5.4 FRACTOGRAPHY

5.4.1 Optical Fractography

Typical macrographs showing relative areas of fatigue, environmental cracking and overload failure are given in Figures 43 and 44. The limits of each type of growth were generally clearly distinguishable, albeit irregular, and enabled planimeter assessments to be made from which the mean crack-lengths could be calculated. Higher standard deviations were recorded for environmental cracks as expected, although there was an overall tendency for variance to increase at small crack lengths. The mean crack lengths were accurate to $\pm$ 0.20 mm and $\pm$ 0.25 mm for fatigue and environmental cracks respectively.

Fatigue crack profiles were all convex, with the greatest extension in the specimen centre, and generally similar on both sides of the specimens. Any marked differences in extension resulted from either misalignment during precracking or from specimens being non-square.

By comparison, under stress-corrosion conditions, propagation in nearly every case extended more at the specimen edges than at the centre producing characteristic concave profiles. The intergranular cleavage nature of

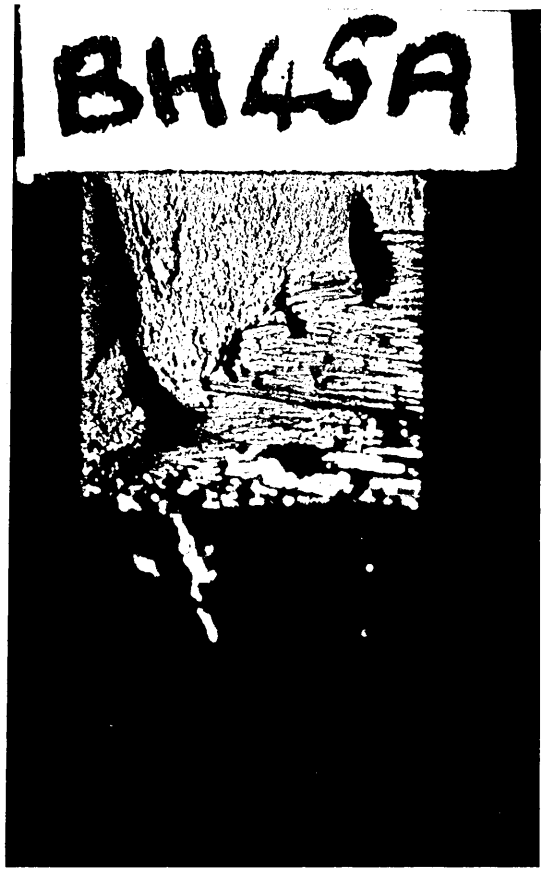

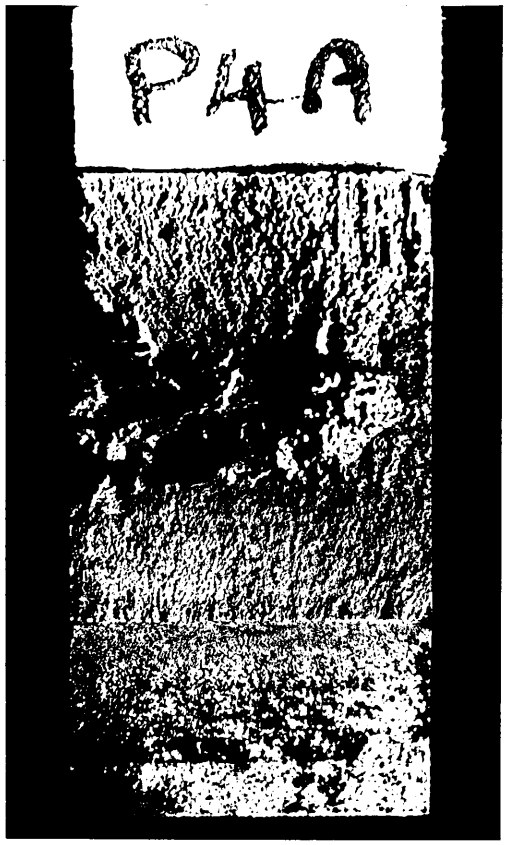

(a) Weld Metal

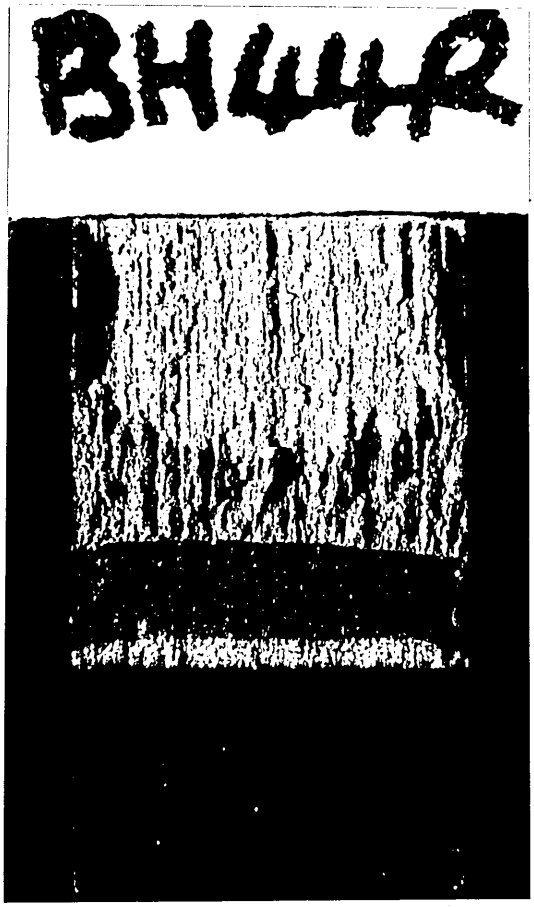

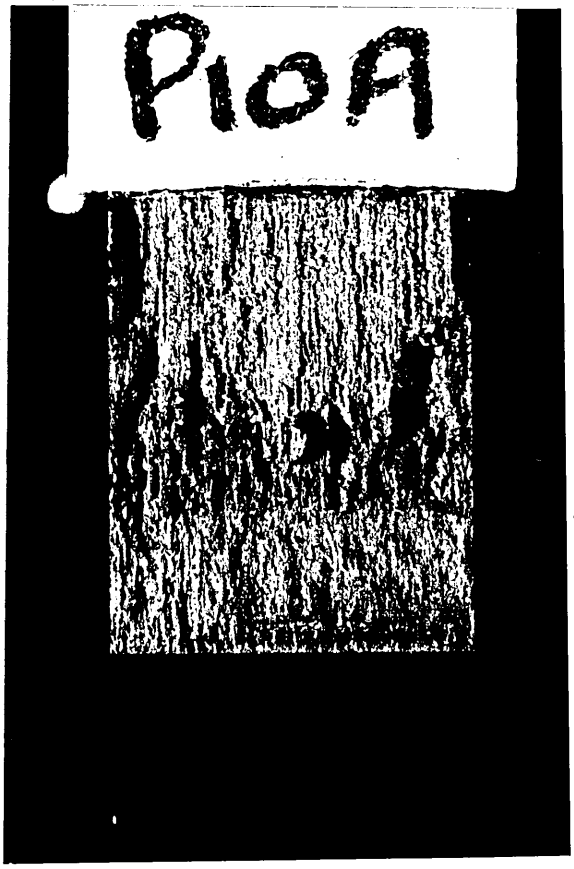

(b) Parent Metal

(All x7 approx)

Figure 43: Fracture Surface Macrographs (a) Weld Metal
(b) Parent Metal

(a)
Dark
Etching
Region

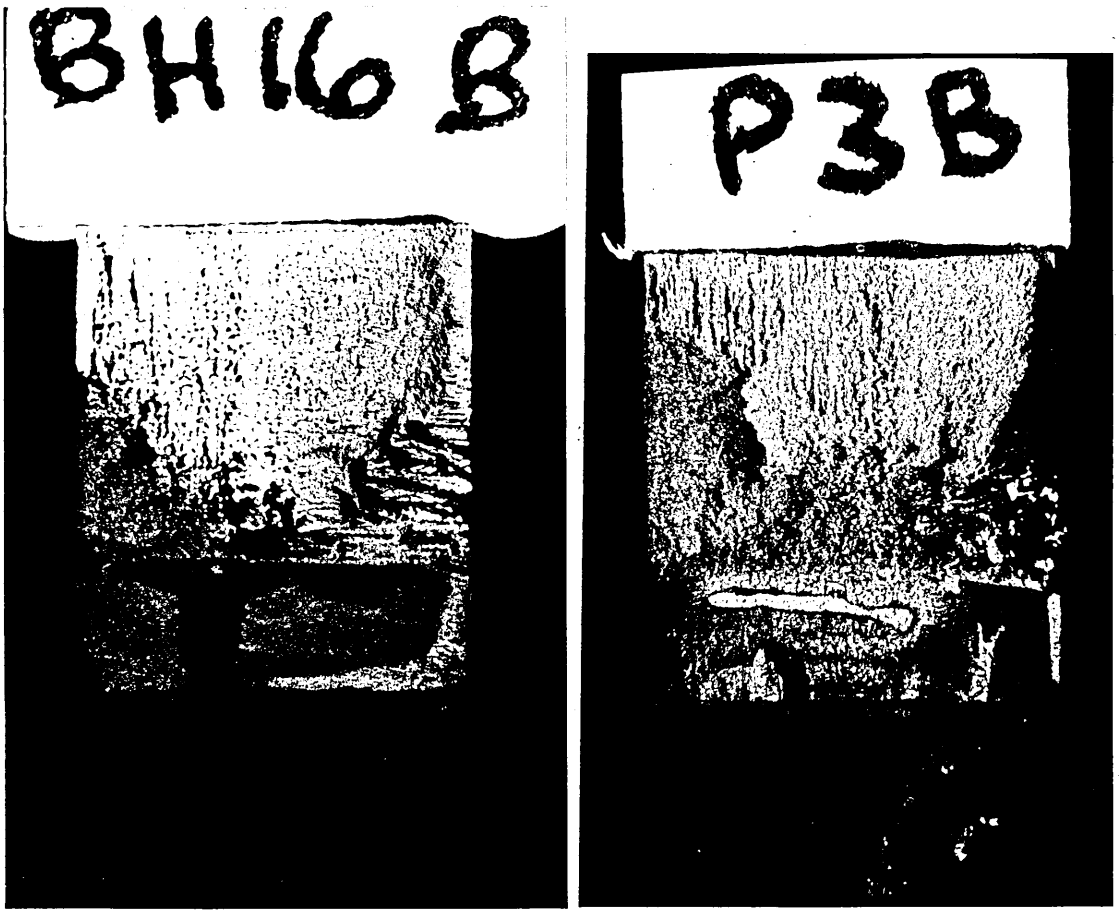

(b)
Interface
Region

(All x7
approx)

Figure 44: Macrographs of (a) Dark-Etching Region
(b) Interface Region

fracture was particularly well defined in weld metal in which the grain size and directionality was much greater than in other regions.

Interface material was usually orientated differently from weld metal and of smaller grain size so that any mixture of the two structures was easily discernible. Fast-fracture surfaces also revealed structural differences but to a much lesser extent.

A noticeable contrast between specimens fractured in air and those in hydrogen sulphide lay in the absence of shear-lips on environmental cracks. Small lips were formed on fast-fracture ligaments, but in no case exceeded 5% of the total crack area.

5.4.2 Scanning Fractography

Two representative specimens from each of the four basic regions of submerged arc welded material were examined by scanning microscopy. At the same time, reference could be made to the corresponding optical micrographs enabling areas of specific interest to be pinpointed. Attention was concentrated on the starts and finishes of environmentally cracked regions since these showed the greatest structural differences.

Various fields from the fracture surfaces of weld metal are shown in Figures 45 to 57. The immediate change in fracture mode following exposure to hydrogen sulphide

is typified in Figures 45 to 54, which show the massive cleavage faces produced by totally intergranular failure. Pure cleavage was maintained as growth proceeded up to the point where the critical stress-intensity was exceeded.

Of the extensive cracking round each grain revealed by scanning microscopy in Figure 53 and indicating multiple crack branching, very few side cracks extended sufficiently far from the main fracture path as to be optically detectable on a transverse microsection. At high initial intensities, environmental cracks developed from the free surfaces only, leaving central regions of the specimen to fracture by ductile dimpling (Figure 47). Some regions also showed cracking along martensite laths within grains.

As expected in vacuum-remelted material, few inclusions were found on environmental crack surfaces and none of those observed appeared to have materially affected the principal direction of crack growth (Figure 54).

Figures 50 to 52 illustrate the transition to fast-fracture resulting in ductile dimpling typical of purely mechanical failure. The fatigue surfaces themselves (Figures 55 and 56) showed the characteristic step-wise growth, although troughs corresponding to macro-striations were barely discernible.

Interface material showed extensive pure cleavage fracture in some areas, together with rougher surfaces

characteristic of crack propagation in parent metal, (Figures 57 to 60).

Environmental cracks in parent metal shown in Figures 61 to 63, appeared to develop much rougher cleavage surfaces than weld metal. In consequence, some specimens with notches nominally at the interface, produced mixed character fracture with equiaxed regions also occurring through recrystallisation during the second welding pass.

Stretch-zones, which form at the start of sub-critical crack growth, proved difficult to observe, perhaps due to lack of experience on the part of the author. However, some examples were found in parent metal samples (Figure 64) although in weld metal, growth appeared to occur without prior plastic deformation at the crack-tip.

Environmental Crack

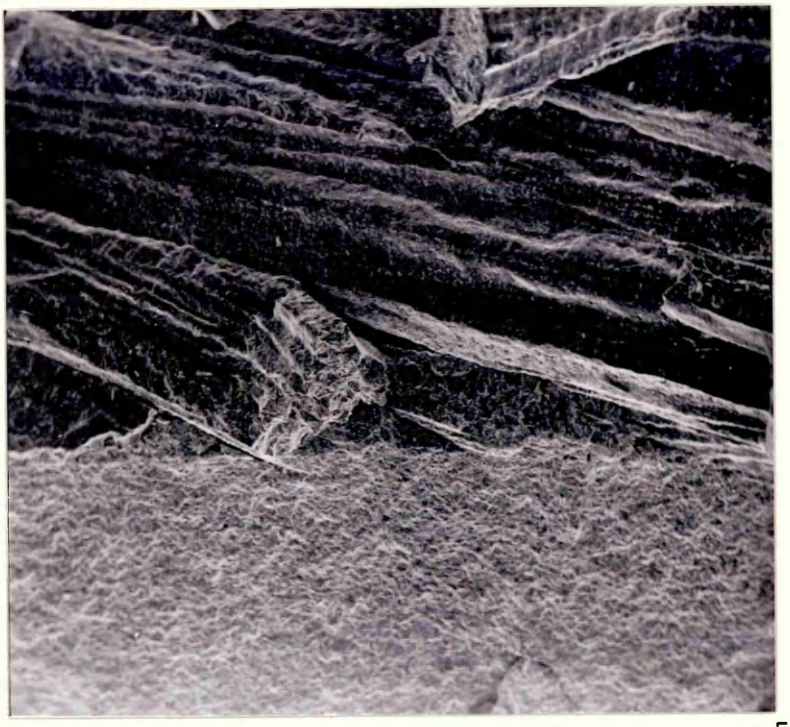

Fatigue

DIRECTION OF PROPAGATION

x50

Figure 45: Weld Metal: Start of Environmental Crack Growth (Centre of BH45A)

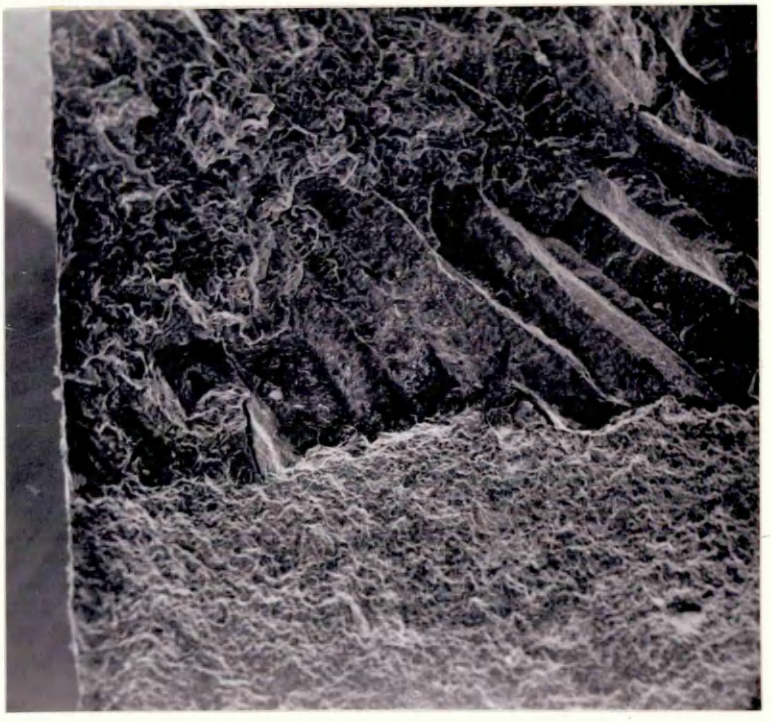

x100

Figure 46: As Above: Environmental Crack Growth at L.H. edge of BH45A, showing change of grain direction

Figure 47. Weld Metal Fracture at High Internal Stress Intensity. Direct Transition between Fatigue and Ductile Dimpled Fast Fracture

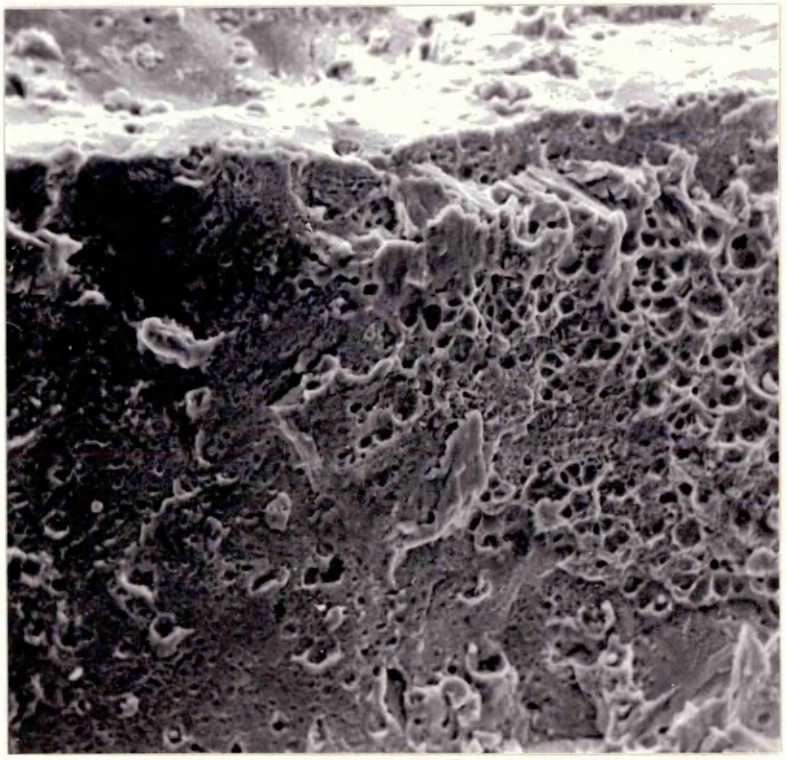

Figure 48: Occurrence of Partial Ductile Fracture at Edge of Environmental Crack Ringed in Figure

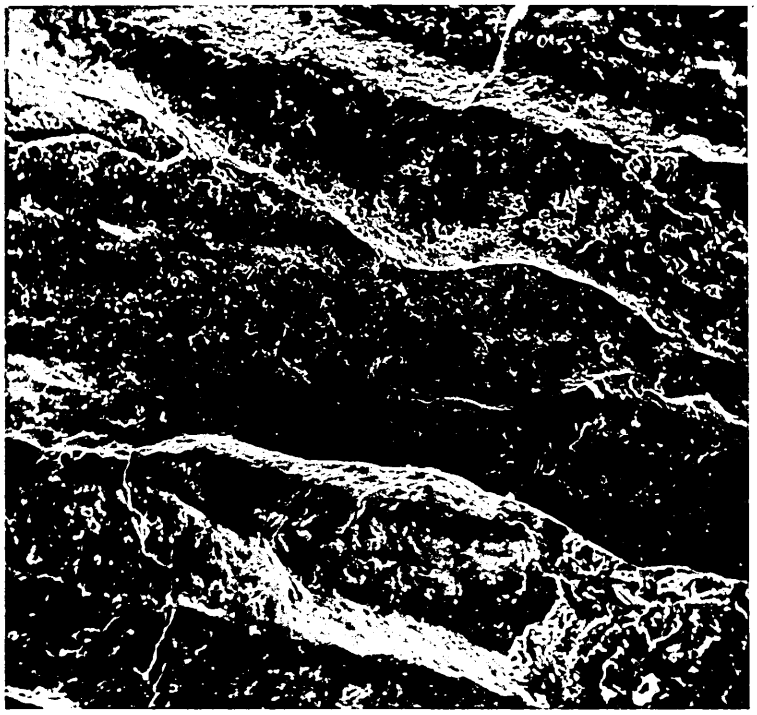

×500

Figure 49: Weld Metal Environmental Crack, showing Pitting of Cleavage Surfaces

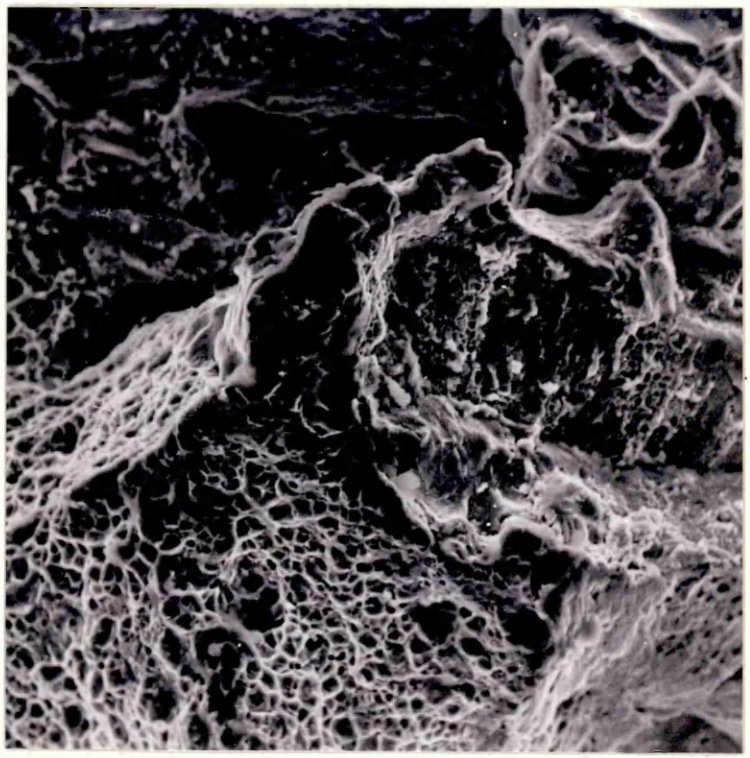

x500

Figure 50 : Weld Metal: Transition Region between Environmental Crack and Fast Fracture

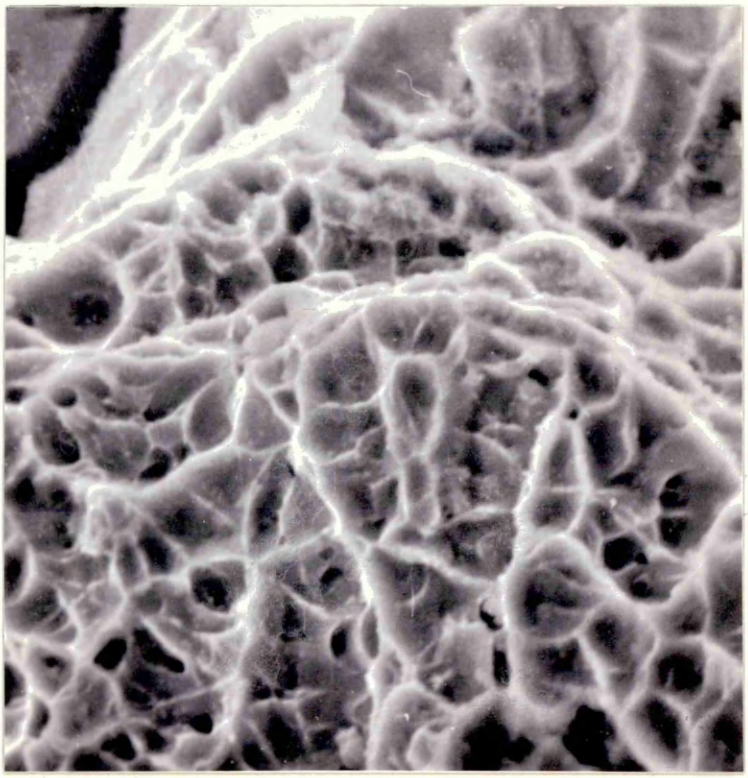

x2000

Figure 51: Weld Metal: Ductile Dimpling in Detail and Start of Shear Lip

TiS_2
inclusion

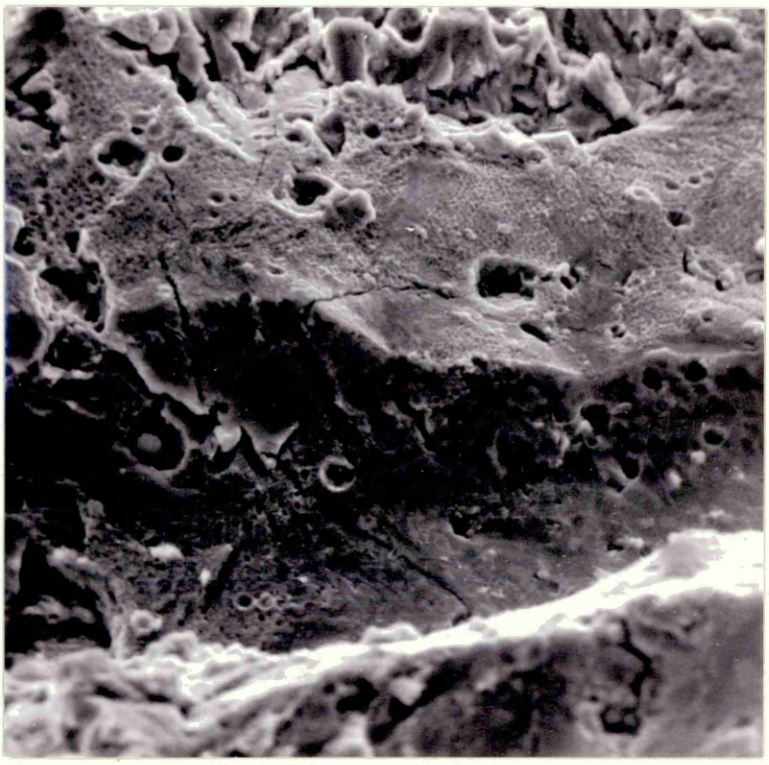

x1000

Figure 54: Weld Metal Environmental Fracture Showing Incipient Cracking through Original Prior Austenite Grain. A TiS_2 inclusion is also visible.

Shear Lip

Fast Fracture

Environmental Crack

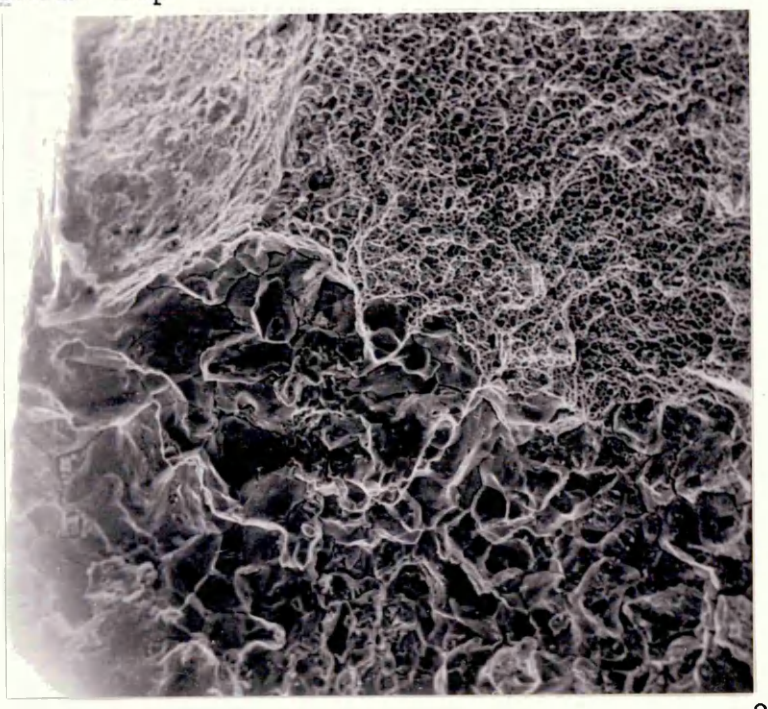

x200

Figure 52 : Weld Metal BH45A: Development of Ductile Dimpling in Fast Fracture Region, together with Start of Shear Lip

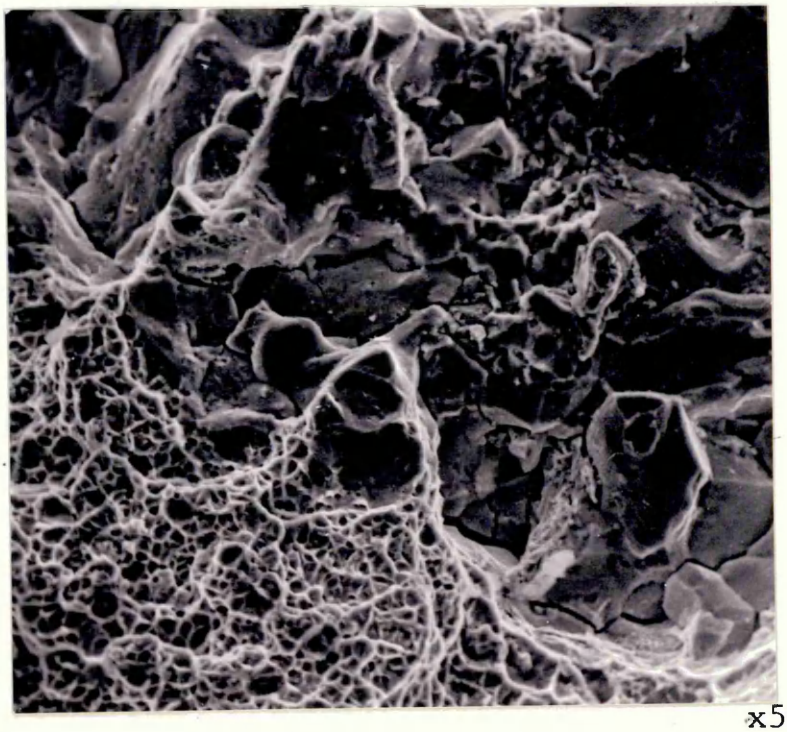

x500

Figure 53: Weld Metal as Above, showing Extensive Intergranular Cracking

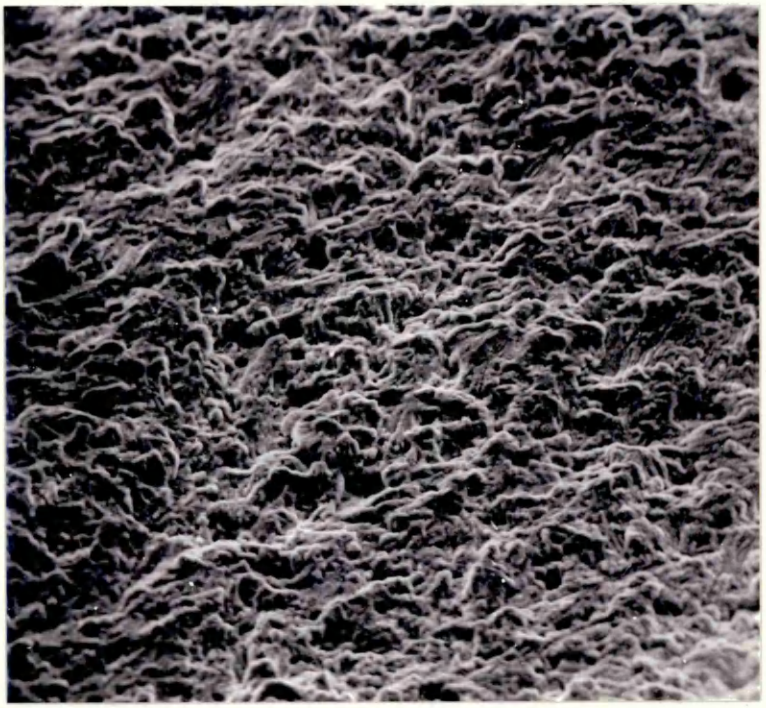

x500

Figure 55: Fatigue Crack Propagation in Weld Metal

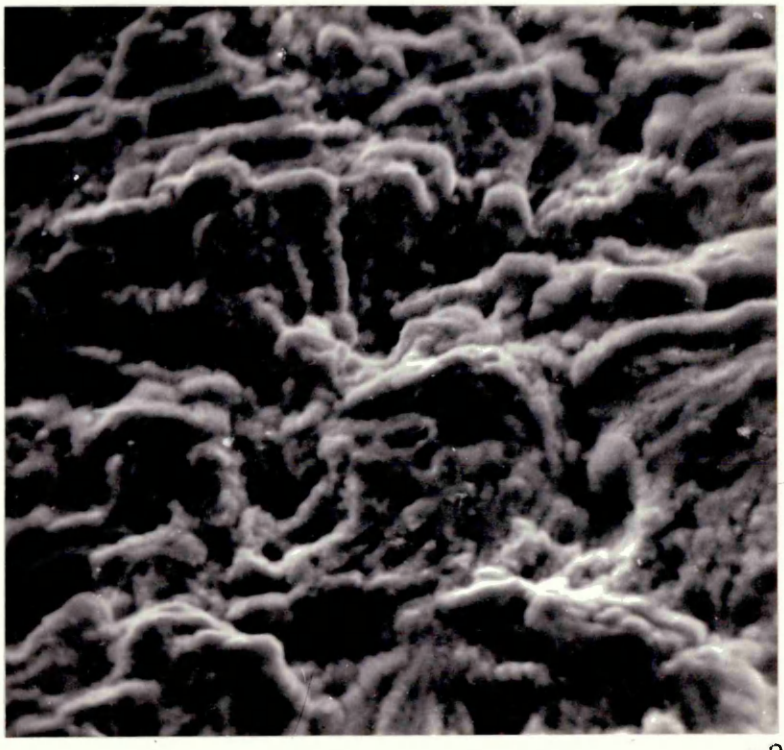

x2000

Figure 56: As Above

x76

Figure 57: Interface Region at Start of Environmental Crack Showing Cleavage through Equiaxed Prior Austenite

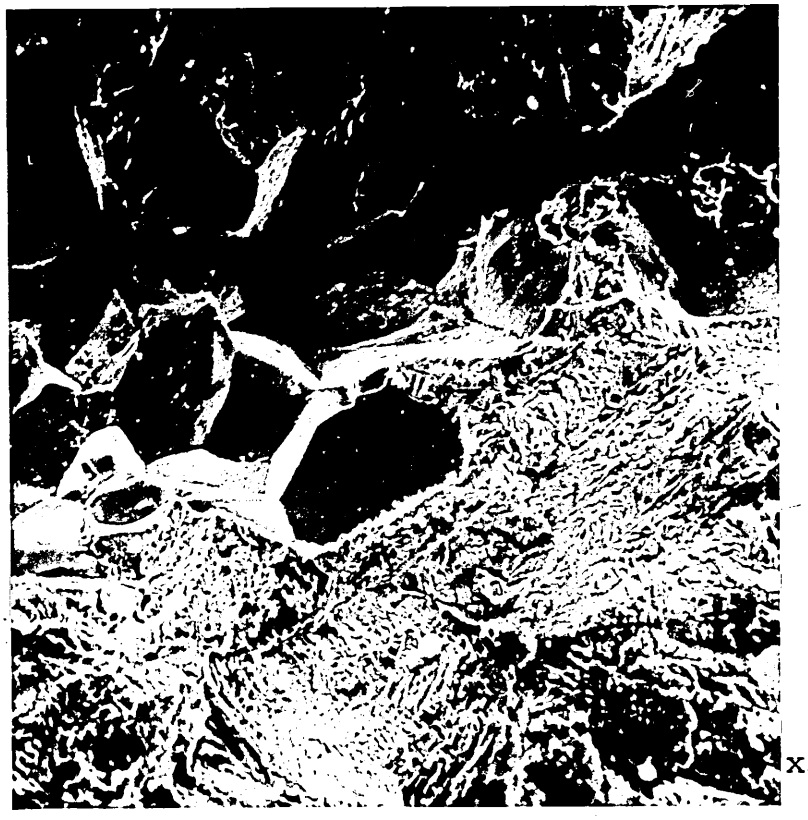

x380

Figure 58: As Above in Detail, Showing Crack Branching which occurred a short time after the start of Environmental Cracking

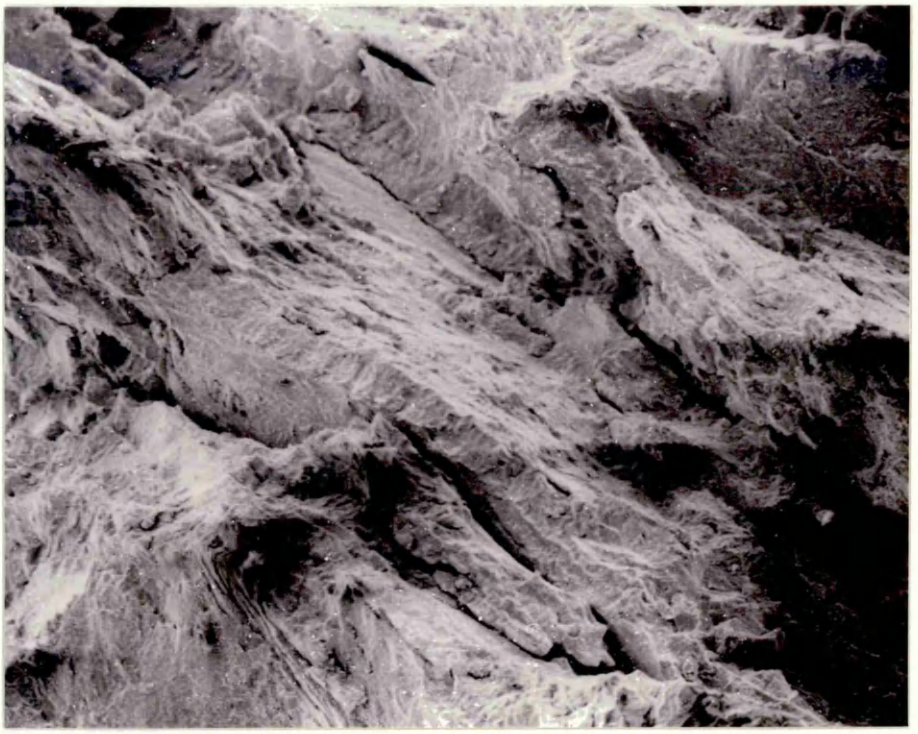

x160

Figure 59: Interface Material Showing Environmental Fracture Producing Rough Cleavage Surfaces Characteristic of Parent Metal

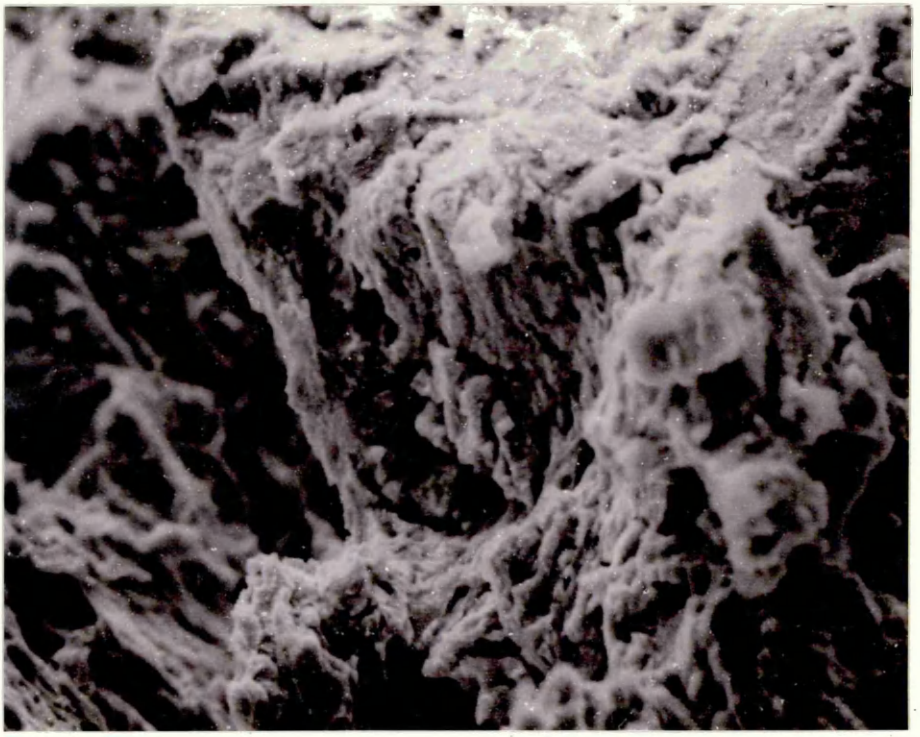

x5000

Figure 60 : As Above Showing Surface Roughness in Detail

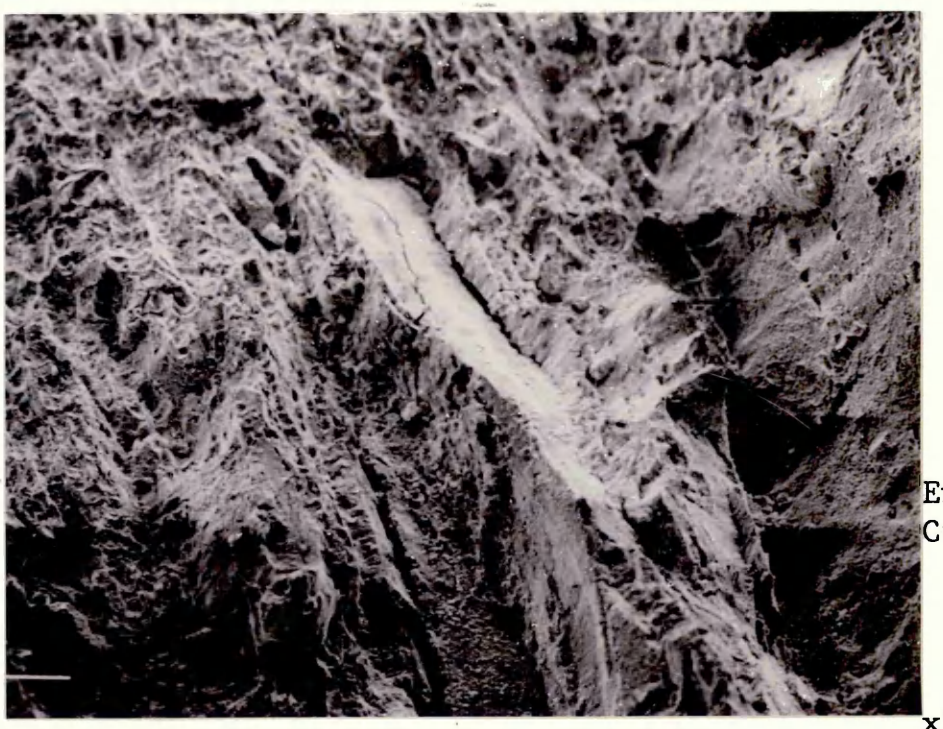

Figure 61 : Parent Metal: Environmental Crack Producing Rough Cleavage Surfaces with Some Incipient Transgranular Cracks

Figure 62: Ringed Area Above in Detail

Possible
Stretch
Zone

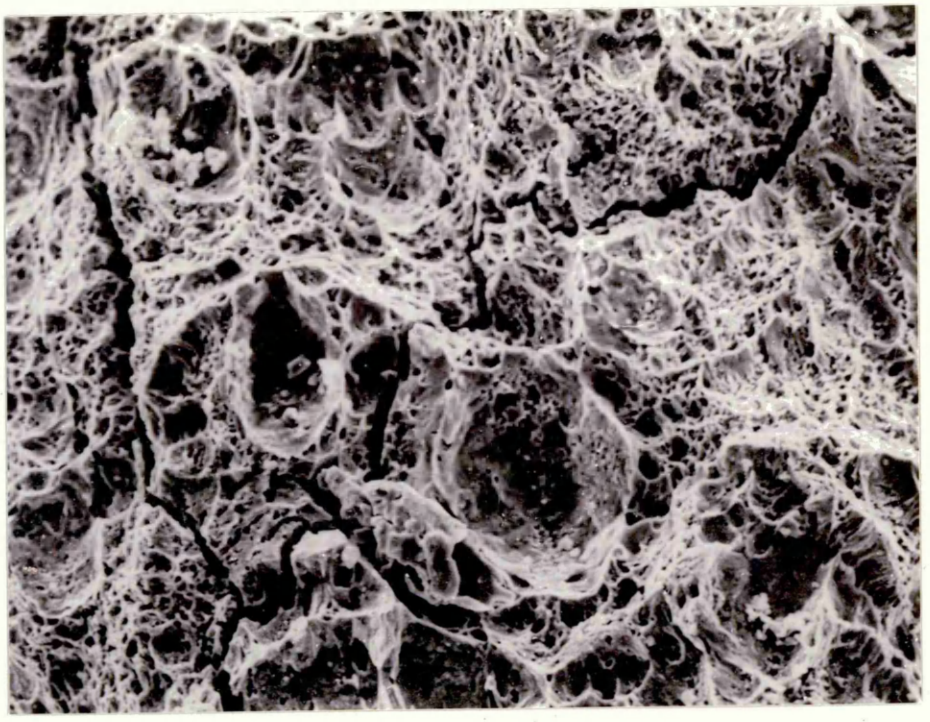

Figure 63: Parent Metal: Mixed Fracture Mode Near Start Of Environmental Crack

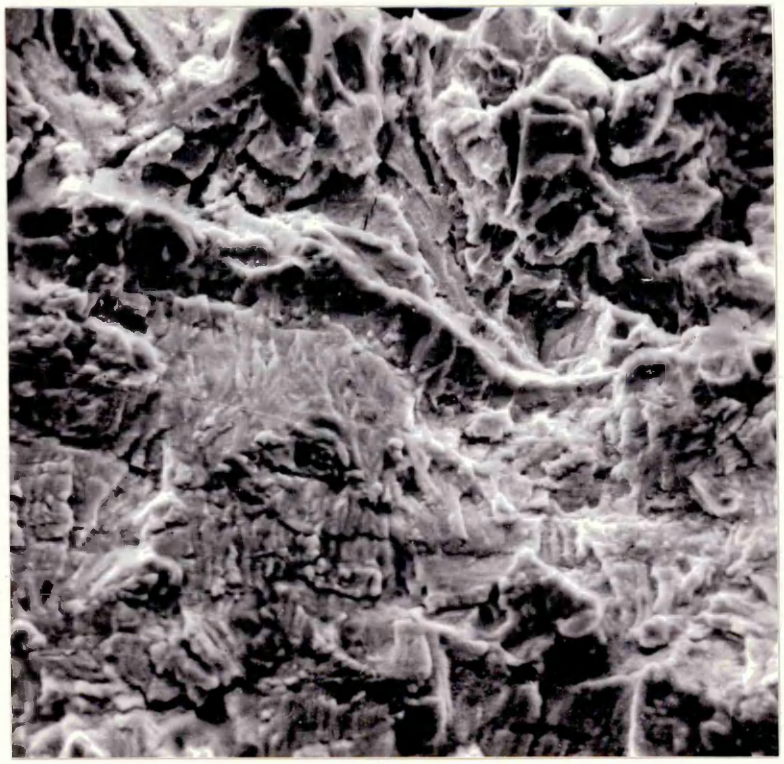

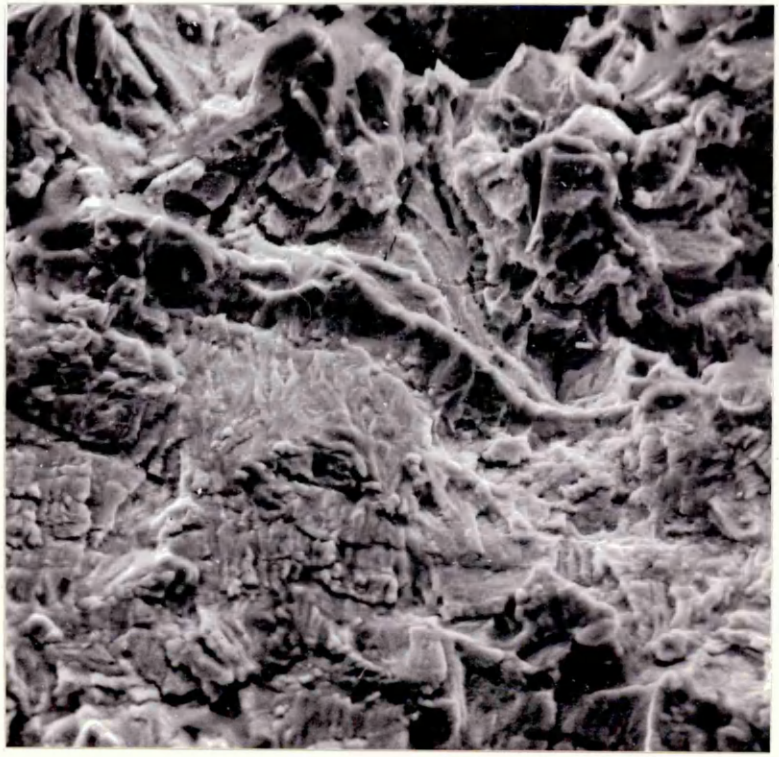

Figure 64: Stretch-Zone Formation at Start of Environmental Crack in Parent Metal

Propagation Direction

x320
(Etched in Mixed Acids)

Figure 65: Truncated Branching in Sample Exposed at High Stress-Intensity

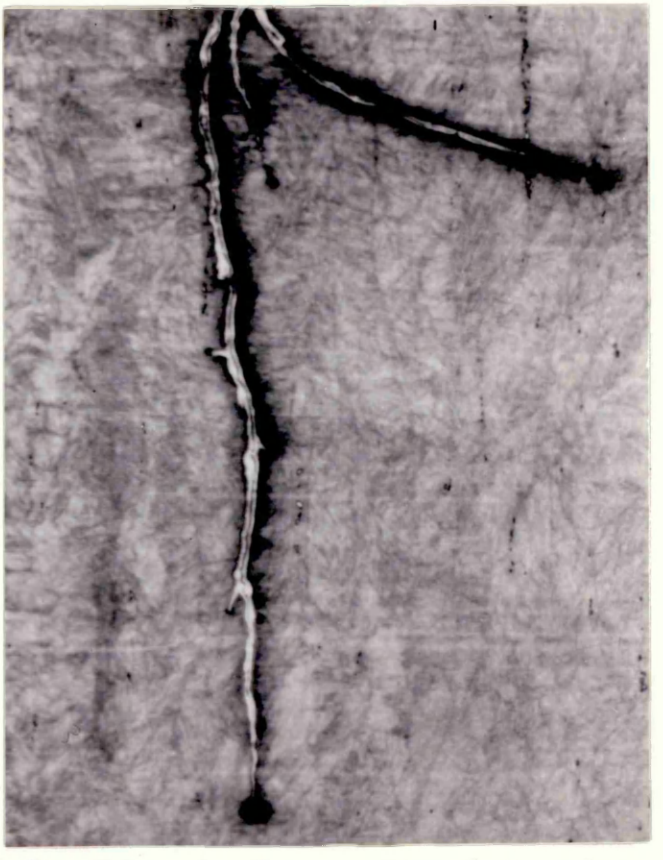

Propagation Direction

Termination

Figure 66: Branched Cracking in Parent-Metal Samples - Low Stress-Intensity

6. DISCUSSION

From the review of literature, it is evident that the limiting stress-intensity for crack propagation, coupled with the propagation rate, presently provide the most valid, if not the most convenient parameters for assessing environmental performance of high-strength materials. Their measurement, however, begs the question of crack initiation, a stage which, for some materials at least, is of major structural importance[136]. Threshold-intensities appear to be measurable and well-defined in the case of high-strength steels in hydrogen containing media[137], although they are much less certain for more ductile materials.

Economic considerations apart, there is no criticism of fracture mechanics based tests for maraging and similar strength steels which cannot equally be levelled at other methods of testing. The principal disadvantages of other methods lie in their unknown initiation and incubation periods, defined in the present work as the time for an initial flow to develop by corrosion and the subsequent period spent in reaching critical conditions for crack growth to start. With smooth specimens, the onset of cracking is difficult to detect and is often a subjective assessment. In addition, the fracture may be very delayed. Smooth specimen endurance per se therefore, can at best

offer only a qualitative indication of material performance.

With precracked samples, conditions at the advancing crack front may also be questionable due to branching and/or uneven propagation, but at least the initial state can be calculated with a reasonable degree of certainty, provided validity criteria are fulfilled. The singular dependence of threshold and cracking rate upon material and environment obtained in plane strain should be a prerequisite for stress-corrosion tests.

6.1 THRESHOLD STRESS-INTENSITIES

The endurances obtained showed a high degree of stress-intensity dependence, and threshold K_{QSCC} values of 20 - 30 $MN/m^{3/2}$ for both weld and parent metal appear likely. Results for mixed microstructures indicated that the threshold values in the heat-affected zone could be marginally higher. Few samples in the present work achieved endurances greater than 400 minutes, so that more precise estimates of thresholds cannot be made. There would have been problems however, in maintaining hydrogen sulphide concentrations during the long term exposures resulting from lower initial stress-intensities. Nevertheless, in future work on this system, a binary search[138] for K_{1SCC} may prove valuable.

The general levels of K_{QSCC} are within the range of reported values for unwelded 250 grade maraging steels

determined in sodium chloride and illustrated in Figure 8, and are also in agreement with those determined using ammonium sulphide solution[119]. It would appear therefore, that weld microstructure removed from their normal residually stressed practical situation are no less resistant to cracking than is parent material, if judgement is based solely on threshold values.

Since maraging steels are conventionally aged after welding in the majority of cases, only structural changes due to variations in peak temperature with distance during the welding cycle would be expected to influence results. Stavros and Paxton[98] produced six markedly differing grain sizes in maraging steel by excessive solution treatment temperatures. On ageing these structures to similar levels of yield stress, all subsequently showed identical K_{1SCC} values in a variety of environmental conditions. Significant differences were obtained, however, by variations in ageing conditions. These results are in accordance with the view that K_{1SCC} is principally yield-stress dependent, in maraging steels, and that the mechanism of cracking is the same in each of the environments tested. Assuming that yield stress and hardness are interdependent, the small variations in hardness found across the weld zone (Figure 28), after ageing would not, therefore, be expected to affect threshold values materially. Those

variations in hardness which do occur do so in agreement with yield stress dependence, with slight softening in the 650°C peak temperature regions giving rise to marginally higher thresholds. Similar independence of threshold values on position across the weld was reported by Gooch[60] for 180 grade material, although there were overall differences between material welded by various methods.

It is possible that K_{1SCC} values are not a sensitive parameter as far as environmental cracking is concerned, since thresholds per se are not an implicit function of endurance. It is more likely that their value is a function of the stress at which hydrogen at the crack tip reaches critical embrittlement concentration. This view is supported by the essentially similar values of threshold intensity found for 835 M 30 steel in hydrogen gas, hydrogen sulphide gas and in salt solution by McIntyre[139].

Gerberich and Chen[140] have noted the absence of any quantitative explanation for threshold existance, in spite of the considerable experimental evidence which is available. By assuming that hydrogen is responsible for environmental failure in high-strength steels, Gerberich and Chen were able to show that the threshold/yield stress dependence for hydrogen-charged 4340 steel was almost identical to that obtained in corrosion experiments.

Despite the considerable scatter, the K_{1SCC}/σ_y

relationship for maraging steels shown in Figure 8 is of similar form, but with much higher threshold values at any given yield-stress, due presumably to a greater tolerance to hydrogen.

Assuming an initially uniform hydrogen content C_o, then the increased concentration under elastic stress at a point r is given by:

$$C_r = C_o \exp\left(\frac{\sigma_{ii} V_H}{3RT}\right) \qquad (18)$$

where σ_{ii} is the sum of the principal normal stresses acting at r, and V_H is the partial molal volume of hydrogen. Hydrogen therefore migrates under the action of the stress field to the region of greatest stress. Liu[80] showed that under crack-opening conditions, then steady-state hydrogen concentration gradients would depend on stress-intensity, according to:

$$C_r = C_o \exp\left(\frac{2(1+\nu)V_H K}{3RT\sqrt{2\pi r}}\right) \qquad (19)$$

where ν = Poisson's ratio, and K is the acting stress-intensity. Thus, at the threshold intensity:

$$K_{Th} = \frac{3RT\sqrt{2\pi r}}{2(1+\nu)V_H} \cdot \log_e \left(\frac{C_r}{C_o}\right) \qquad (20)$$

Equation (20) assumes that purely elastic conditions prevail. However, at the crack tip, the plastic region under plane strain is of radius r, where:

$$r = \frac{K^2}{3\pi\sigma_y^2} \qquad (21)$$

which defines the effective boundary of the elastic/plastic zone.

Substitution into Equation (19) then gives:

$$C_r = C_o \exp\left(\frac{2(1+\nu)V_H\sigma_y}{RT\sqrt{6}}\right) \qquad (22)$$

Gerberich and Chen further suggest that in overall plane-strain conditions, the critical hydrogen concentration round the crack-tip which results in crack extension will be:

$$C_{crit} = C_o \exp\left(\frac{\sigma_y V_H (P-\frac{1}{2})}{RT}\right) \qquad (23)$$

in which P is defined as the maximum principal stress/yield stress ratio and is termed the plastic constraint factor. P is also a function of stress-intensity[141], assumed to be:

$$P = 1 + \alpha\left(\frac{K}{\sigma_y}\right) \qquad (24)$$

where $\alpha \simeq 0.4\ mm^{-\frac{1}{2}}$.

In combination with Equation (23), this gives the following threshold-intensity relationship for hydrogen cracking:

$$K_{Th} = \frac{RT}{\alpha V_H} \cdot \log_e\left(\frac{C_{crit}}{C_o}\right) - \frac{\sigma_y}{2\alpha} \qquad (25)$$

which provides for yield stress and critical hydrogen concentration dependence for K_{Th}. The linear relationship with yield stress may be compared with the published data plotted in Figure 8, for which the least-squares best fit is:

$$K_{1SCC} = 299 - 0.141\ \sigma_y \qquad (26)$$

where K_{1SCC} has the units $MN/m^{3/2}$ and σ_y is in MN/m^2. For this data, the correlation coefficient was -0.85 showing

evidence of linearity at better than the 0.001 level of significance for 37 degrees of freedom. Equation (26) suggests a value of ~3.5 $mm^{-\frac{1}{2}}$ for the term α in Equation(24).

Gerberich and Chen obtained a good correlation between threshold values for 4340, H11 and 300M low alloy steels and those predicted by Equation (25), after assuming that hydrogen solubility was inversely proportional to yield stress, that C_{crit} was 6 p.p.m. and that $\frac{C_{crit}}{C_o} \simeq \frac{3150}{\sigma_y}$ although the correlation coefficients were not quoted.

The same authors also forecast threshold values for maraging steels, assuming that $\frac{C_{crit}}{C_o} \simeq \frac{5500}{\sigma_y}$, but obtained a somewhat poorer correlation. This is to be expected in view of the compositional variations used in maraging alloys to produce the range of yield stresses. It is likely that each composition will have a different critical hydrogen concentration for slow crack growth, and in any case, there is considerable scatter in the K_{1SCC} values, especially in the 1700-2400 MN/m^2 yield-stress range.

6.2 CRACK PROPAGATION RATES

From the characteristic relationships proposed by Carter[76] and shown in Figure 7, two parameters may be extracted, viz.,

(i) The variation of Stage I velocity with intensity, and

(ii) The plateau velocity (Stage II) with its relevant stress-intensity range.

Most of the cracking rates reported for maraging steels are plateau velocities, and few details of Stage I velocity are available. Table 19 compares published values for various maraging steels with those from the present work, and shows differences of almost two orders of magnitude between behaviour in salt solutions and hydrogen sulphide.

Several methods are available for determining crack velocities, some of which give instantaneous values, while others provide mean rates over a range of intensities. Briefly, these methods are as follows:

(i) Direct Division of overall crack length by endurance. This requires incubation periods to be small compared with the total endurance, and ignores any variation in rate during slow growth.

(ii) Continuous Monitoring of crack extension with time. This method relies on a correlation between crack length and either resistance-gauge response or beam position. Obviously, any number of individual measurements can be made during crack growth in any one specimen, provided the calibration is known and the calculated compliance is valid.

(iii) Indirect Method (after Carter[142]). By exposing under identical conditions two geometrically similar specimens, one of which is much wider than the other, then cracking rates can be calculated from the differences in failure times:

MATERIAL	CONDITION	ENVIRONMENT	STAGE II CRACKING		REFERENCE
			RATE (mm/sec)	INTENSITY RANGE ($MN/m^{3/2}$)	
250	AGED	NaCl	1.5×10^{-5}	-	132
"	"	"	1.3×10^{-5}	-	150
"	"	Distilled Water	0.8×10^{-5}	-	142
"	"	Aqueous H_2S	$20\text{-}80 \times 10^{-5}$	30-70	Present Work
"	Welded + Aged	"	$5\text{-}80 \times 10^{-5}$	30-60	"
"	AGED	Hydrogen Gas	200×10^{-5}	30-60	151
300	"	NaCl	23×10^{-5}	28-49	142
"	"	Hydrogen Gas	350×10^{-5}	20-40	151
350	"	NaCl	$200\text{-}2000 \times 10^{-5}$ (No plateau)	15-40	86

Table 19: Cracking Velocities in Plateau Range for Maraging Steels in Various Environments

$$E_n = E_i + an.\left(\frac{da}{dt}\right)^{-1} \quad (25)$$

and $$E_w = E_i + a_w \left(\frac{da}{dt}\right)^{-1} \quad (26)$$

in which E = endurance, a = total crack length, t = time and the subscripts n and w indicate narrow and wide specimens respectively. Since the rate of increase in stress-intensity is greatest in the narrow specimen, $E_n < E_w$, allowing $\frac{da}{dt}$ to be obtained by elimination. Again, only average rates are obtained, so that loading must be in the plateau range.

Strictly, average results are meaningless if both Stage I and Stage II velocities are involved, so that instantaneous measurements should be made where possible. The danger in the latter method lies in crack branching which can occur at intensities $2 \times K_{1m}$, where K_{1m} denotes the transition between Stage I and Stage II cracking. Apparently reproducible results may be obtained from successive measurements made during the life of a single cantilever beam specimen as demonstrated by Mostovoy et al[132], who showed all three stages of cracking to be evident in a sample of 250 grade material.

When initial cracking rates from a number of samples exposed at different K_{1i} values are calculated, much more scatter is evident, as in the results of the present work (Figures 41 and 42). The reasons for this scatter lie in specimen to specimen differences and with variations in crack front profile causing changes in compliance.

A significant feature of the majority of the present tests was a drop in cracking rate after initial growth had commenced. Gerberich, Chen and St. John[143] have applied analysis of hydrogen-stress field interactions at the crack-root to the problem of sub-critical crack growth, in both maraging and 4340 steels. They suggest that crack-tip conditions during Stage I at low stress-intensities are mainly elastic and hence predict a linear relationship between velocity and stress-intensity:

$$\left(\frac{da}{dt}\right)_I \simeq \frac{2(1+\nu)\, C_o D_A V_H}{3d^{3/2}.RT.(C_r - C_o)} \qquad (27)$$

where d is the average grain diameter and D_A is the apparent diffusivity of hydrogen. This equation is derived from Equation (22) combined with a Fick's first law treatment; assuming that the crack grows intergranularly one grain at a time, and that hydrogen collects in this grain by diffusion from those immediately surrounding it.

In Stage II cracking, the plastic zone surrounding the tip effectively blunts the crack, and hydrogen flows away from the tip over approximately one grain diameter. The approximate rate of cracking under these conditions is:

$$\left(\frac{da}{dt}\right)_{II} \simeq \frac{9\, Co\, D_A V_H \sigma_y}{2d.RT\,(C_r - C_o)} \qquad (28)$$

which predicts both yield stress and grain size dependence. In Stage III, the plastic zone predominates at the crack tip, but fracture changes to a ductile mode. The predicted

cracking rate:

$$\left(\frac{da}{dt}\right)_{III} \simeq \frac{9\, C_o\, D_A V_H K^2}{2\, Ed^2\, RT\, (C_r - C_o)} \qquad (29)$$

is highly stress-intensity dependent.

Subsequently, it was found that under load, the crack-tip radius was proportional to $\left(\frac{K_1}{\sigma_y}\right)$, which altered the predicted growth rate in Stage II to:

$$\left(\frac{da}{dt}\right)_{II} \simeq \frac{3\, C_o\, D_A V_H \sigma_y}{d\, RT\, (C_r - C_o)} \log_e \left(1 + \frac{d\sigma_y}{\rho_o K_i}\right) \qquad (30)$$

where ρ is a proportionality constant governing $\left(\frac{K_1}{\sigma_y}\right)$. The effect of this modification to Equation (28) is seen when the rise in K_1 with crack length is included. Equation (30) then predicts a small decrease in cracking rate with K_1, of the order of 2. In view of the size of this decrease, the authors concluded that its presence may have either not been observed or ignored by previous investigations. However, in common with the results of the present work, such decreases have now been found for both 4340 steel and for 250 grade maraging steel.

A further interesting feature of Equation (30) is the greater grain-size dependence of Stage II cracking compared with Stage I. This may well have influenced the present results especially in regions such as the interface, where grain-size varied along the crack path due to directional differences in heat extraction during solidification.

When the performance of single specimens in the present work was examined, a majority showed a reduction in cracking velocity once growth had commenced, and the agreement between Stage II rates was suprising in view of the possible specimen to specimen differences in structure. For weld metal, the Stage II cracking velocity was of the order of 20×10^{-5} mm/sec, commencing at a stress-intensity of 30 $MN/m^{3/2}$. For parent metal, the corresponding data were 25×10^{-5} mm/sec and 32 $MN/m^{3/2}$ respectively. These values are illustrated in Figures 67 and 68. If individual samples are exposed at intensities less than K_{1m}, then successive measurements of crack velocity should yield approximately the same plateau as that derived from the initial velocities measured on a range of samples.

6.3 FAILURE MECHANISMS

It is outside the scope of this work to consider the mechanism of cracking in detail, but the results that have been obtained, in particular the reduction of cracking velocity in Stage II, do lend support to the view that hydrogen is the agent responsible. Additional evidence of its involvement with crack growth in maraging and other high-strength steels is provided by:

(i) Enhanced susceptibility of material polarised cathodically either by applied current or by zinc coupling, as shown by Trueman[53], and by the present work.

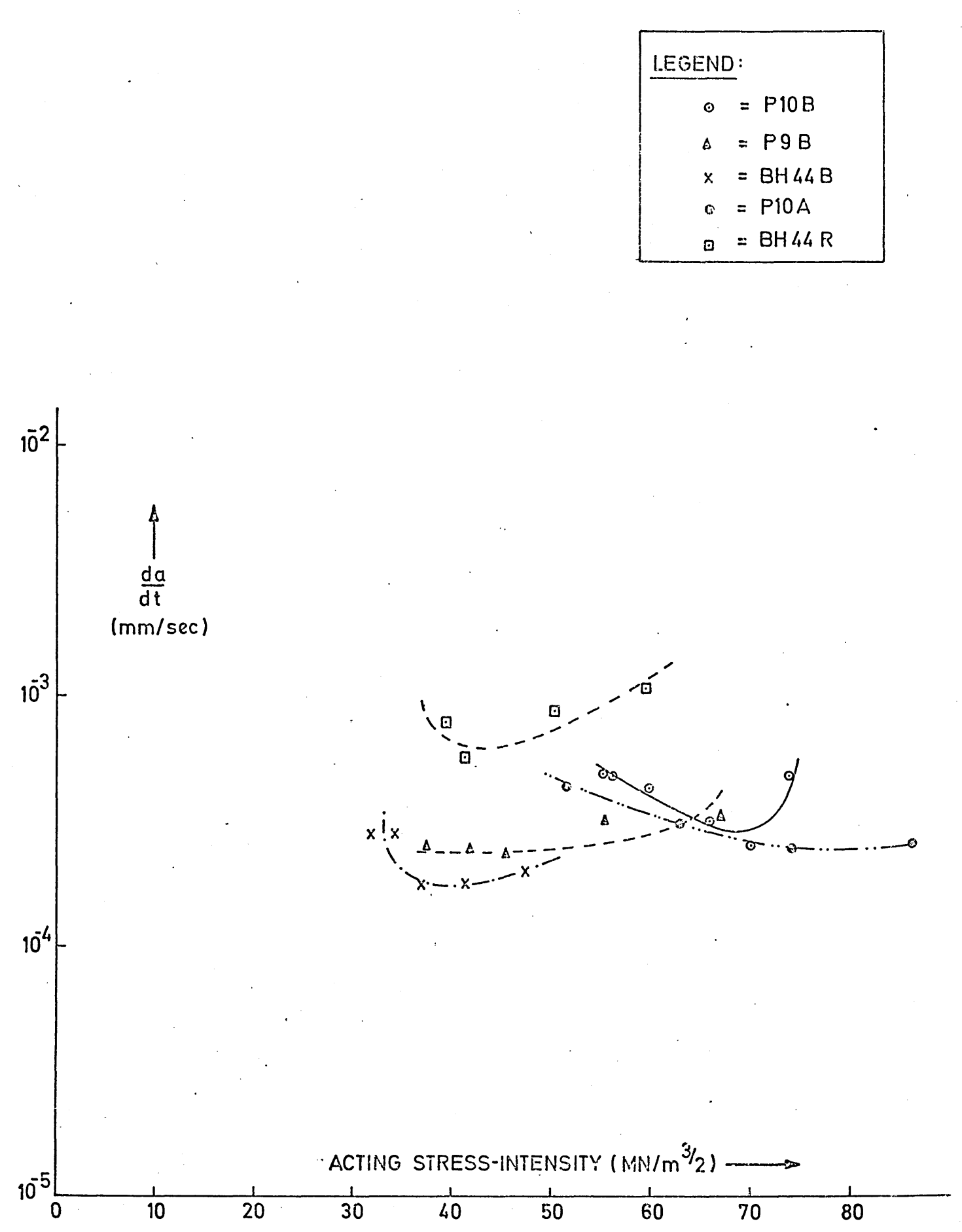

FIG. 67 Stage II velocity variation in maraging steel parent metal.

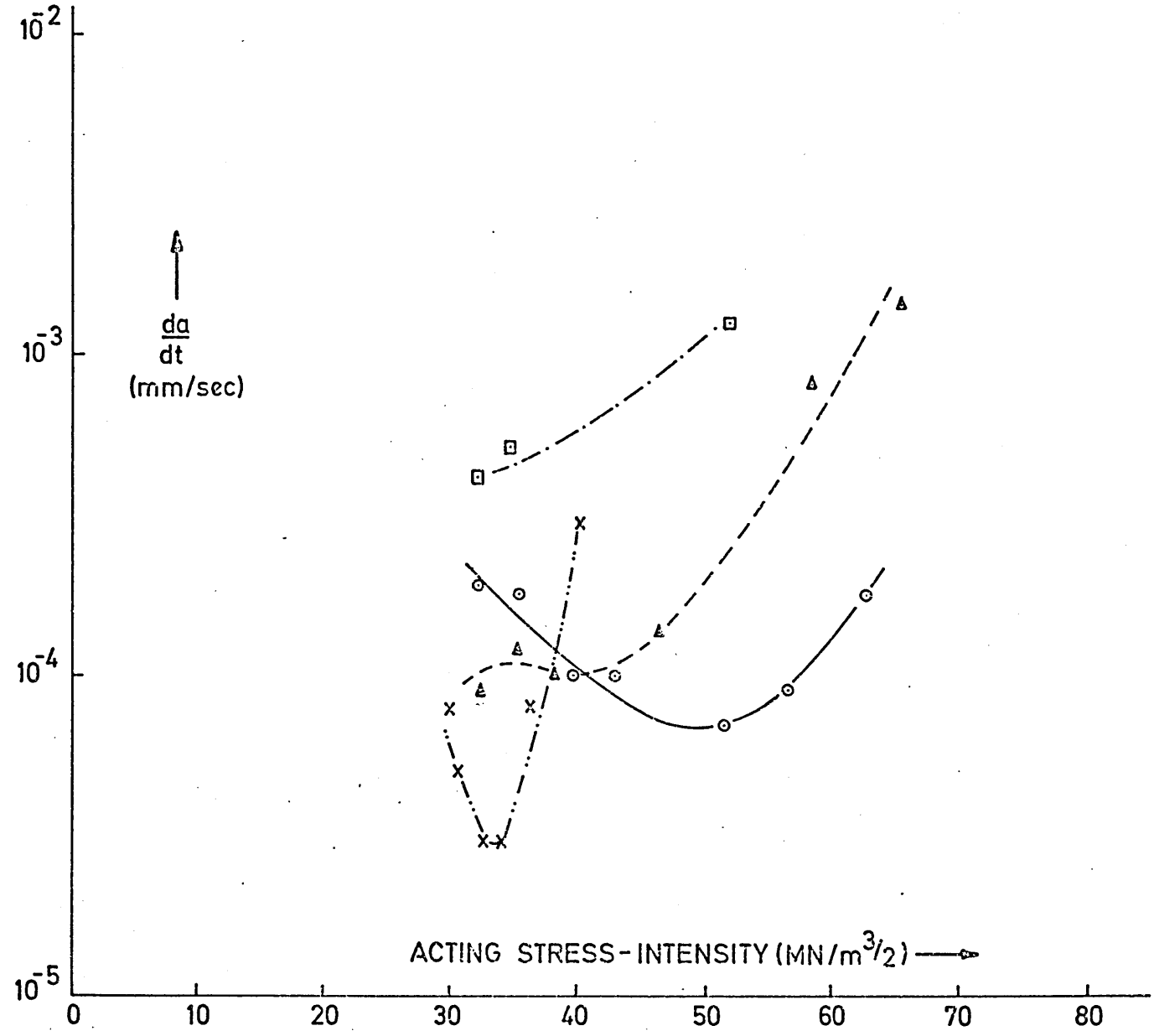

FIG. 68 Stage II velocity variation in submerged-arc welded maraging steel weld metal.

(ii) Generation of cathodic hydrogen even under overall anodic conditions was shown by Smith et al[143] to be possible. Such hydrogen is then capable of diffusion to crack tips.

(iii) Comparable activation energies for cracking and for hydrogen volume diffusion. Johnson and Wilner[144] and Van Sluys[145] measured cracking rates in high-strength steels exposed to water and to moist air, and found similar values of ~ 11 J/mol.K.

(iv) Response to stressing mode. Hayden and Floreen[88] found that increasingly rapid failure occurred under plane stress, pure tensile stress and plane-strain conditions in that order. Failure did not occur under torsional stress, and this cannot be explained by any 'active path' mechanism.

(v) Environment independence of K_{1SCC} as demonstrated by McIntyre[138]. Dautovich and Floreen[133] found similar K_{1SCC} values for hydrogen charged steels and those exposed to sodium chloride solutions.

(vi) Crack velocities proportional to $(\text{pressure})^{\frac{1}{2}}$ indicating relationship with hydrogen solubility.

The experimental evidence for hydrogen embrittlement based failure is impressive, but support for the three main mechanistic theories is still purely circumstantial. Present opinion is in favour of a stress-assisted hydrogen

diffusion mechanism as originally suggested by Troiano[146], which allows critical concentrations to build up at the crack tip. Subsequent fracture may occur by lattice decohesion (following Oriani[147]) or by lowering of the surface energy of the crack[148].

There is no doubt that diffusion rates increase with stress, and that hydrogen diffusion should be greatest in regions of plane-strain. One would, therefore, anticipate cracking to be faster at specimen centres than at their surfaces, so preserving a contour similar to the prior fatigue crack. In the present work however, surface region cracking rates considerably exceeded those in the centres in all but one of the 38 tests in which appreciable sub-critical growth occurred, and produced the U-shaped crack profiles typified in Figures 43 and 44. Only specimen BH 5A (interface zone) showed roughly equal cracking rates across its thickness, for which behaviour no reason was apparent. The differences between sub-critical growth and fast fracture in the surface regions was clearly distinguishable by the development of shear-lips during fast fracture, whereas slow growth was characterised by purely brittle failure.

This behaviour is contrary to the observations of Hayden and Floreen[88], and suggests that other factors are involved. Growth may be controlled by the availability

of hydrogen, easily derived from the bulk hydrogen sulphide solution at the outer surfaces but restricted by diffusion within the crack. The whole problem of hydrogen release on metal surfaces exposed to hydrogen sulphide requires further study to ascertain the reactions involved and the subsequent ingress kinetics. It is possible that the corrosion or catalytic action producing hydrogen is stress-dependent, so that at low stress-intensities, the reaction rate is insufficient to permit the critical concentration of hydrogen to build up at the crack tip.

In this context, at stress-intensities greater than K_{1SCC}, then slow growth commences when the local hydrogen concentration reaches the critical value. Incubation periods, defined here as the time required for pre-existing cracks to commence growth, should reflect the time taken for hydrogen diffusion. Two factors controlling the rate at which critical levels are reached are the stress state and the initial hydrogen concentration at the surface. Assuming that the latter is a function of the surface reaction rate involving the breakdown of hydrogen sulphide, then temperature would affect both the initial hydrogen concentration and its subsequent diffusion to the crack front. In the present work, temperature variations between $0^{o}C$ and ambient occurred during the initial 10-15 minutes of exposure, but their effect has been ignored. Small

changes in apparent crack length at the commencement of tests were assumed to be due to changes in specimen compliance, and incubation measured from the cessation of these changes to the commencement of significant crack growth.

7. CONCLUSIONS

A study has been made of environmental crack growth in submerged-arc welded plate and TIG welded sheet maraging steel exposed to aqueous hydrogen sulphide and sodium chloride respectively. The results enable the following conclusions to be drawn:

(i) Measured in air, the fracture toughness of submerged arc weld metal was $\sim$80 MN/m$^{3/2}$, and was markedly lower than those of either the heat-affected zone or parent metal.

(ii) Submerged-arc weld metal and parent metal show similar resistance to crack growth when exposed to hydrogen sulphide. Their estimated threshold stress intensities were both in the range of 20-30 MN/m$^{3/2}$. Heat-affected zone structures appear to offer marginally greater resistance.

(iii) Stage I crack growth followed by Stage II plateaus occurred in both weld and parent metal. Stage II velocities were of the order of 20×10^{-5} mm/sec over an intensity range of 30 - 50 MN/m$^{3/2}$.

(iv) Crack propagation in all specimens was basically intergranular following prior austenite grain boundaries. Little crack branching was observed.

(v) A reduction in growth rate during Stage II was evident in the majority of samples, regardless of their

thermal history or initial stress level. This supports a previously published observation, and confirms the view that Stage II growth may be inversely related to stress-intensity.

(vi) Crack growth rates measured in hydrogen sulphide are some 1-2 orders of magnitude faster than those in sodium chloride.

(vii) Anodically polarised TIG welded material exposed to aqueous sodium chloride fails intergranularly in the heat affected zone.

(viii) The susceptibility of maraging steel in sodium chloride increases under cathodic polarisation.

(ix) Overall, environmental cracking in maraging steels would appear to involve hydrogen embrittlement.

8. FUTURE WORK

The experimental work carried out has emphasised the specimen to specimen variability likely even with pre-cracked test pieces. Much of this variation appeared to be due to fracture paths passing through inconsistent microstructure associated with a non-planar weld interface A K-type edge preparation would have produced a flatter profile, assuming its practicality with the submerged arc process. However, in future work, the use of simulated heat-affected-zone specimens would improve reproducibility.

Clearly, the mechanism by which hydrogen sulphide causes accelerated failure in maraging steels needs a much closer examination in view of its rapidity and practical importance, and studies of the influence of stress on hydrogen uptake during attack might be profitable. Experiments at various temperatures using hydrogen sulphide gas with different partial pressures of an inert gas may give more insight into the cracking kinetics.

REFERENCES

(1) T. BELL. 'Martensite - Fundamentals and Technology' Ed. E R Petty, 1970, Longmans

(2) CG. BIEBER. Met. Eng. Qtly., 1961, 1 (4), 92

(3) GP. CONTRACTOR. J. Metals, 1966, 18 (8), 938

(4) S. FLOREEN. Met. Revs., 1968, 13, 115

(5) A. MAGNÉE ET AL 'Cobalt Containing High Strength Steels' 1974, Centre d'Information du Cobalt

(6) WD. SWANSON and JG PARR, J.I.S.I., 1964, 202, (2), 104

(7) EA. WILSON 'Diffusionless Transformations in Iron Alloys' PhD Thesis, 1965, University of Liverpool

(8) EA. OWEN and YH. LIU, J.I.S.I., 1949, 163, (2), 132

(9) FW. JONES and WI. PUMPHREY, Ibid, 1949, 163, (2), 121

(10) RF. DECKER, JT. EASH and AJ GOLDMAN, Trans. A.S.M., 1962, 55, 58

(11) BF. REISDORF, Ibid, 1963, 56, 783

(12) H. MARCUS, LH. SCHWARTZ and ME. FINE, Ibid, 1966, 59, 468

(13) JM. CHILTON and CJ. BARTON, Ibid, 1967, 60, 528

(14) P. LEGENDRE and JL. CASTAGNÉ, Met. Constr. Mec., 1968, 100, 105

(15) S. FLOREEN J.I.S.I., 1969, 207, (4), 484

(16) A. MAGNÉE ET AL Cobalt, 1973, No1, P3

(17) JC. HAMAKER and AM. BAYER, Cobalt, 1968, No.38, 3

(18) SJ. MATAS Met. Eng. Qtly., 1964, 4, (2), 48

(19) RPM. PROCTOR and HW. PAXTON, Corr. Sci., 1971, 11, (9), 723

(20) CJ. NOVAK and LM. DIRAN, J. Metals, 1963, 15, (3), 200

(21) AJ. SPITZNER and RH. KALTENHAUSER, Welding J., 1967, 46, (10), 433S

(22) HW. MAYNOR and CC. BUSH, Met. Eng. Qtly., 1966, 6, (1), 20

(23) GJ. SPAEDER. Met. Trans., 1970, 1, (7), 2011

(24) PH. SALMON-COX, BG. REISDORF and GE PELLISER. Trans. A.S.M., 1967, 239, (11), 1809

(25) A. GOLDBERG. Trans. A.S.M. Qtly, 1968, 55, (1), 26

(26) G. SAUL, JA. ROBERTSON and AM. ADAIR. Met. Trans., 1970, 1, (2), 383

(27) CE. WITHERALL ET AL Met. Prog., 1963, 89, (7), 82

(28) DA. CORRIGAN. Weld. J., 1964, 43 , (5) 298S

(29) FH. LANG and N KENYON. W.R.C. Bulletin, 1971, No159

(30) CE. WITHERALL and WA. FRAGETTA. Weld. J., 1962, 41, (11), 481S

(31) CLM. COTTRELL. J.I.S.I., 1965, 203, (6), 597

(32) RJ. KNOTH and FH. LANG. Met. Eng. Qtly., 1966, 6, (2), 49

(33) Z. PALEY. Weld. J., 1969, 48, (6), 245S

(34) CM. ADAMS. and RE. TRAVIS Ibid, 1964, 43, (3), 193S

(35) ML. KOHN. and CD. SCHAPER. Met. Prog., 1964, 85, (2), 93

(36) T. BONISZEWSKI and DM. KENYON. B.W.J., 1966, 13, (7), 415

(37) C. ROBERTS. Weld. and Met. Fab., 1968, 36, (11), 405

(38) FD. DUFFEY and W SUTAR. Weld. J., 1965, 44, (4), 251S

(39) EM. WILSON and AI. WILDMAN. B.W.J., 1966, 13, (2), 67

(40) PA. KAMMER and DC. MARTIN. D.I.M.C. Report, 1966, No229

(41) GP. CONTRACTOR. J.Met., 1966, 18, (8), 938

(42) N KENYON. Weld. J., 1968, 47, (5), 193S

(43) MC. COLEMAN and MF. JORDAN. Met. Tech., 1974, 1, (1), 24

(44) N. KENYON and S. FLOREEN. Weld.J., 1975, 54, (3), 245

(45) AT. D'ANNESSA. Brit. Weld. J., 1967, 14, (2), 62

(46) WA. TILLER ET AL. Acta.Met., 1953, 1, (3), 428

(47) AT. D'ANNESSA. Weld. J., 1966, 45, (10), 569S

(48) PH. SALMON-COX ET AL. Trans. A.I.M.E., 1967, 239, 1809

(49) JJ. PEPE and WF. SAVAGE. Weld. J., 1967, 46, (8), 4115

(50) N BAILEY Met. Const., 1971, 3, (1), 1

(51) A. GOLDBERG. Weld. J., 1968, 47, (5), 200S

(52) RN PARKINS Met Revs., 1964, 9, (35), 201

(53) JE. TRUEMAN and R. PERRY. Brit. Corr. J., 1966, 1, (11), 369

(54) JC. SCULLY and DT. POWELL. Corr. Sc., 1970, 10, 371

(55) JA. FEENEY and MJ. BLACKBURN. 'The Theory of Stress Corrosion Cracking in Alloys', 1971, Nato, Brussels, (Ed JC. Scully)

(56) FF. BOOTH and GEG. TUCKER. Corrosion 1965, 21, (5), 173

(57) AJ. JACOBS and HL MARCUS. Corrosion 1974, 30, (9), 305

(58) BF. BROWN and CD. BEACHEM. Corrosion Science 1965, 5, (11), 745

(59) TG GOOCH, D McKEOWN and D WILLINGHAM Met. Const and B.W.J., 1969, 1, (10), 469

(60) TG GOOCH Welding Research International, 1973, 3, (2), 17

(61) GR IRWIN 'Fracture of Metals' A.S.M., 1948, pp 147-166

(62) E OROWAN Welding J., 1955, 20, (3), 185

(63) GR IRWIN J. App. Mech., 1957, 24, (3), 361

(64) JD ESHELBY 'Fracture Toughness' I.S.I. publication, 1968, pp 30-48

(65) JE STRAWLEY, MH JONES and B GROSS 'Experimental Determination of the Dependence of Crack Extension Force for a Single Edge Notch Tension Specimen' T.N.D. 2396, N.A.S.A., 1964(August)

(66) EF WALKER and MJ MAY 'Compliance Functions for Various Types of Test Specimen Geometry' BISRA Report MG/E/307/67

(67) B GROSS, JE STRAWLEY and WF BROWN Jnr. 'Stress-Intensity Factors for a Single-Notched Tension Specimen by Boundary Collocation of a Stress Function' TN D2395, N.A.S.A., 1964(August)

(68) B GROSS and JE STRAWLEY 'Stress-Intensity Factors for Single Edge-Notch Specimens in Bending or Combined Bending and Tension by Boundary Collocation of a Stress Function' TN D3092, N.A.S.A., 1965(December)

(69)

(70) Materials Research and Standards, 1967, 7, (6),

(71) BF BROWN Materials Research and Standards, 1966, 6, (3), 129

(72) BF BROWN Annual Meeting A.S.T.M., Lafayette, 1965

(73) BF BROWN and CD BEACHEM Corrosion Science, 1965, 5, ( ), 745

(74) SR NOVAK and ST ROLFE Corrosion, 1970, 26, (4), 117

(75) CS CARTER Met. Trans., 1970, 1, (6), 1551

(76) CS CARTER Eng. Fract. Mech., 1971, 3, (1), 1

(77) RP WEI, SR NOVAK and DP WILLIAMS AGARD Conference Proc. No98, Paper 5, Specialists Meeting on Stress Corrosion Testing Methods, 1972

(78) JC SCULLY Metal Science J., 1972, 6, (11), 238

(79) JA FEENY and MJ BLACKBURN 'Theory of Stress-Corrosion Cracking in Alloys' Ed. JC Scully. NATO, Brussels, 1971

(80) HW LIU J. Basic Eng., 1970, 92, (12), 633

(81) MO SPEIDEL 'Theory of Stress-Corrosion Cracking in Alloys' Ed. JC Scully, NATO, Brussels, 1970, p 289

(82) WB HILLIG and RJ CHARLES 'High Strength Materials' Ed VF Zackay, London, 1955, Wiley

(83) TP HOAR 'Fundamental Aspects of Stress-Corrosion Cracking' Ed. RW Staehle et al, 1969, p 638 NACE Houston

(84) HP VAN LEEUWEN Corrosion, 1975, 31, (2), 42

(85) BF BROWN, CT FUJII and EP DAHLBERG J. ElectroChem. Soc, 1969, 116, (2), 218

(86) CS CARTER Eng. Fract. Mech., 1971, 3, (1), 1

(87) SR ANTHONY and J CONGLETON Met. Sc. J., 1968, 2, (4), 158

(88) HW HAYDEN and S FLOREEN Corrosion 1971, 27, (10), 429

(89) DP DAUTOVICH and S FLOREEN 'Stress-Corrosion Cracking and Hydrogen Embrittlement of Iron-Based Alloys' Int. Conf. Unieux, France, 1973, Paper F2

(90) CS CARTER Met. Trans., 1971, 2, (6), 1621

(91) PP PUZAK and EA LANGE N.R.L. Report No6951, 1969

(92) SW DEAN and HR COPSON Corrosion 1965, 21, (3), 95

(93) HP LECKIE and AW LOGINOW Ibid 1968, 24, (9), 291

(94) WW KIRK, RA COVERT and TP MAY Met. Eng. Qtly., 1968, 8 (4), 31

(95) RB SETTERLUND Mat. Prot., 1965, 4, (12), 27

(96) S YAMATOTO and T FUJITA Proceedings of 2nd Int. Conf. on Fracture, Brighton, 1969, Paper 36

(97) WG REUTER and CE HARTBLOWER Eng. Fract. Mech., 1971, 3, (4), 493

(98) AJ STAVROS and HW PAXTON Met. Trans., 1970, 1, (11), 3049

(99) RPM PROCTOR and HW PAXTON Corr. Sci., 1969, 9, (10), 631

(100) DP DAUTOVICH Unpublished work

(101) RN PARKINS and EG HANEY Trans. A.I.M.E., 1968, 242, (9), 1943

(102) JL CASTAGNE Corr. Trait. Prot. Fin., 1970, 18, (4) 218

(103) Report of Committee 1G, Corrosion 1952, 8, (10), 351

(104) M SMIALOWSKI 'Hydrogen in Steel' 1962, p 389 (Pergammon)

(105) JB GREER Mat. Prot., 1975, 14, (3), 11

(106) CM HUDGINS ET AL Corrosion 1966, 22, (6), 238

(107) TM SWANSON and JP TRALMER Mat. Prot., 1972, 11,(1), 36

(108) JP FRAZER and RS TRESEDER Trans. A.S.M.E., 1955, 22, (2), 238

(109) CD KIM and AW LOGINOW Corrosion 1968, 24, (10), 313

(110) RS TRESEDER and TM SWANSON Ibid, 1968, 24, (1), 31

(111) LM DVORACEK Ibid, 1970, 26, (5), 177

(112) A TIRMAN, EG HANEY and P FUGASSI Ibid, 1969, 25,(8), 69

(113) EC GRECO and WF BRICKELL Mat. Prot., 1966, 5,(10), 29

(114) P McINTYRE Pract. Imp. Fract. Inst. Metallurgists Spring Meeting, 1973, Series 2(10) paper 9

(115) P McINTYRE and AH PRIEST 'Accelerated Test Technique for the Determination of K_{1SCC} in Steels' B.S.C. Corporate Laboratories, Report No MG/31/72

(116) P McINTYRE and AH PRIEST 'Hydrogen Induced Sub-Critical Flaw Growth in Steels' B.S.C. Corporate Laboratories Report No MG/23/72

(117) E SNAPE Brit. Corr. J., 1969, 4, (9), 253

(118) LR SCHARFSTEIN J.I.S.I., 1964, 202, (2), 158

(119) P HORSMAN 'Stress Corrosion of Maraging Steels' Sheffield Polytechnic Research Project 1973

(120) N KENYON, WW KIRK and D VAN ROOYEN Corrosion 1971, 27, (9), 390

(121) SM TOY and A PHILLIPS Weld. J., 1970, 49, (11), 487S

(122) AH FREEDMAN J. Materials, 1970, 5, (2), 431

(123) TG GOOCH Welding J., 1974, 53, (7), 287S

(124) W HALL 'Stress Corrosion of Maraging Steels' Sheffield Polytechnic Thesis, 1970

(125) JE STRAWLEY and WF BROWN A.S.T.M. STP-381, 1965, p 133

(126) P MCINTYRE and AH PRIEST B.S.C. Corporate Laboratories Report No MG/ES/274/70, 1970

(127) CE HARTBLOWER, WW GERBERICH and PP CRIMMINS Symposium on Welding Imperfections, Lockheed(Palo-Alto) Laboratories, California, 1966

(128) WW GERBERICH and CE HARTBLOWER Conf. Fund. Asp. S.C. Cracking, Ohio, 1969

(129) SF SWANSON, F CICCI and W HOPPE A.S.T.M. STP-415, 1967, p 312

(130) CE LAUTZENHEISER, AF WHITING and RE WYLIE Mat. Eval., 1966, 24(5), 241

(131) BC SYRETT Corrosion 1971, 27, (7), 270

(132) S MOSTOVOY, HR SMITH RG LINGWALL and EJ RIPLING Eng. Fract. Mechanics, 1971, 3, (3), 291

(133) DP DAUTOVICH and S FLOREEN Met Trans., 1973, 4,(11), 2672

(134) ST ROLFE ET AL 1966(June) Annual Meeting A.S.T.M. (N. Jersey)

(135) RPM PROCTOR and HW PAXTON Corr. Sci., 1971, 11,(6), 723

(136) JE DAVIES J.I.M., 1973, 101, (9), 221

(137) JP HIRTH and HH JOHNSON Corrosion 1976, 32, (1), 9

(138) P McINTYRE and AH PRIEST 'Reproducability of K_{1SCC} Determinations: A Collaborative Investigation' B.S.C. Corporate Laboratories Report No PMC/APE/10/74

(139) P McINTYRE 'Practical Implications of Fracture Mechanisms' Inst. of Metallurgists, Spring Meeting, 1973, Series 2(10), Paper 9

(140) WW GERBERICH and YT CHEN Met. Trans., 1975, 6A,(2), 271

(141) GT HAHIN and AR ROSENFIELD Trans A.S.M., 1966, 59, (6), 909

(142) CS CARTER Corrosion 1971, 27, (11), 471

(143) JA SMITH, MH PETERSON and BF BROWN Corrosion 1970, 26, (2), 53

(144) HH JOHNSON and AM WILNER App. Mat. Res., 1965, 14, (1), 34

(145) WA VAN DER SLUYS Nat. Symp. on Fract. Mechanics 1967 Lehigh University, U.S.A.

(146) AR TROIANO Trans. A.S.M. 1960, 52, (1), 54

(147) RA ORIANI Int. Conf. on Stress Corr. Cracking and Hydrogen Embrittlement of Iron Band Alloys, 1973, Unieux, France

(148) NJ PETCH Phil. Mag., 1956, 1, (10), 331

(149) WW GERBERICH, YT CHEN and C ST JOHN Met.Trans., 1975 6A, (8), 1485

(150) WD BENJAMIN and EA STEIGERWALD A.F.M.L. TR 68-80, 1968

(151) SJ HUDAK and RP WEI (to be published)

STRUCTURE	MEAN NOTCH POSITION (mm)	WIDTH W (mm)	THICKNESS B (mm)	RELATIVE CRACK LENGTH ($^a/W$)	COMPLIANCE Y	MAX. LOAD P_Q (Kg)	FRACTURE TOUGHNESS K_Q ($MN/m^{3/2}$)
Parent Metal	21.7	10.81	6.63	0.526	11.56	682	112.09
	18.7	10.88	6.43	0.517	11.22	701	114.99
	17.7	10.83	6.28	0.545	12.33	642	118.85
	16.7	10.92	6.28	0.496	10.48	677	106.02
	12.3	10.69	6.90	0.530	11.71	716	115.23
	8.7	10.73	6.70	0.540	12.12	778	133.17
	8.7	10.62	5.59	0.534	11.87	589	118.90
Dark Etching Zone Interface	5.3	10.81	6.40	0.505	10.78	693	110.03
	5.2	10.74	6.60	0.511	11.00	753	128.43
	3.3	10.90	6.29	0.497	10.51	640	100.42
	3.3	10.88	6.27	0.508	10.89	630	102.96
Weld Metal	-2.3	10.78	6.62	0.492	10.34	570	84.13
	-2.3	10.86	6.35	0.523	11.44	501	84.98
	-6.1	10.83	6.04	0.512	11.03	460	79.17
	-9.0	10.84	6.65	0.497	10.51	517	76.95
	-10.3	10.74	5.87	0.535	11.91	490	94.06

Table 20: Fracture-Toughness Determinations at Various Weld Positions

MEAN NOTCH POSITION (mm)	WIDTH W (mm)	THICKNESS B (mm)	INITIAL CRACK LENGTH (a/W)	COMPLIANCE Y	LOAD P (Kg)	INITIAL INTENSITY K_{1i} ($MN/m^{3/2}$)	RAW ENDURANCE (mins)	INCUBATION PERIOD (mins)	TI LET
15.0	10.73	5.95	0.490	10.28	321.6	52.59	0.3	0	BH
13.0	10.84	6.16	0.512	11.03	311.6	52.54	3.0	0	BH
24.0	11.46	7.26	0.480	9.99	400.0	50.42	75	10	P
24.3	11.56	6.41	0.490	10.28	335.0	48.99	174	15	P
10.3	10.60	6.22	0.492	10.34	285.0	45.12	9.6	3.6	BH
10.0	10.66	6.10	0.489	10.25	260.0	41.48	15	5.5	BH
10.0	10.58	6.27	0.494	10.41	250.0	39.97	39	9	BH
13.0	10.80	6.18	0.502	10.68	230.0	37.51	15	4	BH
10.0	10.68	6.32	0.463	9.46	260.0	36.93	51	10	BH
9.5	11.55	6.22	0.447	9.02	225.0	33.19	222	48	BH
15.0	10.76	6.31	0.494	10.41	210.0	32.75	294	0	BH
20.7	11.42	6.97	0.471	9.69	250.0	31.89	222	43	P
9.6	10.84	6.18	0.489	10.25	195.0	30.46	573	90	BH

Table 21: Test Data and Endurances for Parent Plate Exposed to Aqueous Hydrogen Sulphide

(Mean Test Temperatures $15^{o}C$, Mean pH 3.5)

MEAN NOTCH POSITION (mm)	WIDTH W (mm)	THICKNESS B (mm)	INITIAL CRACK LENGTH (a/W)	COMPLIANCE Y	LOAD P (Kg)	INITIAL INTENSITY K_{1i} ($MN/m^{3/2}$)	RAW ENDURANCE (mins)	INCUBATION PERIOD (mins)	T LET
-8.6	11.54	7.02	0.487	10.18	270.0	40.73	9	7	P
-4.0	10.87	6.19	0.489	10.25	250.0	38.94	150	15	BH1
-4.0	10.92	6.11	0.533	11.83	210.0	38.15	4	1.2	BH1
-5.5	10.79	6.96	0.460	9.37	300.0	38.12	0.5	0	BH1
-6.0	11.39	6.58	0.489	10.25	250.0	35.77	27	24	BH
-4.8	11.42	5.95	0.479	9.95	210.0	31.97	89	8	BH4
-3.5	11.55	6.54	0.494	10.41	200.0	30.00	432	53	P
-4.1	11.42	7.00	0.479	9.95	230.0	29.25	234	30	P
-6.0	11.36	6.76	0.479	9.93	210.0	29.21	1548	84	BH
-6.0	11.36	6.56	0.494	10.41	155.0	22.63	> 1200	-	BH
-5.5	10.84	5.90	0.512	11.03	110.0	19.36	> 1200	-	BH1

Table 22: Test Data and Endurances for Maraging Submerged-Arc Weld Metal Exposed to Aqueous Hydrogen Sulphi

MEAN NOTCH POSITION (mm)	WIDTH W (mm)	THICKNESS B (mm)	INITIAL CRACK LENGTH	COMPLIANCE Y	LOAD P (Kg)	INITIAL INTENSITY K_{1i} ($MN/m^{3/2}$)	RAW ENDURANCE E_r (mins)	INCUBATION PERIOD (mins)	TE LET
4.0	10.75	5.68	0.507	10.85	300.0	54.21	27	7	BH
-1.0	10.85	5.80	0.500	10.61	250.0	43.05	30	1	BH1
3.0	10.80	5.91	0.472	9.72	250.0	38.80	54	34	BH1
-1.0	10.88	6.19	0.469	9.63	260.0	38.02	0	-	BH1
-0.1	10.81	5.95	0.488	10.21	230.0	37.22	54	0	BH2
3.0	10.74	6.38	0.479	9.93	251.6	37.05	66	20	BH1
-2.0	10.82	6.05	0.478	9.90	240.0	37.02	6	0	BH
-2.0	10.82	6.20	0.539	12.08	200.0	36.73	231	-	BH
-0.1	10.81	6.06	0.510	10.96	210.0	35.82	66	7	BH2
-2.7	11.44	6.72	0.467	9.57	245.0	33.59	297	54	BH1
-2.0	10.83	6.18	0.481	9.99	220.0	33.50	57	0	BH3
1.0	11.55	7.39	0.470	9.66	270.0	32.20	231	0	P

Table 23: Test Data and Endurances for Interface Region of Submerged-Arc Welded Maraging Steel Exposed to Aqueous Hydrogen Sulphide

MEAN NOTCH POSITION (mm)	WIDTH W (mm)	THICKNESS B (mm)	INITIAL CRACK LENGTH (a/W)	COMPLIANCE Y	LOAD P (Kg)	INITIAL INTENSITY K_{1i} ($MN/m^{3/2}$)	RAW ENDURANCE (mins)	INCUBATION PERIOD (mins)	TE LETT
5.4	11.40	6.60	0.474	9.78	375.0	51.03	324	84	BH1
5.5	11.21	6.04	0.504	10.75	290.0	47.80	135	48	BH1
5.3	11.42	6.78	0.481	9.99	285.0	38.54	63	12	BH4
7.0	10.76	6.09	0.494	10.41	231.6	37.43	2.4	0	BH
4.0	10.84	6.20	0.491	10.31	230.0	36.02	420	20	BH1
4.3	11.42	6.42	0.495	10.44	270.0	34.80	507	16	BH4
7.2	11.55	6.42	0.484	10.09	195.0	27.96	> 7000	-	P
5.8	11.36	7.03	0.507	10.85	180.0	25.55	381	60	P
8.0	10.62	6.13	0.498	10.54	125.0	20.45	1890	534	BH1

Table 24: Test Data and Endurances for Dark-Etching Zone of Submerged-Arc Welded Maraging Steel Exposed to Aqueous Hydrogen Sulphide

TEST LETTERS	$(\frac{a_{sc}}{W})$ (per hour)	ACTING CRACK LENGTH $(\frac{a}{W})_{sc}$	FATIGUE PRE-CRACK $(\frac{a}{W})_F$	$(\frac{a_F+a_{sc}}{W})$	COMPLIANCE Y	LOAD P (Kg)	$B\sqrt{W}$ / Y	STRESS INTENSITY K_{Qi} ($MN/m^{3/2}$)	CRACK VELOCIT da/dt (mm/sec
P10B	0.1562	0.0294	0.4808	0.5102	10.96	400	2.2424	55.31	49×10^{-5}
	0.1518	0.0343		0.5151	11.14		2.2061	56.22	48 "
	0.1367	0.0535		0.5343	11.88		2.0687	59.96	43 "
	0.0970	0.0812		0.5620	13.09		1.8775	66.06	31 "
	0.0789	0.0970		0.5778	13.87		1.7719	70.00	25 "
	0.1497	0.1126		0.5934	14.69		1.6730	74.14	48 "
P 9B	0.0789	0.0511	0.4710	0.5221	11.40	250	2.0657	37.53	25×10^{-5}
	0.0743	0.0834		0.5544	12.74		1.8485	41.94	24 "
	0.0720	0.1059		0.5769	13.82		1.7040	45.49	23 "
	0.0970	0.1583		0.6293	16.85		1.3976	55.47	31 "
	0.1037	0.2051		0.6761	20.34		1.1578	66.96	33 "
BH44B	0.0857	0.0219	0.4470	0.4689	9.63	225	2.1951	31.78	28×10^{-5}
	0.0857	0.0464		0.4934	10.39		2.0345	34.29	28 "
	0.0581	0.0651		0.5121	11.03		1.9165	36.40	18 "
	0.0558	0.1014		0.5484	12.47		1.6952	41.16	18 "
	0.0628	0.1410		0.5880	14.39		1.4690	47.49	20 "
P10A	0.1323	0.0168	0.4900	0.5068	10.86	335	2.0068	51.76	43×10^{-5}
	0.0970	0.0743		0.5643	13.20		1.6511	62.92	31 "
	0.0766	0.1192		0.6092	15.59		1.3979	74.31	24 "
	0.0789	0.1583		0.6483	18.18		1.1988	86.65	25 "

Table 25: Crack-Velocities and Related Data: Maraging Steel Parent Metal

TEST LETTERS	$(\frac{a_{sc}}{W})$ (per hour)	ACTING CRACK LENGTH $(a/W)_{sc}$	FATIGUE PRE-CRACK $(a/W)_F$	$(\frac{a_F+a_{sc}}{W})$	COMPLIANCE Y	LOAD P (Kg)	$\frac{B\sqrt{W}}{Y}$	STRESS INTENSITY K_{Qi} $(MN/m^{3/2})$	CRAC VELOC $\frac{da}{d}$ (mm/se
BH44R	0.2613	0.0000	0.4940	0.4940	10.41	250	1.9591	39.57	77x1(
	0.1924	0.0142		0.5082	10.89		1.8728	41.39	56 "
	0.2942	0.0720		0.5660	13.28		1.5357	50.48	86 "
	0.3691	0.1170		0.6110	15.70		1.2990	59.68	108 "
BH23A	0.7000	0.0142	0.4918	0.5060	10.82	230	1.8770	38.00	210x1(
BH40B	0.5852	0.0269	0.4961	0.5231	11.44	285	1.7701	49.93	172x1(
BH42A	0.0370	0.0219	0.4861	0.5080	10.89	195	1.8459	32.76	11x1(
BH22B	0.1924	0.0219	0.4634	0.4853	10.13	260	2.0389	39.50	57x1(
BH22A	0.4486	0.0116	0.4887	0.5003	10.61	260	1.8777	42.94	133x1(
BH25A	0.1148	0.0511	0.4944	0.5455	12.35	210	1.6760	38.95	34x1(

Table 25 : (Continued)

TEST LETTERS	$(\frac{a_{sc}}{W})$ (per hour)	ACTING CRACK LENGTH $(a/W)_{sc}$	FATIGUE PRE-CRACK $(a/W)_F$	$(\frac{a_F+a_{sc}}{W})$	COMPLIANCE Y	LOAD P (Kg)	$\frac{B\sqrt{W}}{Y}$	STRESS INTENSITY K_{Qi} ($MN/m^{3/2}$)	CRACK VELOCIT da/dt (mm/sec
P 4B	0.0605	0.0319	0.4715	0.5034	10.72	230	2.2066	32.32	19x10⁻
	0.0559	0.0605		0.5302	11.79		2.0063	35.55	18 "
	0.0319	0.0925		0.5640	13.19		1.7934	39.77	10 "
	0.0319	0.1148		0.5863	14.30		1.6542	43.11	10 "
	0.0219	0.1627		0.6342	17.15		1.3793	51.71	7 "
	0.0270	0.1840		0.6555	18.75		1.2616	56.53	9 "
	0.0511	0.2055		0.6770	20.85		1.1345	62.86	16 "
P 4A	0.0270	0.0245	0.5038	0.5283	11.64	200	1.9094	32.48	9x10⁻
	0.0344	0.0488		0.5526	12.66		1.7556	35.33	12 "
	0.0319	0.0744		0.5782	13.87		1.6024	38.70	10 "
	0.0440	0.1236		0.6274	16.72		1.3293	46.65	14 "
	0.2469	0.1776		0.6814	20.90		1.0634	58.32	80 "
	0.4368	0.2055		0.7093	23.41		0.9494	65.32	140 "
BH 9A1	0.0245	0.0116	0.4855	0.4971	10.51	210	2.1678	30.04	8x10⁻
	0.0142	0.0194		0.5049	10.78		2.1135	30.81	5 "
	0.0116	0.0368		0.5223	11.41		1.9968	32.61	3 "
	0.0116	0.0488		0.5343	11.88		1.9178	33.95	3 "
	0.0245	0.0698		0.5553	12.79		1.7814	36.55	8 "
	0.0925	0.0970		0.5825	14.11		1.6147	40.33	30 "

Table 26 : Crack Velocities and Related Data: Submerged-Arc Welded Maraging Weld Metal

TEST LETTERS	$(\frac{a_{sc}}{W})$ (per hour)	ACTING CRACK LENGTH $(a/W)_{sc}$	FATIGUE PRE-CRACK $(a/W)_F$	$(\frac{a_F+a_{sc}}{W})$	COMPLIANCE Y	LOAD P (Kg)	$\frac{B\sqrt{W}}{Y}$	STRESS INTENSITY K_{Qi} ($MN/m^{3/2}$)	CRACK VELOCI da/dt (mm/se
BH45A	0.1280	0.0511	0.4769	0.5280	11.64	210	2.0380	31.95	41x10
	0.1627	0.0721		0.5490	12.50		1.8978	34.31	51 "
	0.3891	0.1819		0.6588	18.90		1.2551	51.88	123 "
P 5B	0.7000	0.0168	0.5273	0.5441	12.30	270	1.9390	43.18	210x10
BH 9B1	0.6237	0.0084	0.4816	0.4900	10.28	250	2.1826	35.52	196x10

Table 26 : (Continued)